学位申請論文

松本　充弘

Thesis :

Molecular Orientation near Liquid-vapor Interface of Hydrogen-bonding Systems

Mitsuhiro Matsumoto

Mitsuhiro Matsumoto

Dec. 15, 1988

ぬばたまのわが黒髪にふりなずむ天の霜雪取れば消につつ

万葉集　巻七

Dew and frost, which is falling on my black hair
from the haven, is disappearing on my palm.

in MAN'YŌSHŪ, Vol.7.

Acknowledgments

The author is much grateful to Professor Nobuhiro Gō and Dr. Yosuke Kataoka for their extensive support, helpful discussion, and constant encouragement.

Dr. Shuichi Nosé kindly advised me about molecular dynamics simulation technique, and Professor Keith E. Gubbins gave me important suggestion and information about their works on interfacial systems. The author heartily thanks them.

The simulations and various analyses have been executed in the Kyoto University Data Processing Center and the Computer Center of the Institute for Molecular Science.

Abstract

The various anomalies of liquid-vapor interface of strongly hydrogen-bonding fluids are well known and the main cause has been considered to be some molecular orientational ordering near the surface. While a few of simulational works to investigate the ordering, especially for water, have been already reported, no conclusive results are obtained yet. We executed the large-scale molecular dynamics simulations of water surface for wide temperature range from 250 K to 400 K and found that two typical orientations exist near the surface, instead of one orientation usually stated. We analyzed the orientational tendency in detail and compared it with experimental results; thermodynamic measurements, ellipsometry, and surface potential measurement. Although the water model is rather simple, good agreement with thermodynamic measurements was obtained; in particular the empirically observed anomalous temperature dependence of surface excess entropy was well reproduced, which suggests the validity of computer simulation for studies of interfacial systems. As to the ellipsometry we pointed out that the usual assumption in experiments about the shape of density profile is doubtful for water surface. The surface potential that we evaluated from the simulation agrees quantitatively with recent experiments, which conversely supports the assumption in experimental measurements.

We carried out the similar simulation and analysis for the surface of methanol to consider the role of hydrogen bonding in more detail. Methanol shows much stronger orientational tendency due to its hydrophobic methyl group; in this sense methanol can be considered as one of the simplest models of surfactant. Comparing these results (water and methanol) we discussed the origin of the orientational ordering for strongly hydrogen-bonding systems.

TABLE OF CONTENTS

I

Wie zwei weiße Tauben fliegen wir selig ins Blau!
Flüsse im Frühlicht! Gottesacker im Wind und der Geruch
der unendlichen Felder, vor sie abgehauen werden!

Bertolt Brecht, BAAL

Like two white doves let's fly into the blue sky with joy!
The river flow in dawn! The graveyard in wind and
the scent of the boundless field before mowing!

I. Introduction

Water, of course as one of the most important substances on our earth, has long been a central topic of science, not to mention the speculative philosophy of the Ancient Greek and mystic alchemy of the Middle Age. It is a well known fact that water plays various important roles in living bodies, such as metabolism and keeping of homeostasis. Also the climate on the earth is kept stable and suitable for life owing to the existence of water (moisture and the sea). The details of properties and functions of water in various forms have been clarified little by little, but the most part of them still remains unresolved.

In particular interfacial systems of aqueous solutions, including ionic solutions, polymer solutions etc., have been attracting special interest lately. Thermodynamic properties of interface, such as surface tension and surface excess entropy, have been long investigated since the last century, but it was only recently that the microscopic (molecular-level) understanding of interfacial phenomena began to progress. Many novel and important systems and phenomena have been fully studied and reported up to now; e.g., micells of various surface active agents (surfactants), membranes, and films. By the way, do we completely understand how water molecules behave in such systems? The answer is, of course, no. There are few bridges connecting the thermodynamic properties and molecular behaviors as yet.

Fortunately scientists of today in these fields can use the highly developed computer facilities; high-speed vector processors, large main

memory, graphic terminals, etc. Among the fields having much benefits from them, quantum chemistry and computer simulation are the two main ones. In particular the investigation of liquid structure on molecular level has shown a great progress due to the computer simulation using the pair potential calculated with the approach of quantum chemistry.

Now we feel that the ability of computer has reached the stage of making possible the study of more subtle problems, i.e., inhomogeneous or interfacial systems. As described in Sec.Ⅱ, some results have been already reported on such systems of simple fluids (monatomic and diatomic ones), to which a lot of physicists (and some chemists) are paying more and more attention. However, more interesting systems (from the view point of chemists), the interfaces of strongly hydrogen-bonding fluids, have not been fully researched in this way because the interactions between molecules are too complicated. In this work I report one of the most simple examples of such study, the liquid-vapor interface of strongly hydrogen-bonding substances, water and methanol.

It is well known that the liquid-vapor interface of such substances itself shows some unique, or anomalous, features; e.g., surface tension is much larger than other simple fluids. We could find in this work that a part of the cause is the orientational ordering of molecules near the surface due to the hydrogen bonding and reported some experimental evidences to be compared with it. Our final goal exists, however, not only in knowing what occurs near the liquid-vapor interface, but also in understanding the more general molecular behaviors under various inhomogeneous circumstances. This work gives a new direction to future study of interfacial systems.

II

Luogo è là giù da Belzebù remoto
 tanto quanto la tomba si distende,
 che non per vista, ma per suono è noto
d'un ruscelletto che quivi discende
 per la buca d'un sasso, ch'elli ha roso,
 col corso ch'elli avvolge, e poco pende.

Dante Alighieri, La Divina Commedia

Down there, from Beelzebub as far removed as his tomb extends,
is a space not known by sight, but by the sound of a rivulet
descending in it along the hollow of the rock which it has
eaten out in its winding and gently sloping course.

THE DIVINE COMEDY

Ⅱ. Historical Background

In this section I briefly describe the background of our work. The study of interfacial systems, of course, has long history since the last century. It was only recently (in the 1950's), however, that the elucidation of interfacial phenomena in molecular level began. The effort of studying them in detail is continuing even now with approaches of statistical mechanics and computer simulations. To make the description concise, I will limit the topics to the case of liquid-vapor interface.[1-5] Researches on other systems, especially on liquid-liquid and liquid-solid interfaces, are also rapidly developing recently.[6-8]

A. Thermodynamics and statistical mechanics

Study of interfacial systems started probably for the capillary phenomena,[2] which are now explained as a balance between the surface tension and the gravity. The surface tension, which was often referred to as an evidence of the existence of attractive interaction between molecules (or atoms) by many scientists such as P.S.Laplace (1749-1827) and T.Young (1773-1829), was thermodynamically founded in the last century by J.C.Maxwell (1831-1879), Lord Rayleigh (1842-1919), and J.W.Gibbs (1839-1903). In particular Gibbs established the general foundation of thermodynamics and statistical mechanics, one application of which is the notion of "surface excess quantity"; this is the basic idea when one considers the interfacial

phenomena. For example, the surface tension γ, which is almost the only directly measurable thermodynamic quantity, is naturally related to the surface excess (Helmholtz) free energy within this framework. As a result of that, the temperature derivative of γ is the surface excess entropy s_s; for details, see Sec. Ⅲ Many people experimentally measured γ and s_s of various substances, including organic compounds and liquid metals, and tried to find out some empirical rules describing the relation of γ and the temperature T. Among them one of the most successful ones is the law of Eötvös-Ramsay-Shields-Katayama,[4,9,101,102] which is represented as

$$\gamma (M/\rho)^{2/3} = k(T_c - T - \tau), \qquad (Ⅱ-1)$$

where M is the molecular weight, ρ the liquid density, and T_c the critical temperature. Then k and τ are almost constant ($k \sim 2$ $cm^2 g^{1/3} s^{-2} K^{-1}$ and $\tau \sim 6$ K) for usual liquids. Some examples of the value of k are listed in Table Ⅱ-1, from which one can see that this simple relation holds rather well. It was considered that the extraordinarily low values for water, methanol, ethanol, etc. suggest some anomaly such as dissociation or association. As easily understood by differentiating the both sides of Eq.(Ⅱ-1) with T, k is nearly equal to the molar surface excess entropy. Therefore the low value of k suggests also existence of some structural change near the surface, as described later

Statistical mechanical treatment of the interfacial systems began more lately in the 1950's. The first subject was how to connect γ (excess free energy) and the molecular distribution near the surface. Roughly speaking,

there are two ways; one is the mean field theory[103-106] based upon the van der Waals-type free energy expression, and the other is the capillary wave theory.[3,107] The former theory is a kind of variational method in which the free energy of the whole system is expanded with respect to the local density and then minimized. In the latter theory, the density variation near the surface is considered as superposition of capillary waves. Since both theories predict almost the same results for thermodynamic properties such as γ and density variation unless the condition is very severe (e.g., near the critical point), they are equally often used in analyses of experimental results (x-ray diffraction, etc.) with some modifications if necessary.

B. Computer simulation of simple fluid

Another way of studying interfacial systems on microscopic (molecular) level is to execute computer simulations on these systems. When the pair interaction model potential is accurate enough to represent the real systems, computer simulation gives us much detailed information, such as local density, many body distribution functions, and time correlation functions; here we do not refer to many body interactions, which become important particularly in liquid metals. The various simulation techniques have been well known in liquid physics; microcanonical molecular dynamics (MD) method, constant temperature MD method, constant pressure MD method, Brownian dynamics method, Monte Carlo (MC) method, etc.[7,8,10]

The history of application of computer simulation techniques to interfacial systems is, however, not so long; the work of Croxton and

Ferrier[108] in 1971 on liquid-vapor interface of two dimensional Lennard-Jones (LJ) fluid is perhaps the first one. Since then many of such simulations[2] have been executed to study the interfacial properties; mainly on surface tension, the shape of density profile (local density variation), two-body correlation functions, and capillary waves. Since computer facilities were quite limited in the initial age of simulation, the number of particles was only some hundreds. As a result of that the statistical error was rather large and controversy sometimes occurred on the reliability of conclusions; one of the biggests was whether the density profile is oscillatory or not. At present it is no more remarkable that the number of particles is more than 10,000 and the problem of statistics does not seem serious. For example, the density profile was settled to be monotonic for LJ system.[2,109]

C. Computer simulation of molecular fluid

While interfacial systems of simple (monatomic) fluids attract attention mostly of physicists, study of more real systems, i.e., molecular fluids, has gradually become an interesting subject for chemists. Among various molecular systems, diatomic (dumbbell type) molecules and Stockmayer models (LJ interaction + a point electric dipole) are probably the most simple ones. These systems have been extensively studied[1,110-113] through perturbation technique and integro-differential equation approach fully developed in liquid state physics.

In particular the effect of electric multipole is very important when one wants to consider the orientational ordering of molecules from the

viewpoints of multipole interactions; the dipole (and the quadrupole also) has the effect of aligning molecules parallel to the surface. This was also confirmed by computer simulations[110-113].

As far as we noticed, more complicated systems have been rarely investigated. The almost only exception is the case of water, as described next.

D. Characteristic features of strongly hydrogen-bonding fluids

It is a well known fact that water has large surface tension, which contributes to various phenomena, such as sea wave, surface rise in capillary, dews rolling on waxed floor, etc. Other hydrogen-bonding liquids (e.g., methanol) are also known to show rather large surface tension.

Based upon the anomaly of Eötvös constant described above, Good[114] collected surface entropy data of various substances near its triple point temperature T_t and proposed that the molar surface entropy can be taken as a criterion of grouping the substances. In particular, the group of associating liquids, including water, formic acid, methanol, formamide, methyl amine and hydrogen cyanide, shows extraordinary low surface entropy (Fig. II-1). Good tried to explain it by considering entropy deficit due to some molecular orientation, the cause of which he thought was hydrogen bonding. Although we criticize his idea in Sec. VI based upon our simulational results, it still holds true in some cases, especially for methanol.

Another famous topic concerning water surface was the existence of some

phase transition around room temperature which Drost-Hansen suggested from the measurement of the surface tension.[115] It seems now that almost all experimentalists are denying the possibility of such phenomenon,[116,117] but quite recently it was reported that more accurate measurement may detect the transition.[118]

Theoretical studies of water surface have also long history. In 1951 Weyl[119] suggested by considering the difference of polarizability of hydrogen atom and oxygen atom that water molecules near the surface prefer to have their dipoles directed toward the interior of liquid phase, i.e., O^{2-} is in the vapor-side and H^{+} is in the liquid-side. Stillinger and Ben-Naim[120] (SB) obtained the similar result from electrostatic calculation of a simple model of water molecules (point dipole + point quadrupole). On the other hand, assuming a simple exponential decay of orientational ordering coherence and evaluating the surface excess free energy, Fletcher[121] concluded that the orientation of the lowest free energy is that with the protons directed outwards. Most recently in 1981 Croxton[122] adopted the model almost similar to that of SB and, by introducing a dipole order parameter, obtained the same result as Fletcher's. Up to the present these two contradictory predictions (Fig. Ⅱ-2) exist concerning the orientational tendency of water molecules. It appears, however, that the most relevant difference between the calculation of SB and that of Croxton is not the method itself but the value of quadrupole moment of the model water molecule ; SB used Q_{zz}= +0.364 DÅ (1DÅ = 3.336×10^{-40} Cm^2) and Croxton adopted the values of opposite sign (Q_{xx}=-6.56, Q_{yy}=-5.18, Q_{zz}=-5.51 DÅ). The values of the quadrupole moment of water experimentally measured or quantum-mechanically calculated most

recently[12] are rather different from both of these; e.g., Q_{XX}=+2.63, Q_{yy}= -2.50, Q_{ZZ}=-0.13 DÅ.[123] Considering that the orientational ordering is determined mostly by the coupling term of the dipole and the quadrupole,[1,112,113] it is natural that change of the sign of the quadrupole moment causes the opposite predictions for orientation.

Another possible theoretical approach is the perturbation technique; however, usual perturbation from simple model is considered to be rather difficult because water molecules have large dipole moment and other higher multipole interactions are also relevant. As far as we noticed no such rigorous theoretical treatments were reported.

E. Computer simulation of water surface

While it is considered to be rather difficult to experimentally detect the molecular orientation near the liquid-vapor interface, computer simulation is a hopeful approach. Simulation of aqueous systems is, however, much more difficult than that of simple fluids because the interaction between molecules is very complicated for aqueous systems. As far as we noticed, a MC calculation of Borštnik, Janežič, and Ažman[124] in 1980 is the first to simulate the liquid-vapor interfacial properties of water with MCY potential[125]; in that they reported the shape of the density profile, the surface tension, the excess energy, and the orientational structure of molecules. But the number of molecules they used was only 64 due to the poor ability of computer in those days, so their system appears to be too small to extract some definite conclusion. Lee and Scott[126] used a MC umbrella

sampling technique with 256 particles to calculate the surface tension of water and reported a value 97±6 dyn/cm at 298 K for ST2 potential.[127] Townsend, Gryko, and Rice[128] also studied ST2 water (free cluster of 1000 or 512 particles) at 300 K by MD simulation and confirmed the existence of orientational ordering (tendency of lying down on the surface); their data of contour plot of orientational distribution is shown in Fig. II-3, in which one can certainly see some orientational ordering, but we have an impression that the statistical error is rather large. More recently Christou et al.[129] executed MC simulation on a film of the Rowlinson model water[130] (the number of molecules N=216, the temperature T=298 K and 363 K). Brodskaya and Rusanov[131] did MD simulation on a cluster of ST2 water (N=15～64 and T=222 K～314 K), and Wilson et al.[132] carried out MD simulation on water surface of 342 TIPS4P model molecules[133] at T=325 K, both of them obtained some evidences of orientational ordering. A part of their results are shown in Figs. II-4～II-6. Christou et al. calculated the electrostatic potential profile, $\chi(z)$ in Fig. II-4, and suggested that the potential difference, the surface potential, may be induced due to the molecular orientation at low temperatures. Brodskaya and Rusanov investigated atomic density profiles (Fig. II-5) and found that density of oxygen is larger than that of hydrogen in the inner part of the surface, which means that water molecules tend to project hydrogen atoms toward the vapor phase. Wilson et al. also calculated the distribution functions of the molecular orientation (Fig. II-6) and supported the lying-down orientation. They also estimated the surface potential[134] and suggested the strong model-dependence, for which we will later discuss the validity of their calculation in detail.[135]

Thus not a few of simulational study have been already reported and the existence of some orientational ordering is perhaps established; there seems to exist, however, no consensus as to the detailed picture of the molecular orientation of water, nor any established relations between the simulational results and experimental ones (e.g., the anomaly of surface entropy). One of the main reasons for this situation is that the insufficient simulational average due to the poor ability of computers; in particular, it seems as yet that the system size (number of molecules) is too small and the temperature range is too narrow.

In order to elucidate the nature of liquid-vapor interface of water in more detail and to discuss the relation to the thermodynamic anomaly, we have executed the MD simulation for much larger system and wider temperature range. Moreover, the surface of methanol, known nearly as anomalous as water surface, was also investigated through simulation to be compared with water. As the results of such large-scale simulations, we found two typical orientation instead of one orientation for water and could clarify the role of hydrogen bonding in the ordering, as fully described in the following sections.

Table Ⅱ-1. Examples of the value k in the Eötvös-Ramsay-Shields-Katayama's law, Eq.(Ⅱ-1). The unit is $cm^2g^{1/3}s^{-2}K^{-1}$. Data are taken from Ref.13.

Ar	2.336	Cl_2	2.413	CH_4	2.083	$CH_3(CO)CH_3$	1.966
Kr	2.217	F_2	1.419	C_2H_6	2.518	$(C_2H_5)_2O$	2.006
Xe	1.913	O_2	2.364	CH_3OH	0.911	CH_3COOH	1.476
Hg	1.236	CO_2	2.070	C_2H_5OH	1.251	Benzene	2.629
Na	0.781	H_2O	0.948				

[Figure captions in Sec. II]

Fig. II-1. Frequency distribution of molar surface entropy values of various substances (Good, 1957, Ref.114).

Fig. II-2. Two different predictions about the typical orientation of water molecules near liquid-vapor interface; (a) Weyl (Ref.119), Stillinger and Ben-Naim (Ref 120), and (b) Fletcher (Ref 121) and Croxton (Ref 122).

Fig. II-3. Contour plot of molecular orientational distribution obtained by Townsend et al. (Ref.128) ϕ is the angle between the surface normal and the molecular symmetry axis.

Fig. II-4. Surface potential profile obtained by Christou et al. (Ref.129)

Fig. II-5. Atomic density profiles calculated by Brodskaya and Rusanov (Ref 131); ρ_O for oxygen (solid lines) and ρ_H for hydrogen (dotted lines), respectively The five figures (a~e) correspond to samples of various temperatures and number of particles.

Fig. II-6. Distribution functions of the angle between the molecular dipole and the inward-pointing surface normal obtained by Wilson et al. (Ref 132) The layer 1 is the most outward (vapor side) layer of the surface.

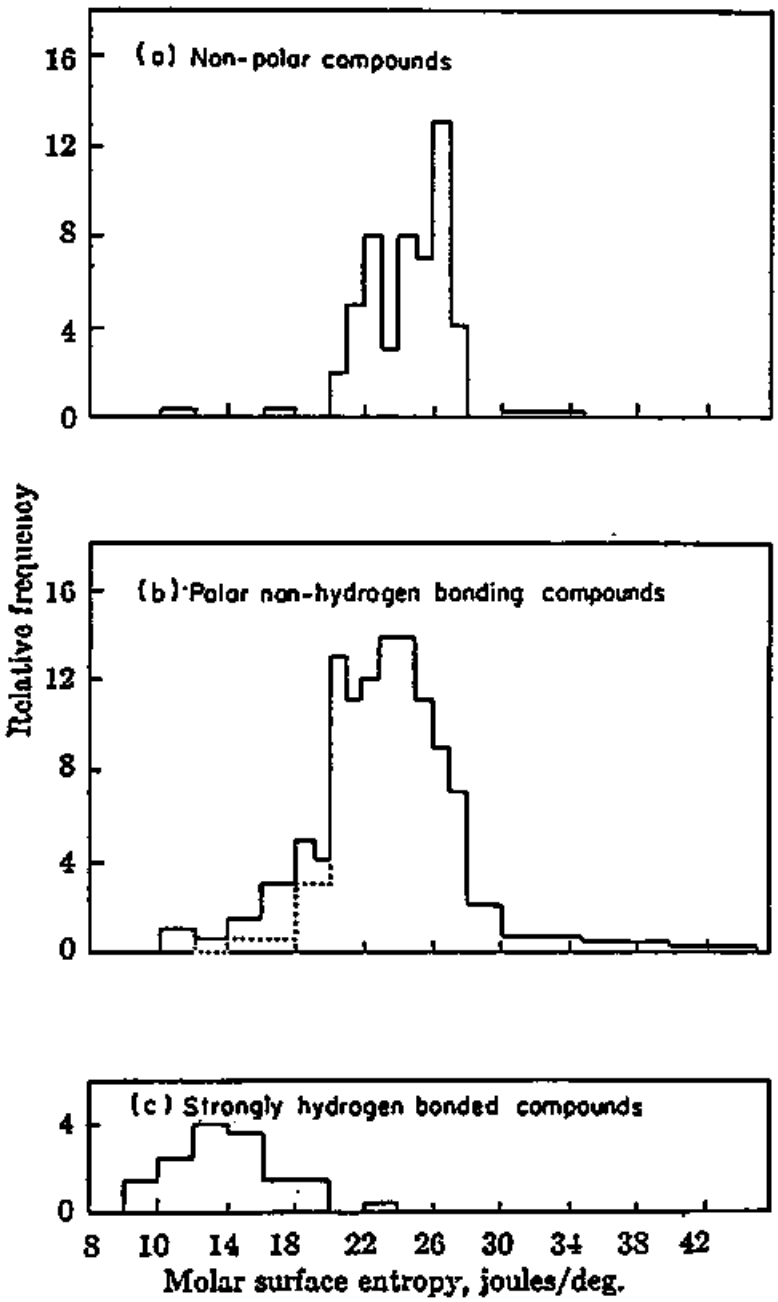

Fig. II-1. (R.J.Good, 1957)

(a) Weyl, Stillinger & Ben-Naim

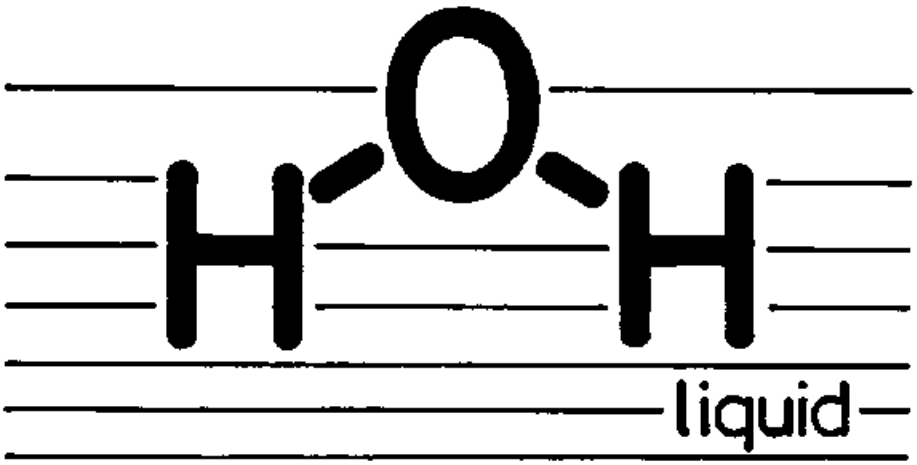

(b) Fletcher and Croxton

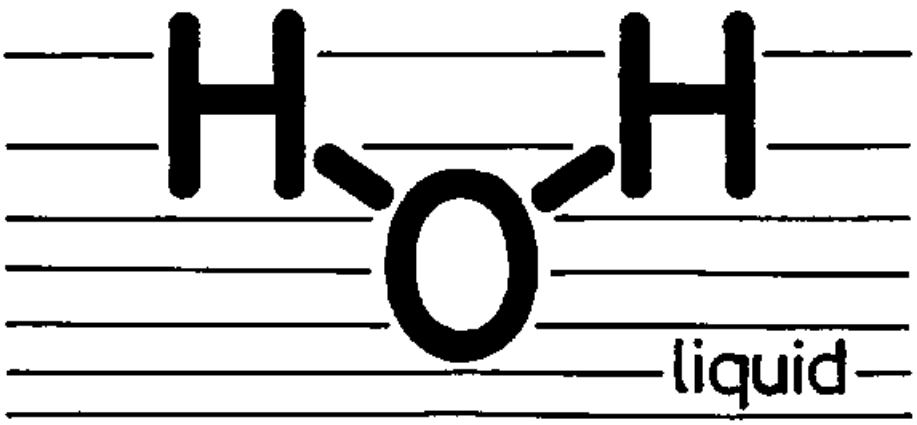

Fig. II-2.

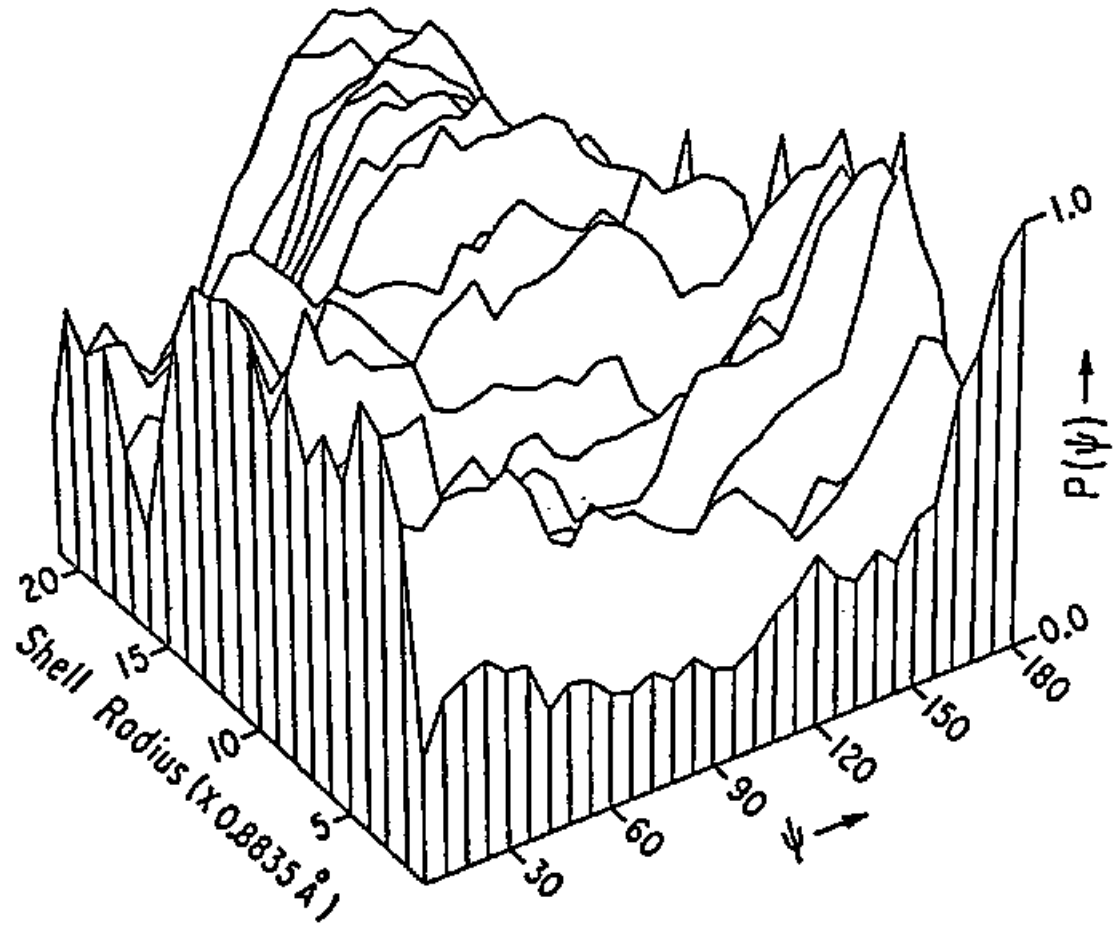

Fig. II-3. (R.M.Townsend, J.Gryko, and S.A.Rice, 1985)

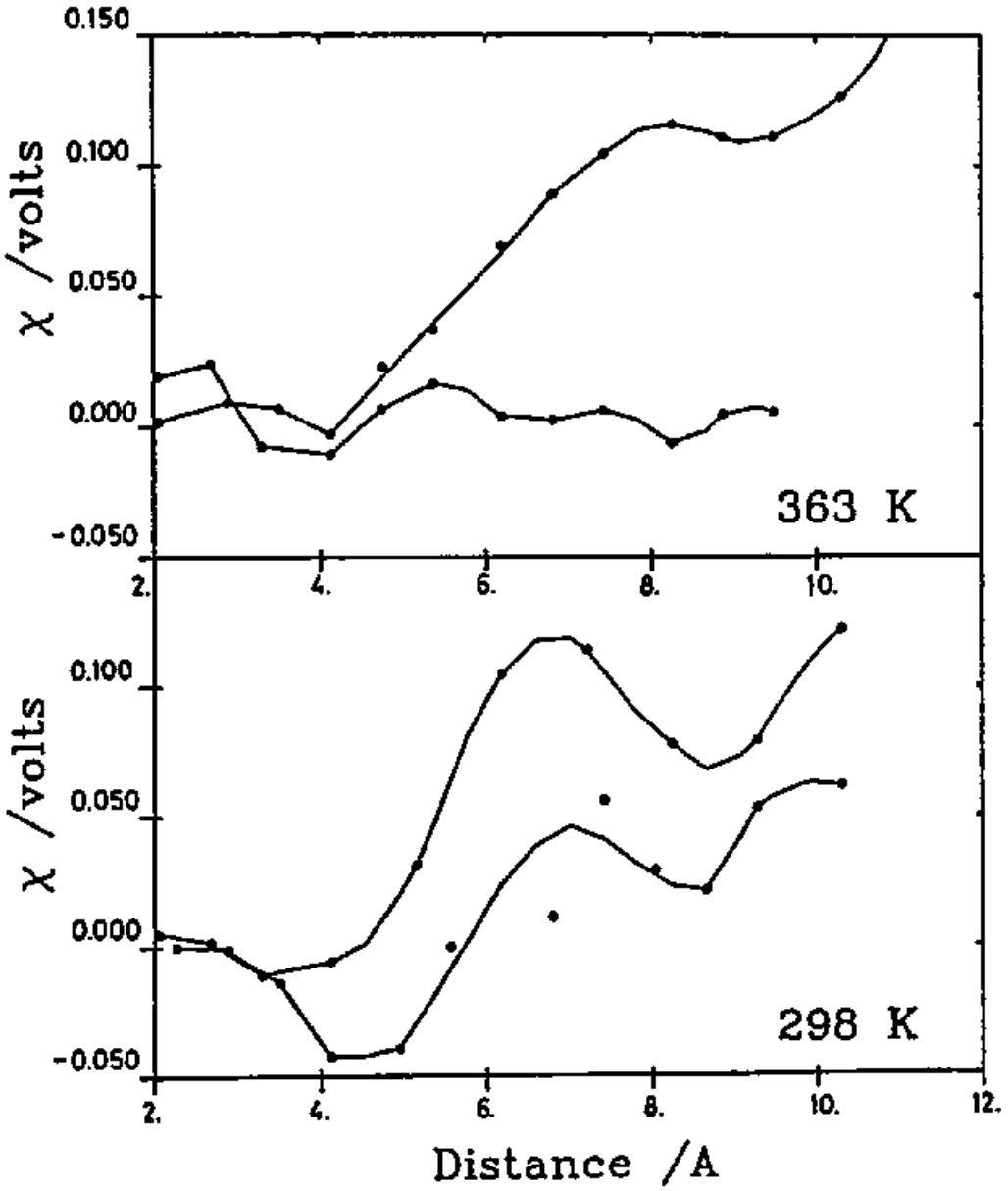

Fig. II-4.
(N.I.Christou, J.S.Whitehouse, D.Nicholson, and N.G.Parsonage, 1985)

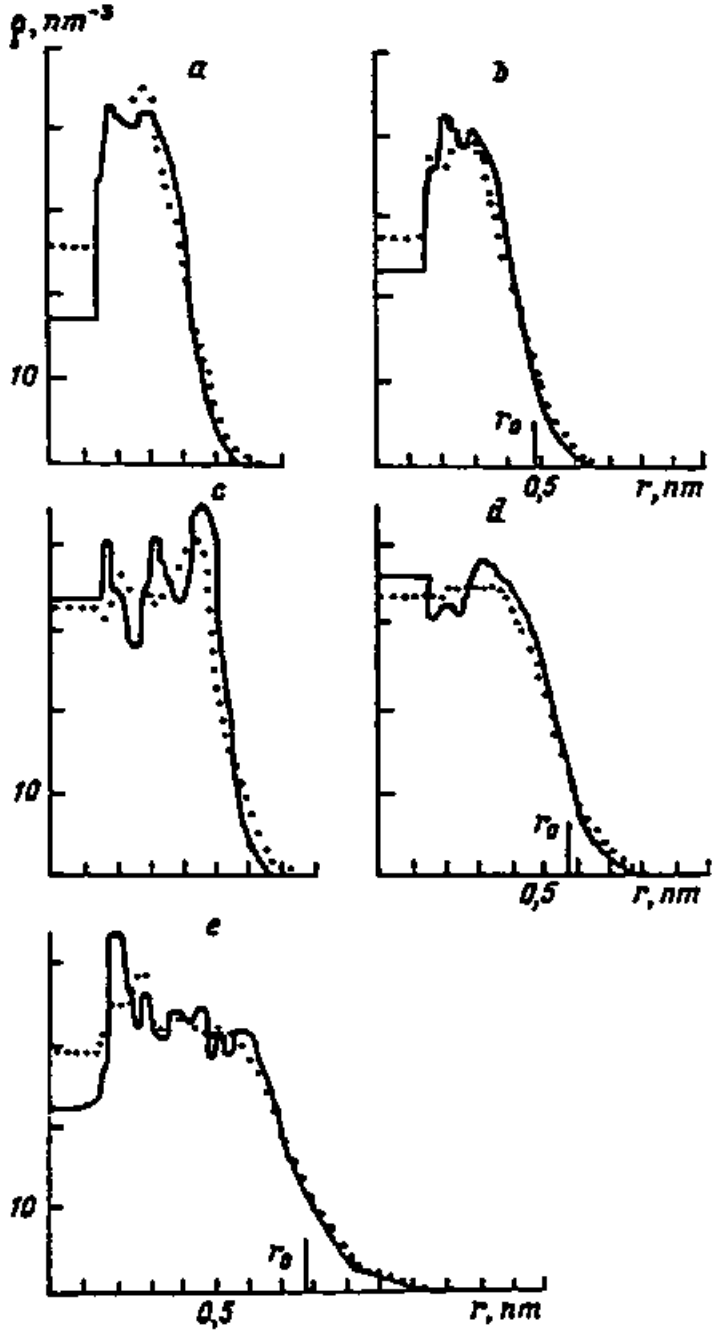

Fig. II-5. (E.N.Brodskaya and A.I.Rusanov, 1987)

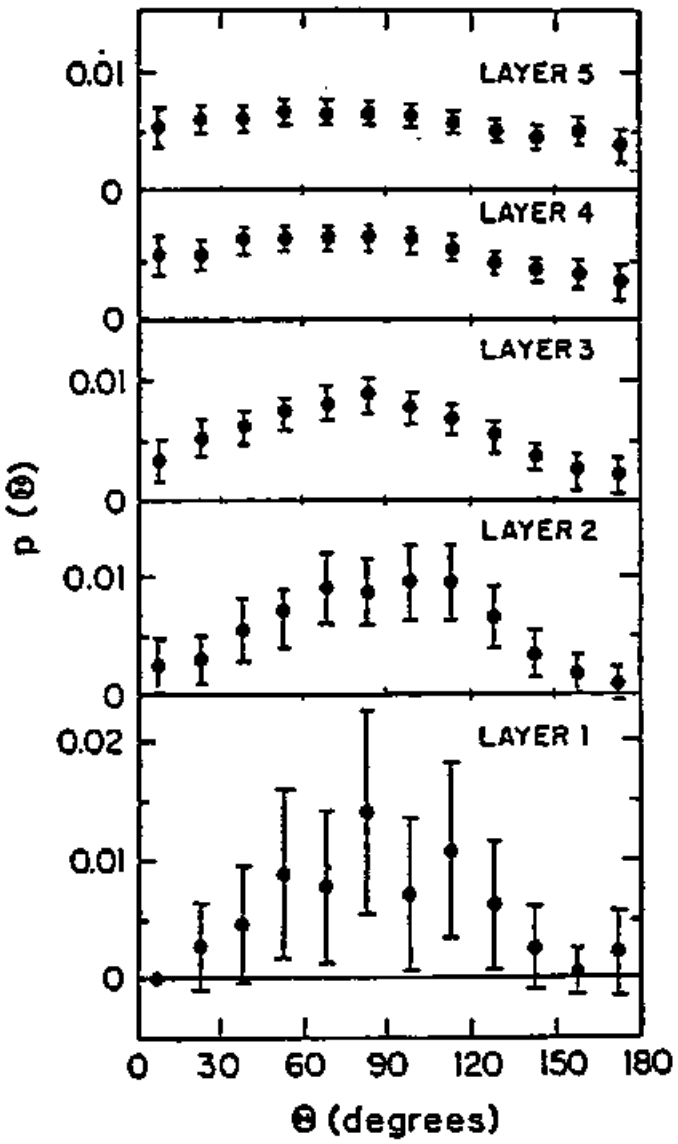

Fig. II-6. (M.A.Wilson, A.Pohorille, and L.R.Pratt, 1986)

III

καί κεν ἐν Ἄργει ἐοῦσα πρὸς ἄλλης ἱστὸν ὑφαίνοις,
καί κεν ὕδωρ φορέοις Μεσσηΐδος ἢ Ὑπερείης
πόλλ' ἀεκαζομένη, κρατερὴ δ' ἐπικείσετ' ἀνάγκη·

Ὅμηρος, ΙΛΙΑΔΟΣ

Before another woman's loom in Argos
it may be you will pass, or at Messeis
or Hypereia fountain, carrying water,
against your will iron constraint upon you.

Homer, THE ILIAD

Ⅲ. Thermodynamics and Statistical Mechanics of Interfacial Systems

The aim of this section is to give the thermodynamic and statistical mechanical formulas used in our work; extensive description of more general interfacial systems can be found in other orthodox textbooks.[2,4,9]

Assume that N particles are interacting each other in a cell of volume V at temperature T and that this system is not uniform but has a planar interface (liquid-vapor, for example) of area A (Fig.Ⅲ-1), i.e., the state point of the system is just on the coexistence line. The following conditions define the volume of each phase, V_l and V_v for liquid and vapor, respectively:

$$\begin{aligned} V &= V_l + V_v \\ N &= n_l V_l + n_v V_v, \end{aligned} \qquad (Ⅲ\text{-}1)$$

where n_l and n_v are the number density of bulk liquid and vapor, respectively. In other words, Eq.(Ⅲ-1) determines the position of the Gibbs (geometrical) surface.[9] Then it is generally impossible to represent other thermodynamic quantities of the whole system as a simple sum of those of bulk phases, but one needs to add the "surface term", which should be proportional to the surface area A. For example, the internal energy U, the Helmholtz free energy F, and the entropy S of the whole system are represented as follows:

$$U = u_l V_l + u_v V_v + u_s A,$$
$$F = f_l V_l + f_v V_v + f_s A, \qquad (\text{Ⅲ-2})$$
$$S = s_l V_l + s_v V_v + s_s A,$$

where u_l is the internal energy of bulk liquid per unit volume, u_v that of bulk vapor, and u_s the so-called "surface excess energy", etc. These quantities of lower case letter are dependent only on the temperature T, when considering that the system is in the coexistent state. These U, F, and S are related each other by the well-known thermodynamic equation:

$$F = U - TS. \qquad (\text{Ⅲ-3})$$

From this equation the following relation among surface excess quantities is easily derived:

$$f_s = u_s - Ts_s. \qquad (\text{Ⅲ-4})$$

Next let us consider virtual expansion of the area A with the volume and the temperature fixed. The force per unit length acted in this process, the so-called "surface tension" γ, is equal to the virtual work W (or the free energy change) needed for the expansion by unit area:

$$\gamma = dW/dA$$
$$= (\partial F/\partial A)_{T,V,N}$$

$$= f_S. \qquad (\text{Ⅲ-5})$$

Therefore the derivative of γ with respect to T gives s_S:

$$s_S = - d\gamma/dT. \qquad (\text{Ⅲ-6})$$

In experimental studies, γ is almost the sole measurable quantity, so one uses Eq.(Ⅲ-6) to obtain s_S and then Eq.(Ⅲ-4) to estimate u_S. In computer simulations, on the other hand, differentiation of γ with T, Eq.(Ⅲ-6), would need exhaustive computational resources because one must obtain precise values of γ at small interval of T for numerical differentiation. In simulation, however, both γ and u_S can be easily calculated; u_S is calculated according to the definition, Eq.(Ⅲ-2), and as to γ one utilizes statistical mechanical expressions (see next paragraph). We can, therefore, avoid the troublesome numerical differentiation. Although this way of using the elementary equation, Eq.(Ⅲ-4), to evaluate the interesting and important quantity s_S does not seem such a novel approach, its usefulness is not so widely recognized as far as we noticed. We will show in Sec.Ⅴ how well this approach works.

In order to calculate γ by computer simulation, the following virial expression[2,136] is convenient:

$$\gamma = \frac{1}{2}\int_{-\infty}^{\infty} dz_1 \int d\Omega_1 dr_2 d\Omega_2 \; \rho^{(2)}(r_1, \Omega_1, r_2, \Omega_2)$$

$$\times \left[\frac{1}{2}\left\{x_{12}\frac{\partial}{\partial x_{12}} + y_{12}\frac{\partial}{\partial y_{12}}\right\} - z_{12}\frac{\partial}{\partial z_{12}}\right] u(r_1, \Omega_1, r_2, \Omega_2)$$

$$= \int_{-\infty}^{\infty} dz_1 \left[-\frac{1}{2}\{P_{xx}(z) + P_{yy}(z)\} + P_{zz}(z)\right], \qquad (\text{III-6})$$

where $\rho^{(2)}(r_1, \Omega_1, r_2, \Omega_2)$ and $u(r_1, \Omega_1, r_2, \Omega_2)$ is the pair distribution and the pair potential, respectively; r_i and Ω_i is the position and the orientation of the i-th molecule. P_{jj} (j=x,y,z) represents the local pressure tensor The last line of Eq.(III-6) can be rewritten as a simpler form by defining the pressure normal and tangential to the surface, P_n and P_t, respectively:

$$\gamma = \int_{-\infty}^{\infty} dz \left[P_n(z) - P_t(z) \right],$$

$$P_n(z) = P_{zz}(z), \qquad (\text{III-7})$$

$$P_t(z) = \frac{1}{2}\left[P_{xx}(z) + P_{yy}(z) \right],$$

where we assume for simplicity that the interface is a plane normal to the z-axis.

As to the definition of the local pressure tensor we adopted Harashima's[137] here; i.e., the virial term $r(\partial u/\partial r)$ is counted just on the position of each molecules. Another way of calculating the local pressure, that is due to Irving and Kirkwood[138]; i.e., the virial term is counted at all places between the two molecules with some appropriate weight. It has

been pointed out by simulational study[139] that these two ways of definition give different local pressure tensor profile, but the calculations of γ and other surface excess quantities are not affected at all because of spatial integration with respect to z.

[Figure caption in Sec. Ⅲ]

Fig. Ⅲ-1. Schematic figure of an interfacial system.

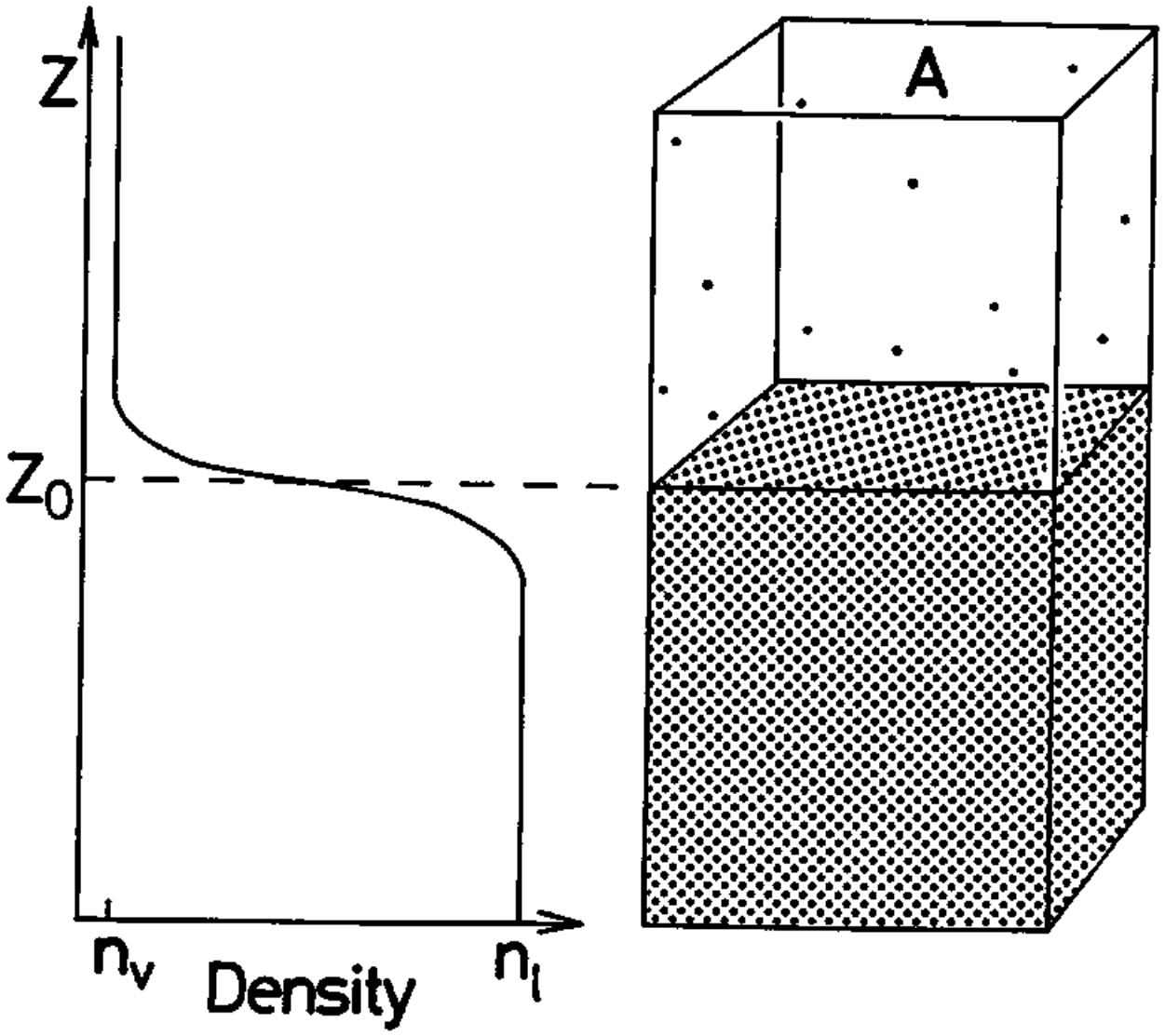

Fig. Ⅲ-1.

IV

Вода и землю точит и камень долбит.
РУССКАЯ ПОСЛОВИЦА

Water bores even the earth and caves a stone.
A RUSSIAN PROVERB

Ⅳ. Method of Computer Simulation

In this section I explain our simulation technique. The basic idea is quite simple; microcanonical (constant energy and constant volume) molecular dynamics simulation (MD) of liquid film, which should be thick enough to avoid the interference of both sides, is executed and various properties of its free surface (liquid-vapor interface) are investigated. For our first aim, study of molecular orientation, Monte Carlo simulation would also do, but MD simulation can give us dynamic properties such as various time correlation functions, as well as static properties, though analysis of dynamic properties is not reported here.

Up to now such simulational studies on interfacial systems of molecular fluid have been rarely reported although the importance of simulation is widely recognized.[1,2,7,8] The main difficulty is the computer ability as already described in Sec.Ⅱ. Since the interface is two dimensional system, whereas bulk fluid is three, a huge number of particles is needed to obtain reliable statistical average. For simulation of bulk fluid 200～500 particles are usually used, but at least 1000 particles are necessary for simulation of interfacial system because only 100～200 out of 1000 are the "interfacial particles" It is only a few years ago that Lennard-Jones (monatomic) interfacial system with much larger number of particles was simulated by MD method.[2,109,140] Since there exists more complex interaction in molecular systems, especially in strongly hydrogen-bonding fluids such as water and methanol, the simulation of such systems needs much more computer

resources and therefore what we had to pay most attention was how to simulate the system efficiently.

A. Simulation of water

Kataoka recently reported[141] the equation of state of fluid water calculated with non-empirical Carravetta-Clementi[142] (CC) pair potential by MD simulation technique. It is shown in his paper that this CC potential can semi-quantitatively reproduce various properties of real water, and the equation of state is given in analytical form for wide range of pressure and temperature, from which one can easily get the liquid-vapor coexistence line. We therefore used CC potential here to utilize the equation of state to check our results. For the detail of CC potential, see Appendix A.

The MD program in our study is based on one of CCP5 simulation program library. MDMPOL of Smith and Fincham for microcanonical MD simulation of polyatomic rigid molecular liquids,[143] but we have much improved it with tabulation and second order interpolation technique of some mathematical functions (EXP, SQRT, and ERFC) in order to speed up the program; see Appendix B. The way of time integration is Verlet's leap frog method,[144] which calculates momentum $p_i(t)$ and position $r_i(t)$ of the i-th molecule alternatively:

$$p_i(t+\Delta/2) = p_i(t-\Delta/2) + \Delta f_i(\{r(t)\}),$$
$$r_i(t+\Delta) = r_i(t) + \Delta p_i(t+\Delta/2)/m, \qquad \text{(IV-1)}$$

where Δ is the step size of time integration, m the mass of each molecule, and $f_i(\{r\})$ the force that the molecule feels. As to the rotational motion we adopt the quaternion representation,[145] which is superior to the Euler angle representation because the former has no singular point. For the long range Coulomb term the usual Ewald summation technique[146,147] is used; the electrostatic potential ϕ that the charge q_0 at position r_0 feels is expressed as follows:

$$\phi(r_0) = \frac{1}{\varepsilon\Delta}\sum_{G}\frac{e^{-G^2/4\eta}}{G^2}\left[\sum_{t} q_t e^{-iG\cdot(r_t-r_0)}\right] - \frac{q_0}{2\pi\varepsilon}\sqrt{\frac{\eta}{\pi}} + \frac{1}{4\pi\varepsilon}\sum_{t\neq 0}\frac{q_0}{|r_t-r_0|}\,\mathrm{erfc}\left(\sqrt{\eta}\,|r_t-r_0|\right), \qquad \text{(IV-2)}$$

$$\mathrm{erfc}(x) = \frac{2}{\sqrt{\pi}}\int_x^\infty e^{-t^2}dt$$

where ε is the dielectric constant, Δ the volume of unit cell, G the reciprocal lattice vector, and η the parameter for which one should empirically choose the optimal value for rapid convergence in G-summation. The error function erfc(x), one of intrinsic functions in FORTRAN language, is very time-consuming, so we apply the tabulation and interpolation technique (Appendix B) to it.

The simulation cell, as shown in Fig.IV-1, is a rectangular prism of dimensions $L_x=L_y=32.5$ Å and $L_z=120$ Å, in the middle of which we placed 1000

water molecules interacting with CC potential. We adopted a complete three dimensional periodic boundary condition (PBC) rather than the usual two dimensional periodicity of only X and Y directions, because the usual Ewald summation technique can be applied for the complete periodicity without any modification. The cutoff radius of short range potential (exponential and error function term) is 12Å, which is a little larger than the usual one (7.5Å～10Å); instead we did not add any long-tail correction because the evaluation of the correction was difficult for such inhomogeneous systems as this. Recently it is reported[148] that such truncation may affect the thermodynamic properties such as the surface tension, but there seems to be no good remedy. The liquid layer exists between about 40Å and 80Å, and the interference of liquid layers due to the periodicity along Z axis is found to be negligible. Although it is well known in classical thermodynamics that films of pure liquid is not stable but at most quasi-stable, we did not apply any external field potentials (e.g., gravitation-like) in our simulation to stabilize the layer, but the layer was found to be stable enough and did not break into small clusters in the temperature range we calculated (250 K ～ 400 K, see Table Ⅳ-1), the reason of which we guess is the periodicity of X and Y directions; we also examined the sample of T=450 K, but molecules made several clusters after 10,000 step run. Notice here that the critical temperature T_c of CC water[141] is near 603 K but the triple point temperature T_t is not known so far; we guess that it exists between 250 K and 275 K, though. The total energy conservation is quite well, within ±0.01%. The CPU time is 0.5～0.8 s/step (varying with the density of liquid phase) on FACOM VP-200 vector processor at Kyoto University Data Processing Center.

The initial configuration is the lattice of cubic ice I_c. After equilibrating process of about 10,000 steps (5 ps) at 400 K, we started sampling and averaging for about 7 ps. To get lower temperature samples, we cooled gradually the system of higher temperature and annealed it for about 5000-7000 steps. Sampling was repeated several times, and the error estimation was done by comparing these results; other detailed simulational conditions are listed in Table Ⅳ-1.

B. Simulation of methanol

The MD program for the simulation of methanol is almost the same that we use to simulate the water system described above. The intermolecular potential for methanol is Jorgensen's empirical TIPS model,[149] which treats a methanol molecule as a rigid one with three interaction sites (hydrogen atom, oxygen atom, and methyl group); for the detail, see Appendix A. Although the thermodynamic properties (critical temperature T_c, triple point temperature T_t, etc.) of TIPS methanol are not well known yet, we simulate this system in the temperature range of 160 K~350 K. The experimental values[13] of T_c and the melting temperature under the atmospheric pressure T_m is 512.58 K and 175.7 K, respectively.

The simulation cell is also a rectangular prism of a slightly larger size, $L_x=L_y=39$ Å and $L_z=120$ Å, in the middle of which we also placed 1000 methanol molecules. The liquid layer exists between about 35 Å and 85 Å. The cut-off length for short range interaction is 15 Å. Without any external field this layer is stable enough in the temperature range that we examined;

at T=400 K, however, the liquid layer broke up and the molecules made some clusters after the simulational run of several picoseconds. The step size of time integration is chosen to be $0.70 \sim 0.85 \times 10^{-15}$ s so that the total energy conservation is within $\pm 0.01\%$. As to other simulational conditions in detail, see Table Ⅳ-2. Because of the simplicity of TIPS potential (3-site model and no exponential functions) the CPU time is only about 0.3 s/step on FACOM VP-400E, which is much shorter than that in the case of CC water because CC water is 4-site model and its dispersion force is represented with time-consuming exponential functions.

The initial configuration is FCC lattice with random molecular orientation. After equilibrating process for about 20 ps at 350 K, the system seemed to reach thermodynamic equilibrium and then we started sampling and averaging. To get samples of lower temperatures, we cooled gradually the system of higher temperature and annealed it for a few picoseconds. Sampling was repeated several times (the duration of each sampling is 24.5 ps~ 27.2 ps), and the error estimation was done by comparing these results.

C. Simulation of Lennard-Jones system

In order to investigate the difference of the nature of the interface of strongly hydrogen-bonding fluids (water and methanol) from that of simple fluids, we also execute MD simulation of the liquid-vapor interface of LJ system. The interaction potential u(r) is the usual 12-6 form, i.e.,

$$u(r) = 4\varepsilon \left[(\sigma/r)^{12} - (\sigma/r)^{6} \right], \qquad (Ⅳ\text{-}1)$$

where the particle diameter, σ = 3.405 Å, and the potential depth, ε/k_B = 119.8 K (k_B is the Boltzmann constant), are those for Ar,[150] since Ar system has been most widely studied by simulations.[2,7,8,10] The simulation cell is similar to that described previously, but the size is $L_x=L_y=32$ Å and $L_z=90$ Å. The number of particles is also 1000, and the complete PBC is also adopted. The cutoff radius is 15 Å. We simulated this system at three temperatures, T=120 K, 100 K, and 80 K; the triple point temperature T_t is known to be about 79 K by simulation.[150] Other simulational conditions are given in Table Ⅳ-3. The CPU time is about 0.1 s/step on FACOM VP-200. Starting from FCC lattice placed at the center of the unit cell (between z~20 Å and 70 Å) and after equilibrating the system at T=120 K for about 10,000 steps (50 ps), we sampled and averaged data for time duration of 450 ps (T=120 K) ~ 1200 ps (T=80 K). For lower temperatures, the gradual cooling and annealing was repeated several times.

Table Ⅳ-1. Simulation conditions and some results for water system; averaged temperature <T> is evaluated from averaged kinetic energy <KE> as <T>=<KE>/3k_B, where k_B is the Boltzmann constant. Bulk liquid density ρ_l is obtained from least-square parameter fitting to hyperbolic tangent function, Eq.(V-5). P is the pressure of bulk phases.

Setting temperature(K)	Step size (10^{-15}sec)	Number of step	<T> (K)	ρ_l (g cm^{-3})	P (MPa)
400	0.5	15000×3	405.2 ±1.0	0.7564±0.0006	-2.38 ±0.91
350	0.5	16000×3	351.5 ±0.5	0.8196±0.0005	-3.98 ±0.77
300	0.5	14000×3	299.7 ±1.0	0.8599±0.0004	-6.20 ±0.29
275	0.6	13000×4	276.7 ±1.7	0.8678±0.0005	-8.07 ±1.20
250	0.7	13000×6	248.8 ±1.9	0.8736±0.0006	-7.33 ±2.89

Table Ⅳ-2. The same as Table Ⅳ-1 for methanol system.

Setting temperature(K)	Step size (10^{-15}sec)	Number of step	<T> (K)	ρ_l (g cm^{-3})	P (MPa)
350	0.70	35,000×4	340.9±2.2	0.6198±0.0002	-1.24±0.98
300	0.75	35,000×4	297.7±1.7	0.6879±0.0002	-2.73±0.88
250	0.85	32,000×4	255.3±2.0	0.7437±0.0003	-3.10±1.21
200	0.85	32,000×5	205.1±1.1	0.7981±0.0002	-4.01±1.36
160	0.85	32,000×6	161.5±0.5	0.8409±0.0004	-7.23±1.81

Table Ⅳ-3. The same as Table Ⅳ-1 for Lennard-Jones system.

Setting temperature(K)	Step size (10^{-15}sec)	Number of step	<T> (K)	ρ_l (g cm^{-3})	P (MPa)
120	5.0	30000×3	118.90±0.42	1.1506±0.0016	1.180±0.085
100	6.0	30000×6	100.55±1.03	1.2904±0.0014	0.335±0.045
80	8.0	30000×5	79.96±0.17	1.4174±0.0021	0.022±0.020

[Figure caption in Sec. Ⅳ]

Fig.Ⅳ-1. Simulation cell.

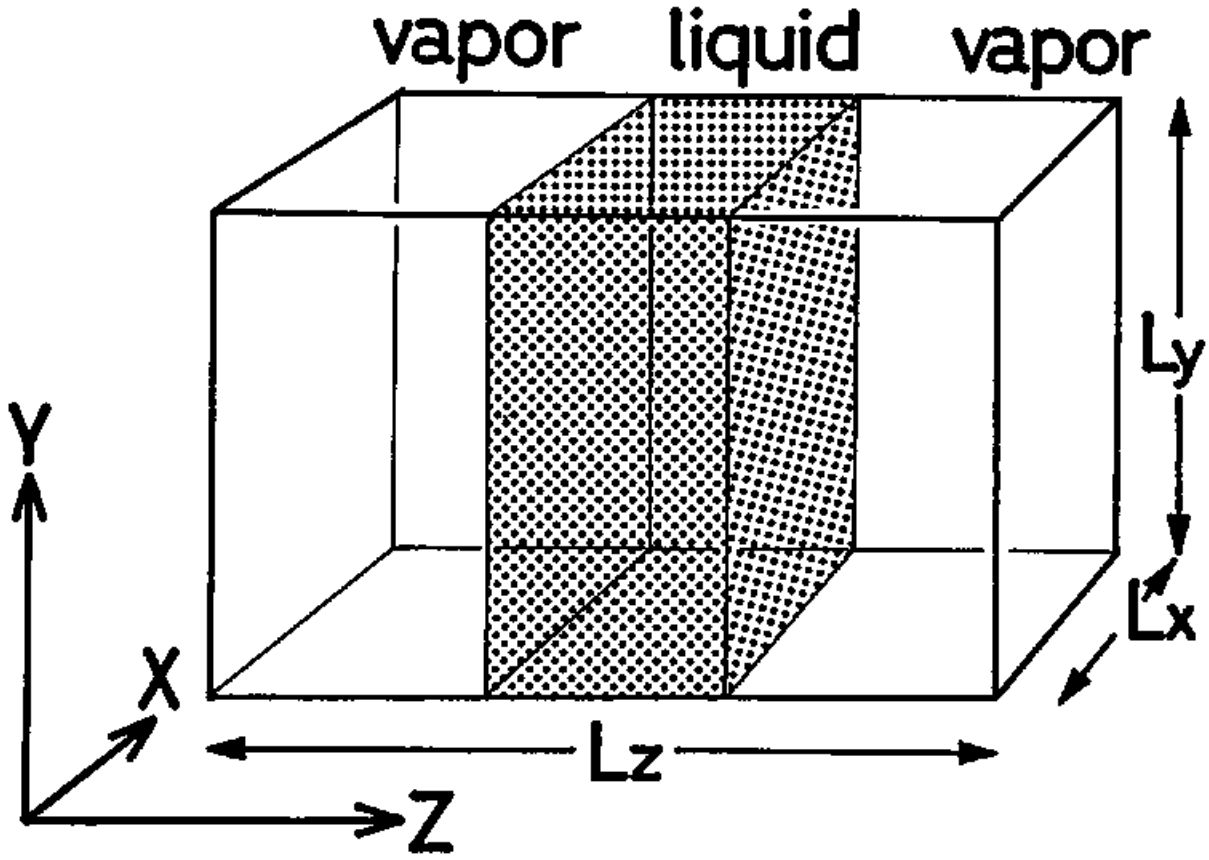

Fig. Ⅳ-1.

V

覆杯水於坳堂之上、則芥爲之舟。
置杯焉則膠、水淺而舟大也。

莊子

When a glass of water is spilled over a hollow, dust floats there to become a boat.
When a glass is put there, however, it touches the bottom of water, because the water is too shallow to float it.

Chuang-tzu

V. Results

The results directly obtained from our computer simulations are described in this section.

Before giving the detail, I would like to mention here that the simulation of interfacial systems is not so difficult on high-speed vector processors of today as it may seem. The convergence of various statistical average is rapid enough unless the condition is so severe (e.g., the temperature is close to T_t or T_c). The averaged temperature T (kinetic energy), the pressure P, and the bulk liquid density ρ_l of the system are tabulated in Table Ⅳ-1, Ⅳ-2, and Ⅳ-3, for water, methanol, and Lennard-Jones system, respectively; ρ_l is obtained by parameter-fitting, see below. Since we use the microcanonical MD method, the averaged temperature is a little different from the aimed one. The slightly negative pressure is probably due to the periodic boundary condition. The state points are well on the coexistence line, which is in Ref.141 for CC water and in Ref.151 for LJ system.

A. Profiles and parameter fitting

To begin with, we show the one-body distribution function $\rho(z)$, the so-called "density profile", and the local potential energy function u(z), the "energy profile". We divided the simulation cell into layers of thickness 2Å for water and methanol, 1Å for LJ, and statistically averaged

the density (number of molecules whose center of mass exists in that layer) or the potential energy of the layers; it would be better to adopt thinner layers, say 0.2Å, to obtain more detailed data, but much more computation would be required to get meaningful statistical average. Strictly speaking, the definition of u(z) is not unique; the problem is where we count the pair potential energy $u(r_1,r_2)$ between particle 1 and particle 2, that is similar to the problem of virial calculation.[137,138] In this work we arbitrarily divided $u(r_1,r_2)$ in half and counted them on r_1 and r_2, like Harashima's treatment of virial; however, this does not at all affect the calculation of the surface excess quantities in the following subsection because such quantities are obtained after integration of u(z) with respect to z.

The data are parameter-fitted to some analytical functions. For density profile, three functional forms have been proposed[1]; the hyperbolic tangent (tanh, or the Fermi) type[104] derived from the van der Waals mean field theory.

$$\rho(z) = \tfrac{1}{2}(\rho_l+\rho_v) + \tfrac{1}{2}(\rho_l-\rho_v)\tanh(z/2\delta), \qquad (V\text{-}1)$$

the Fisk-Widom type[105] based upon another mean field theory,

$$\rho(z) = \tfrac{1}{2}(\rho_l+\rho_v) + \tfrac{1}{2}(\rho_l-\rho_v)\frac{\sqrt{2}\tanh(z/2\delta)}{\sqrt{3-\tanh^2(z/2\delta)}}, \qquad (V\text{-}2)$$

and the error-function type[107] from the capillary wave theory,

$$\rho(z) = \tfrac{1}{2}(\rho_l+\rho_v) + \tfrac{1}{2}(\rho_l-\rho_v)\mathrm{erfc}(z/2\xi), \qquad (V\text{-}3)$$

where ρ_l and ρ_v are the density of bulk liquid and vapor, respectively, and δ and ξ are the parameters of surface thickness. The usual 10-90 thickness t, which is the distance between the position of $\rho(z)=\rho_v+0.1(\rho_l-\rho_v)$ and $\rho(z)=\rho_v+0.9(\rho_l-\rho_v)$, is related $t=4.394\delta$ for tanh profile, $t=5.064\delta$ for Fisk-Widom profile, and $t=2.563\xi$ for error-function profile. It is already well known that the difference among these three becomes larger near the critical point, but within the temperature range we studied here these functions give almost the same results. In Fig. V-1 we show some examples of the parameter-fitting result for water surface; except the vapor-side region the three profiles are nearly the same. Hereafter we adopt the tanh profile, which is the most tractable for analysis of data. For energy profile, though it does not seem as yet that there exist any definite functions, we also adopt the tanh profile:

$$u(z) = \frac{1}{2}(u_l+u_v) + \frac{1}{2}(u_l-u_v)\tanh(z/2\delta), \qquad (V-4)$$

where u_l and u_v are the potential energy density of bulk liquid and vapor, respectively.

We used the program SALS for nonlinear least-square fitting developed by Oyanagi et al.,[152] in which we adopted modified Marquardt method (Fletcher's algorithm). The parameters to be determined are ρ_l, ρ_v, z_{d0} (position of the center of the transition layer), and $t_d=4.394\delta$ (10-90 surface thickness) in

$$\rho(z) = \frac{1}{2}(\rho_l+\rho_v) + \frac{1}{2}(\rho_l-\rho_v)\tanh[(z-z_{d0})/2\delta], \qquad (V-5)$$

and u_l, u_v, z_{u0}, and $t_u=4.394\delta$ in

$$u(z) = \frac{1}{2}(u_l+u_v) + \frac{1}{2}(u_l-u_v)\tanh[(z-z_{u0})/2\delta]. \qquad (V-6)$$

The fitting results are listed in Tables V-1, V-2, and V-3. Generally speaking, the thickness t and the position z_0 of density profile differ from those of energy profile. Concerning z_0, that of energy surface always exists inner, or in liquid side for all three systems. This fact is easily understood if we remind that the local potential energy is in proportion not to the local density itself but, quite roughly speaking, to the square of it.

We first investigate the surface thickness t for three systems (Figs. V-2, V-3, and V-4); as to the ellipsometric surface thickness t_d^{el} we will define and discuss it later in Sec. VI. For LJ surface t_d is much smaller than t_u in low temperature region (near the triple point T_t), but for water t_d and t_u are almost the same even at the lowest temperature. Methanol shows an intermediate feature; t_d is a little smaller than t_u. The precise reason of this phenomenon is not understood, but it suggests that the liquid-vapor interface of water is energetically very sharp in comparison with the simple fluid. Since the properties of bulk liquid of methanol is less abnormal than water, it is not so difficult to understand the feature of methanol surface. It is probable that some ordering of molecules due to hydrogen bonding causes the stabilization of potential energy.

Next we look at the profiles themselves. The density profile and the energy profile are shown in Figs. V-5, V-6, and V-7; the units are reduced as position $z^*=z/\sigma$, density $\rho^*=\rho N_A \sigma^3/M$, and energy $u^*=u\sigma^3/k_B\varepsilon$, where N_A is the Avogadro number, 6.0225×10^{23}. and k_B is the Boltzmann constant, 1.3805×10^{-23} J/K. σ and ε are the Lennard-Jones parameters and M is the molecular weight for each molecule[14]:

System	σ :molecular diameter	ε :potential depth	M
Water	2.641 Å	809.1 K	18.02 amu
Methanol	3.626 Å	481.8 K	32.04 amu
LJ	3.405 Å	119.8 K	39.95 amu

It is obvious that the middle of the system (right side of the figures) is completely bulk liquid from the view point of density and potential energy. The the simulated film, therefore, is thick enough so the two surfaces in the simulation cell do not appear to interfere with each other; remember that the cut-off radius is 12Å (or 4.54σ) for water, 15Å (4.14σ) for methanol, and 15Å (4.41σ)for LJ, respectively, while the thickness of the film is 33~37Å for water, 41~56Å for methanol, and 46~55Å for LJ.

The simulation data are well-fitted to tanh functions (Eqs. V-6 and V-7) for methanol and LJ, but great misfit is observed for the density profile of water; in particular, near the liquid side of the surface, the density seems to be higher than that of the bulk liquid, which suggests the existence of some structural change.

As to the reduced thickness t_d/σ, that of water is a little less than that of LJ (Tables V-1 and V-3). It is often said from ellipsometric experiments[1] that the thickness of water surface ($t_d/\sigma \sim 1$) is much smaller than that of other liquids ($t_d/\sigma \sim 2$), which is counted as one of anomalous properties of water and is also attributed to hydrogen bonding, but we cannot find such remarkable tendency from our simulational results. One probable explanation of this discrepancy is the misfit of the density profile with the tanh function. This point will be discussed in more detail in Sec. VI.

Recently Braslau et al.[153] executed the x-ray small angle reflectivity measurement of water and reported the "surface roughness" $\langle u^2 \rangle = 3.24 \pm 0.05$ Å at T=25 ℃. Since $\langle u^2 \rangle$ can be interpreted as the mean-square amplitude of capillary waves,[3,107,154] the 10-90 thickness t_d is related to it as $t_d = 2.563 \langle u^2 \rangle$. Their result therefore gives $t_d = 8.304 \pm 0.128$ Å, which is much larger than our result, $t_d = 5.148$ Å at T=300 K. One probable reason of this disagreement is the suppression of capillary waves in our system due to the finite size of the simulation cell. As to methanol, we cannot find so far any direct experimental estimations of surface thickness, except ellipsometric technique, which is discussed later, but the agreement between our simulation and the ellipsometry seems to be good.

B. Surface excess quantities

Once the position of Gibbs surface, z_{d0}, is determined, we can evaluate various surface excess thermodynamic quantities through the relations already

described in Sec. Ⅲ Since we assume the tanh-type profiles, we can calculate the excess energy u_S analytically from Eq.(2) as follows:

$$u_S = \int_{-\infty}^{\infty} u(z)\,dz - \left[\int_{-\infty}^{z_{d0}} u_V\,dz + \int_{z_{d0}}^{\infty} u_l\,dz\right]$$

$$= \frac{u_l - u_V}{2}\left[\int_{-\infty}^{z_{d0}}\left\{1 + \tanh\frac{z - z_{u0}}{2\delta_u}\right\}dz + \int_{z_{d0}}^{\infty}\left\{-1 + \tanh\frac{z - z_{u0}}{2\delta_u}\right\}dz\right]$$

$$= (u_l - u_V)\cdot(z_{d0} - z_{u0}). \qquad (V\text{-}7)$$

This formulation suggests that the accuracy of the calculation depends mostly on the precision of $z_{d0}-z_{u0}$, which becomes worse at low temperatures. The excess entropy s_S is evaluated through the following thermodynamic relation [see Eq.(Ⅲ-4)]:

$$\gamma = u_S - Ts_S, \qquad (V\text{-}8)$$

where T is the absolute temperature of the system. The results are listed in Tables V-4, V-5, and V-6. The last column of each table is the molar surface entropy, which is the excess entropy of the one mole molecules existing near the surface, defined by Good[114] as follows:

$$s^A = 1.10\times(M/\rho_l)^{2/3}N_A^{1/3}s_S, \qquad (V\text{-}9)$$

where 1.10 is a (rather arbitrary) factor reflecting the way of packing of molecules. Error estimation is done by comparison of several simulational runs, see Tables Ⅳ-1 ～ Ⅳ-3 as to the length of each run.

For the surface tension of water, an analytical functional form fitted to experimental data is given by Vargaftik et al.[155] for temperature range of 273.15 K≦ T ≦ T_c:

$$\gamma = B[1-T/T_c]^{\mu}[1+b(1-T/T_c)], \qquad (V-10)$$

T_c= 647.15 K (the critical temperature),

B = 235.8 erg/cm^2,

b = -0.625,

μ = 1.256,

from which one can calculate s_S and u_S as

$$s_S = -d\gamma/dT$$

$$= B[1-T/T_c]^{\mu}[\mu/(T_c-T) + b(1+\mu)/T_c], \qquad (V-11)$$

and

$$u_S = \gamma + s_S T$$

$$= B[1-T/T_c]^{\mu}[1 + b + \mu T\{1/(T_c-T)+b/T_c\}]. \qquad (V-12)$$

This empirical formula (solid lines) is compared with our simulated one in Fig. V-8. The dotted line in the top of the figure shows the temperature derivative calculated from Eq.(Ⅲ-8). As to the empirical formula of γ of methanol, we use the following equation linear to the temperature[156] for 10 ℃≦ T ≦ 60 ℃:

$$\gamma = a - bT, \tag{V-13}$$

T in Celsius degree,

a = 24.0 erg/cm^2.

b = 0.0773 erg/cm^{2}K.

In the lower temperature region, the deviation from the linearity is evident,[157] but at present no reliable empirical function applicable for wide temperature range are available for us. Because of the linearity, u_S and s_S is independent of temperature:

$$s_S = b, \tag{V-14}$$

and

$$u_S = a + 273.15b. \tag{V-15}$$

The results are shown in Fig. V-9.

From these figures and tables we can point out the following facts as general features; (1) For LJ system, the calculated γ is in good accordance with simulational results of other groups,[2] though there is a slight discrepancy for u_s especially near T_t. The equation (Ⅲ-4), therefore, is proved to be very useful to estimate the surface excess entropy. (2) For water and methanol the simulated γ and u_s are both smaller than experimental ones, which can be attributed to some defect of the molecular interaction potential models. Whereas both energy density and free energy density are considered to be strongly dependent on the number density of molecules, the density of bulk liquid in equilibrium with its vapor as a result of simulation is a little smaller than real one for both CC water and TIPS methanol; for example, see the table below.

System	ρ_l (g/cm^3) Simulation	Experiment
water at 300K	0.88	1.00
methanol at 300K	0.69	0.79

(3) In spite of the above discrepancies between simulations and experiments, the surface entropy s_s agrees quite well with experimental values for any systems, which suggests that s_s, the quantity reflecting the structure of the interface, is less dependent on potential model than γ and u_s and encourages us to investigate the interfacial properties with simulational approach.

As is already described in Sec.Ⅱ, one of anomalous characters of

surface of strongly hydrogen-bonding liquids is the smallness of the molar surface entropy, s^A. This feature is evident in the tables; the value is 0.7~1.3 R for water, about 0.9 R for methanol, but 2.3~2.5 R for LJ system, where R is the gas constant, 8.314 J/K mol.

Another characteristic property of water surface is the fact that the excess entropy s_s lowers as the temperature decreases to T_t. This is clearly shown in Fig. V-8. On the other hand, s_s hardly changes near T_t for LJ system (see Table V-6). The tendency of entropy decrease with fall of temperature is also weak for methanol except the lowest temperature. Here again is shown another evidence of some structural ordering of surface of water near T_t. The similar suggestion is offered when we look upon the temperature-dependence of u_s; that of water rapidly decreases with temperature decreasing, which means that some energetical stabilization takes place, but LJ system does not show such tendency. A rather simple cluster model of water may give the reason of these phenomena, as proposed by Luck.[157]

C. Orientational structure

In order to investigate one of the most interesting features, molecular orientational ordering near the surface, we define angle variables to represent the orientation of each molecule and take statistical averages of them from the simulation data. Since the molecular symmetry of water and methanol is different, we describe the procedure separately.

(I) Water

A water molecule has C_{2v} symmetry. We use, therefore, the following two angle variables (Fig. V-10); the angle between the dipole of the molecule (C_2 axis, from oxygen atom to M site) and the space fixed Z-axis (from liquid-side to vapor-side), θ, and the rotational angle around the C_2-axis, ϕ; ϕ is defined to be 90° when the line connecting two hydrogen atoms is parallel to the X-Y plane, or the surface. Owing to the symmetry of the molecule and the system, the range of the variables is $0° \leqq \theta \leqq 180°$ and $0° \leqq \phi \leqq 90°$, respectively.

First, we show in Fig. V-11 the statistical average of these variables, $<\theta>$ and $<\phi>$, as functions of the position z. At higher temperatures (T=400K or 350K) one cannot see any deviations from random orientation; notice that the complete randomness gives $<\theta>=90°$ and $<\phi>=45°$ by definition. At lower temperatures ($T \leqq 300$ K) there is a small deviation, i.e., $<\theta><90°$ and $<\phi>>45°$, which means the preference for the orientation of the molecule with its one H atom projecting towards the vapor.

To look upon the tendency in more detail, we show some contour maps of (θ, ϕ) distribution, $P(\theta, \phi)$, in Figs. V-12 for T=300 K and V-13 for T=400 K; the distribution is divided by $\sin\theta$ in order to be normalized to unity when the orientation is completely random. Five different shades are used according to its value, see the figure caption; the darkest one, which represents the region of $P(\theta, \phi) \geqq 1.3$, shows the most preferable molecular orientation. It is obvious that there are two typical orientations which a water molecule takes near the surface, though the peaks are quite broad. In the vapor-side of the surface the peak of the distribution exists around $\theta \sim$

50° and $\phi \sim 0°$, which means that the water molecule is projecting its one H atom to the vapor phase as was observed in the results of $<\theta>$ and $<\phi>$. In the liquid-side of the surface, on the other hand, the peak being around $\theta \sim 110°$ and $\phi \sim 90°$ suggests that the molecule prefers to lie down on the surface with its both two H atoms slightly projected into the liquid phase. The latter tendency of orientation continues rather deeper into the liquid phase, say about 10Å. The two typical orientations are schematically shown in Fig. V-14. The Croxton's estimation[122] is qualitatively in accordance with this vapor-side orientation, and the Stillinger and Ben-Naim's one[120] corresponds to the liquid-side orientation. Since the local density of the liquid side is much higher than that of the vapor side, the "lying-down" orientation plays a more important role in considering various interfacial phenomena, such as the surface potential and the ellipticity coefficient, as seen later in Sec. VI.

As the temperature increases, these orientational tendencies are rapidly weakened, as is easily understood. At lower temperatures (T=275 K and 250 K, distributions are not shown here), however, the orientational ordering is not developed so much, contrary to our expectation. The reason may be partly because the transition layer becomes so thin that the almost opposite tendencies of orientation are not observed separately; notice that we statistically averaged the orientational distribution every 2Å, and the surface thickness $t_d \sim 3.5$Å at these lowest temperatures.

(2) Methanol

Since the symmetry of a methanol molecule, C_s, is lower than that of a

water molecule, the definition of orientational angles is a little more complicated (Fig. V-15). We first consider the principal axes of inertia tensor of a methanol molecule; $\vec{X}$, $\vec{Y}$, $\vec{Z}$ in order of their principal values. This $\vec{Y}$ corresponds to the C_2 symmetry axis of a water molecule. Then the first variable θ is defined as the angle between this $\vec{Y}$ and the surface normal vector $\vec{Z}$ (from liquid to vapor); the range of θ is $0^\circ \leqq \theta \leqq 180^\circ$. The second variable ϕ is the angle between $\vec{X}$ and $\vec{Y}\times\vec{Z}$ ($\times$ represents the vector product, so $\vec{Y}\times\vec{Z}$ is the normal vector of $y-Z$ plane); this means that ϕ is the rotational angle around $\vec{Y}$ The range of ϕ is also $0^\circ \leqq \phi \leqq 180^\circ$.

Fig. V-16 is the averaged values of these variables as functions of position z, from which one can observe that some ordering exists even at high temperatures. Figs. V-17 and V-18 are examples of contour map of (θ, ϕ) distribution. One can read from these figures that a single broad but very high peak of $P(\theta, \phi)$ exists around $\theta \sim 110^\circ$ and $\phi \sim 0^\circ$. This suggests that a methanol molecule near the surface prefers to project its methyl group to vapor phase, as schematically shown in Fig. V-19.

The following two points seem to be very important when one compares the feature of methanol surface with that of water surface; (1) the tendency of orientational ordering of methanol molecules is much stronger than that of water [notice that the darkest shade in Figs. V-17 and V-18 corresponds to the region of $P(\theta, \phi) \geqq 1.6$, whereas the one in Figs. V-12 and V-13 corresponds to $P(\theta, \phi) \geqq 1.3$], and (2) this ordering of methanol exists up to the highest temperature, T=350 K, as well as in low temperature range, whereas the ordering of water almost disappears in $T \geqq 350$ K. The reason of

these phenomena is now obvious when one looks at the preferable orientation in Fig. V-19; the methyl group, as a hydrophobic part which is unable to take part in hydrogen bonding, is put out toward vapor phase so that liquid phase is energetically stabilized. Water, however, does not have any hydrophobic parts, therefore such apparent orientational tendency is not observed. In this sense methanol can be regarded as one of the simplest models for surfactants.

Table V-1. Parameter-fitting results of density-profile and energy-profile of water surface; hyperbolic tangent functions are assumed, see Eqs.(V-5) and (V-6). ρ_l (ρ_v) and u_l (u_v) are the density and the potential energy of bulk liquid (vapor) phases, respectively, t is the 10-90 thickness, and z_0 is the position of the center of surface; there are two surfaces (left and right) in our simulation cell, see Fig.IV-1. The molecular diameter σ is 2.641 Å (Ref.14).

Density profile	T (K)	ρ_l (g cm^{-3})	ρ_v (g cm^{-3})	t_d (Å)	t_d (σ)	z_{d0}(Å) (left)	z_{d0}(Å) (right)
	400	0.7564	0.0022	7.989	3.02	40.459	77.997
	350	0.8196	0.0009	5.771	2.19	42.098	76.518
	300	0.8599	0.0004	5.148	1.95	42.726	75.664
	275	0.8678	0.0000	3.614	1.38	43.033	75.356
	250	0.8736	0.0001	3.560	1.35	42.905	75.370

Energy profile	T (K)	u_l (kJ cm^{-3})	u_v (kJ cm^{-3})	t_u (Å)	t_u (σ)	z_{u0}(Å) (left)	z_{u0}(Å) (right)
	400	-1.3239	0.0001	7.042	2.67	41.171	77.316
	350	-1.5954	0.0001	6.020	2.28	42.689	76.004
	300	-1.8223	0.0001	4.764	1.80	43.110	75.198
	275	-1.9094	0.0001	3.966	1.50	43.386	75.032
	250	-2.0101	0.0000	3.301	1.25	43.006	75.223

Table V-2. The same as Table V-1 for methanol surface. The molecular diameter σ is 3.628Å (Ref.14).

Density profile	T (K)	ρ_l (g cm^{-3})	ρ_v (g cm^{-3})	t_d (Å)	t_d (σ)	z_{d0}(Å) (left)	z_{d0}(Å) (right)
	350	0.6198	0.0035	9.561	2.64	31.301	87.399
	300	0.6879	0.0021	7.445	2.05	33.406	84.040
	250	0.7437	0.0000	6.181	1.70	35.419	82.246
	200	0.7981	0.0000	4.208	1.16	37.229	81.094
	160	0.8409	0.0000	4.240	1.17	38.340	79.984
Energy profile	**T (K)**	**u_l (kJ cm^{-3})**	**u_v (kJ cm^{-3})**	**t_u (Å)**	**t_u (σ)**	**z_{u0}(Å) (left)**	**z_{u0}(Å) (right)**
	350	-0.4717	0.0015	9.713	2.68	32.188	86.269
	300	-0.5946	0.0011	7.712	2.13	34.176	83.307
	250	-0.7130	0.0012	6.484	1.79	36.044	81.889
	200	-0.8398	0.0012	4.981	1.37	37.670	80.538
	160	-0.9454	0.0016	5.005	1.38	38.805	79.469

Table V-3. The same as Table V-1 for LJ surface. The molecular diameter σ is 3.405Å (Ref.150).

Density profile	T (K)	ρ_l (g cm^{-3})	ρ_v (g cm^{-3})	t_d (Å)	t_d (σ)	z_{d0}(Å) (left)	z_{d0}(Å) (right)
	120	1.1506	0.0593	10.668	3.13	16.808	71.312
	100	1.2904	0.0136	8.148	2.39	18.323	68.104
	80	1.4174	0.0004	5.450	1.60	20.480	66.234

Energy profile	T (K)	u_l (kJ cm^{-3})	u_v (kJ cm^{-3})	t_u (Å)	t_u (σ)	z_{u0}(Å) (left)	z_{u0}(Å) (right)
	120	-0.1352	0.0005	10.811	3.18	18.960	69.171
	100	-0.1739	0.0008	8.965	2.63	20.271	66.083
	80	-0.2154	0.0004	7.239	2.13	21.996	64.582

Table V-4. Surface excess thermodynamic quantities of water; surface tension γ, surface excess internal energy u_s, surface excess entropy s_s, and molar surface entropy sA defined in Eq.(V-9). R is the gas constant, 8.314 $JK^{-1}mol^{-1}$.

T (K)	γ (erg cm^{-2})	u_s (erg cm^{-2})	s_s (erg $K^{-1}cm^{-2}$)	sA (R)
400	11.7 ± 1.8	92.3 ±2.1	0.199±0.010	1.84±0.09
350	18.7 ± 2.3	88.2 ±6.2	0.198±0.024	1.74±0.21
300	30.5 ± 2.7	77.4 ±7.5	0.156±0.034	1.32±0.29
275	41.0 ± 6.2	64.6 ±2.7	0.085±0.033	0.72±0.28
250	36.7 ±13.2	24.9 ±4.6	-0.047±0.072	-0.39±0.60

Table V-5. The same as Table V-4 for methanol.

T (K)	γ (erg cm^{-2})	u_s (erg cm^{-2})	s_s (erg $K^{-1}cm^{-2}$)	s A (R)
350	8.21±1.93	47.7±6.3	0.122±0.019	1.00±0.16
300	14.53±1.27	44.8±1.6	0.101±0.010	0.89±0.09
250	18.83±3.51	43.5±1.6	0.097±0.021	0.90±0.19
200	28.38±7.58	41.9±5.3	0.091±0.063	0.89±0.61
160	41.39±9.79	46.4±2.8	0.031±0.078	0.31±0.78

Table V-6. The same as Table V-4 for LJ.

T (K)	γ (erg cm^{-2})	u_S (erg cm^{-2})	s_S (erg K^{-1}cm^{-2})	s A (R)
120	5.89± 0.49	29.13±0.08	0.195±0.005	2.32±0.06
100	9.59± 0.83	34.68±0.65	0.250±0.015	2.50±0.15
80	14.34± 0.75	34.18±1.47	0.248±0.028	2.33±0.26

[Figure captions in Sec. V]

Fig. V-1. Examples of parameter-fitting result of density profile of water; (a)T=300 K and (b)T=400 K.

Fig. V-2. Temperature dependence of the surface thicknesses t_d (from density profiles, solid line), t_u (from energy profile, dashed line), and t_d^{el} (from ellipticity coefficient, dotted line, see Sec. VI) for water surface.

Fig. V-3. The same as Fig. V-2 for methanol surface.

Fig. V-4. The same as Fig. V-3 for LJ surface.

Fig. V-5. Density profiles $\rho^*(z^*)$ and energy profiles $u^*(z^*)$ in reduced units for water surface; solid lines are tanh functions least-square fitted to the simulation data. $z^*=z/\sigma$, where σ=2.641 Å is molecular diameter (Ref.14).

Fig. V-6. The same as Fig. V-5 for methanol surface. The molecular diameter σ is 3.626 Å (Ref.14).

Fig. V-7. The same as Fig. V-5 for LJ surface. The molecular diameter σ is 3.405 Å (Ref.150).

Fig. V-8. Surface excess quantities of CC water (circles) compared with the experimental data (Ref.155, solid lines); (a) surface tension γ, (b) excess internal energy u_s, and (c) excess entropy s_s. The dotted lines are temperature derivative of the surface tension calculated from Eq.(III-6).

Fig. V-9. The same as Fig. V-8 for methanol. The experimental data is taken from Ref. 156.

Fig. V-10. Variables used to represent the orientation of a water molecule. ϕ is defined to be 90° when the straight line connecting both hydrogen atoms is parallel to the surface.

Fig. V-11. Averaged orientational angles of water, $\langle\theta\rangle$ and $\langle\phi\rangle$. The arrows show the position of the Gibbs surfaces.

Fig. V-12. Contour maps of (θ, ϕ) distribution of water at T=300 K, normalized to unity if the orientation is completely random; the ranges corresponding to the various shades are described above the first figure. The position of the Gibbs surface is z=42.7 Å.

Fig. V-13. The same as Fig. V-12 for T=400 K. The position of the Gibbs surface is z=40.5 Å.

Fig. V-14. Two most typical orientations of water molecules near the surface.

Fig. V-15. Variables used to represent the orientation of a methanol molecule. The three axes, x, y, and z are the principal axes of inertia tensor, and Z is the surface normal from liquid to vapor.

Fig. V-16. Averaged orientational angles of methanol, $\langle\theta\rangle$ and $\langle\phi\rangle$. The arrows show the position of the Gibbs surfaces.

Fig. V-17. Contour maps of (θ, ϕ) distribution of methanol at T=200 K; the ranges corresponding to the shades are described above the first figure. The position of the Gibbs surface is z=37.2 Å.

Fig. V-18. The same as Fig. V-17 for T=350 K. The position of the Gibbs surface is z=31.3 Å.

Fig. V-19. The most typical orientation of methanol molecules near the surface.

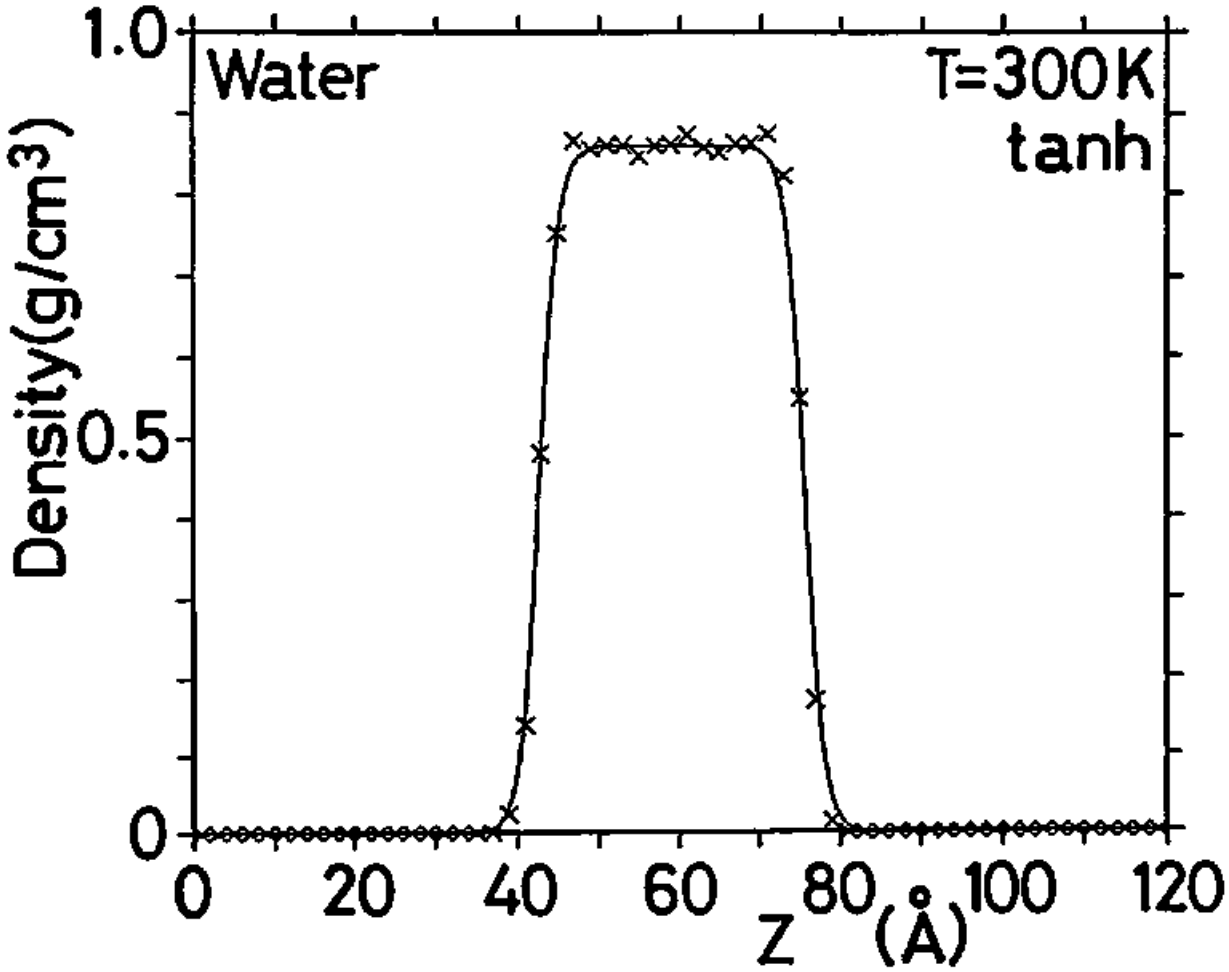

Fig. V-1. (a) Tanh profile.

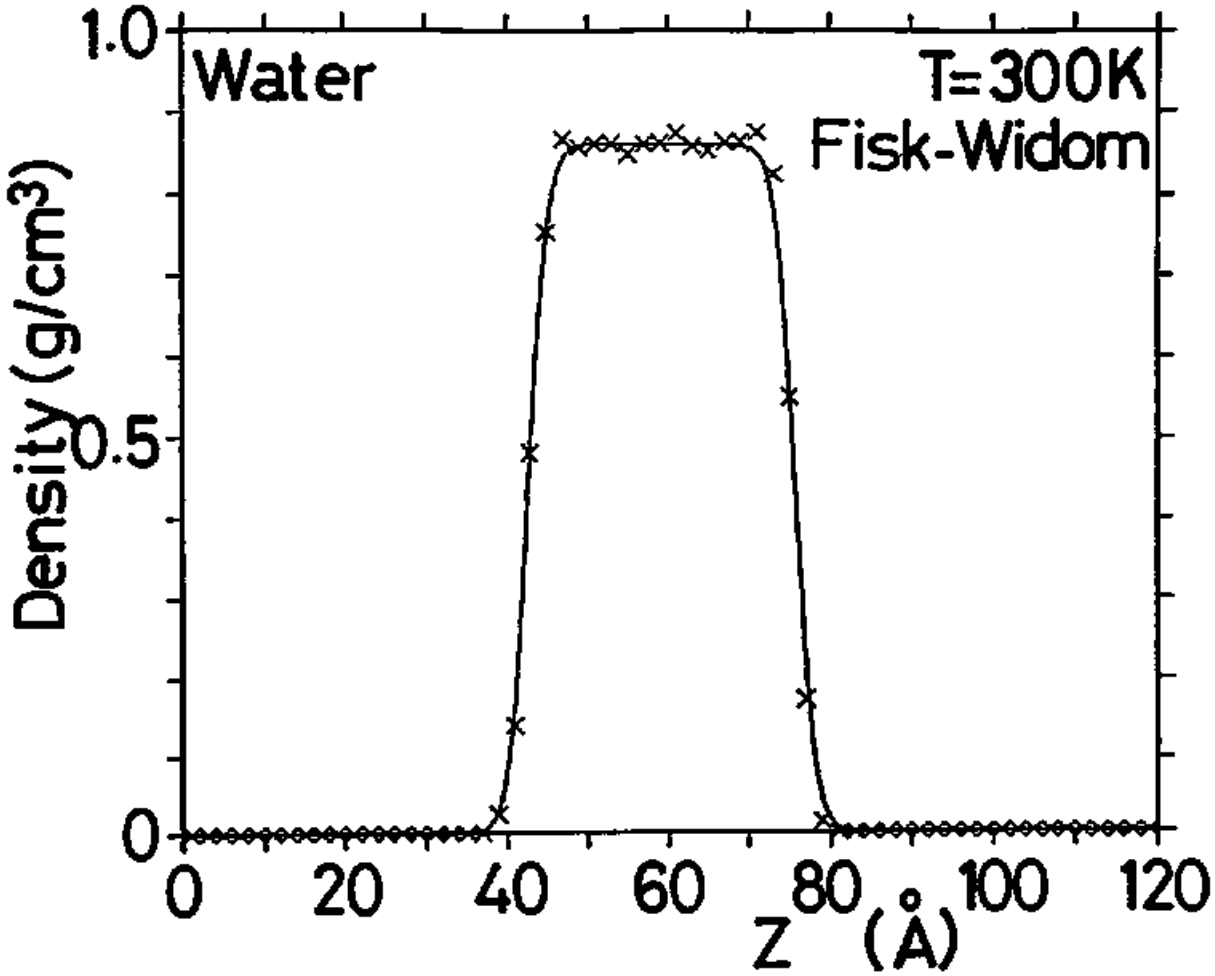

Fig. V-1. (a) Fisk-Widom profile.

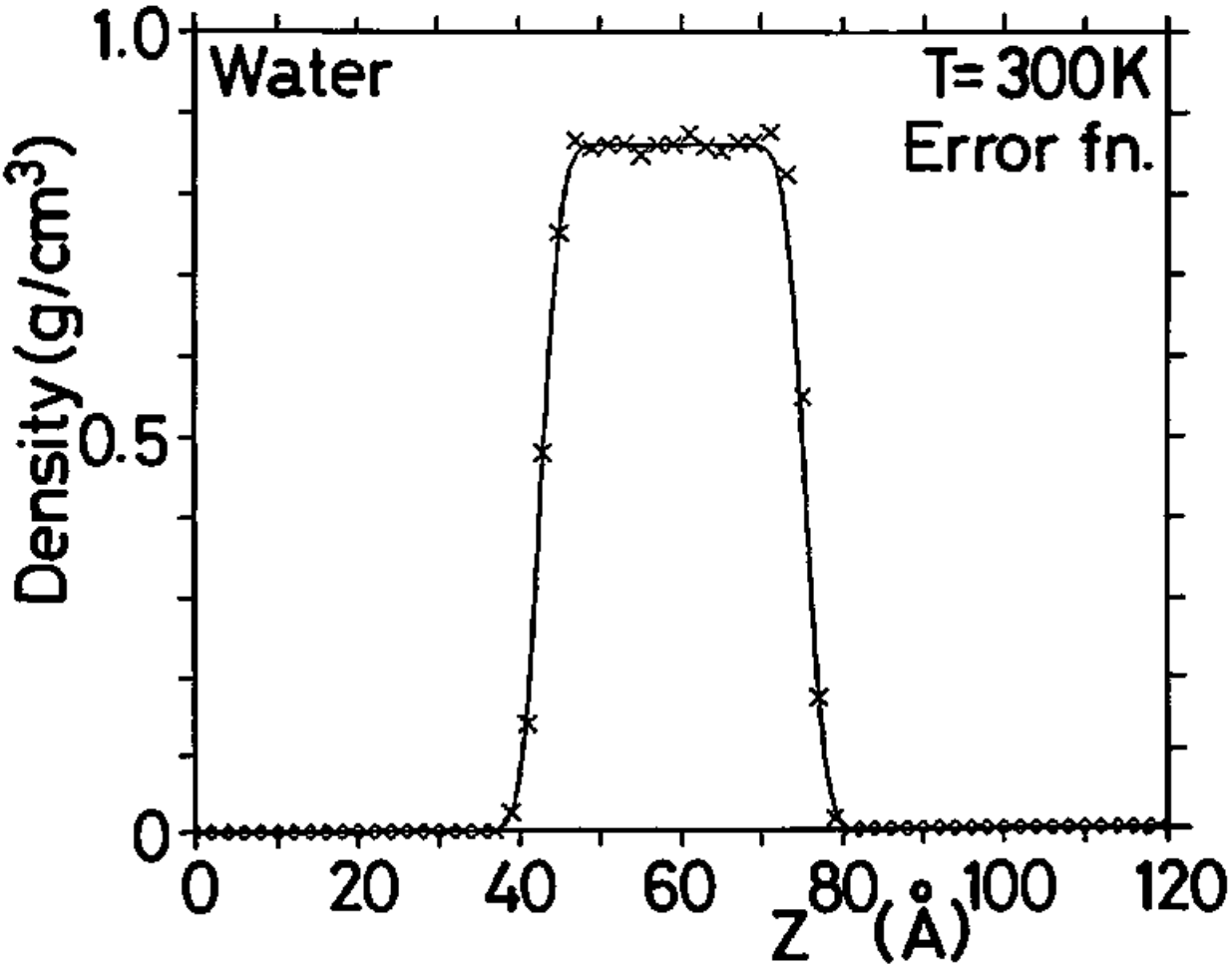

Fig. V-1. (a) Error function profile.

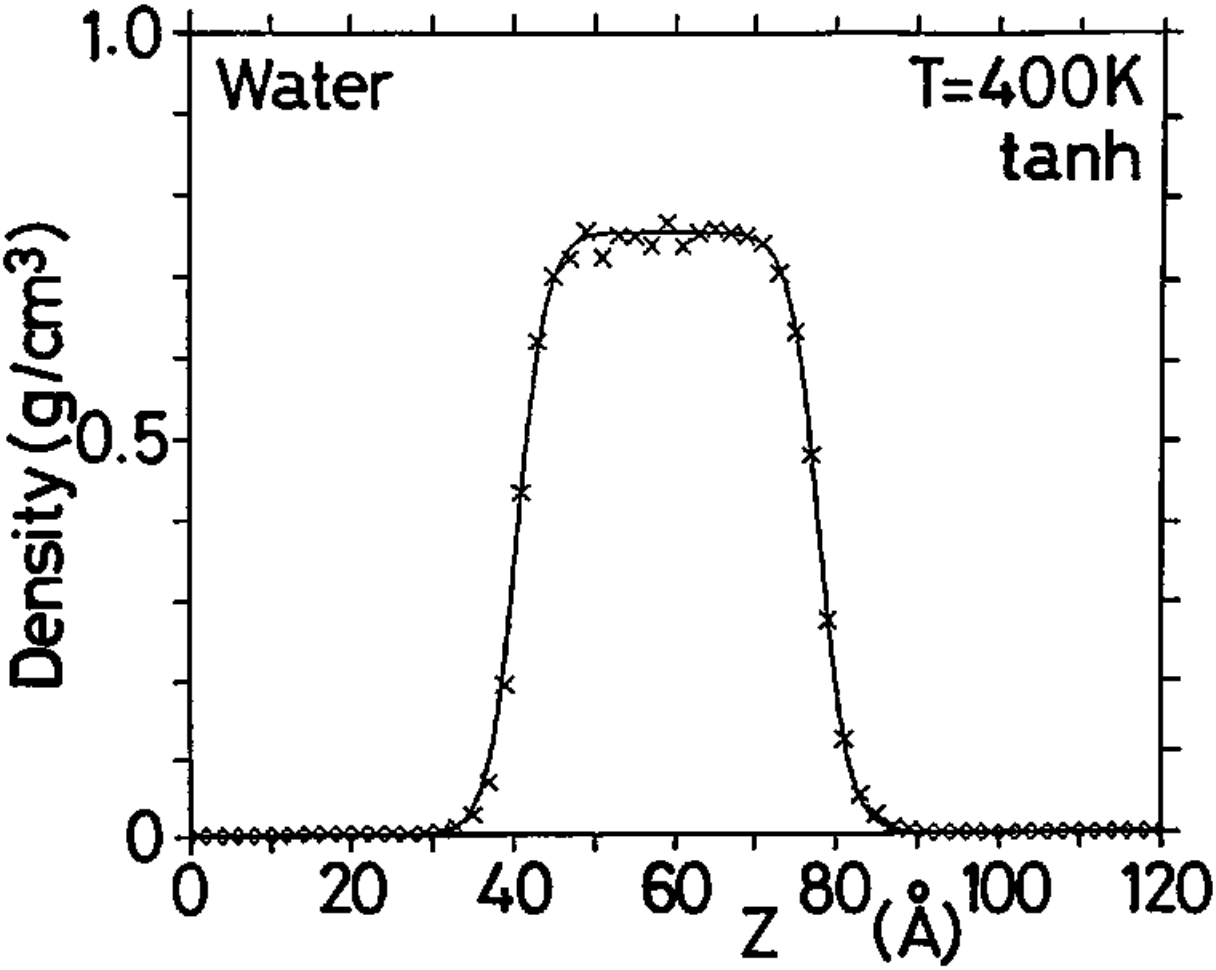

Fig. V-1. (b) Tanh profile.

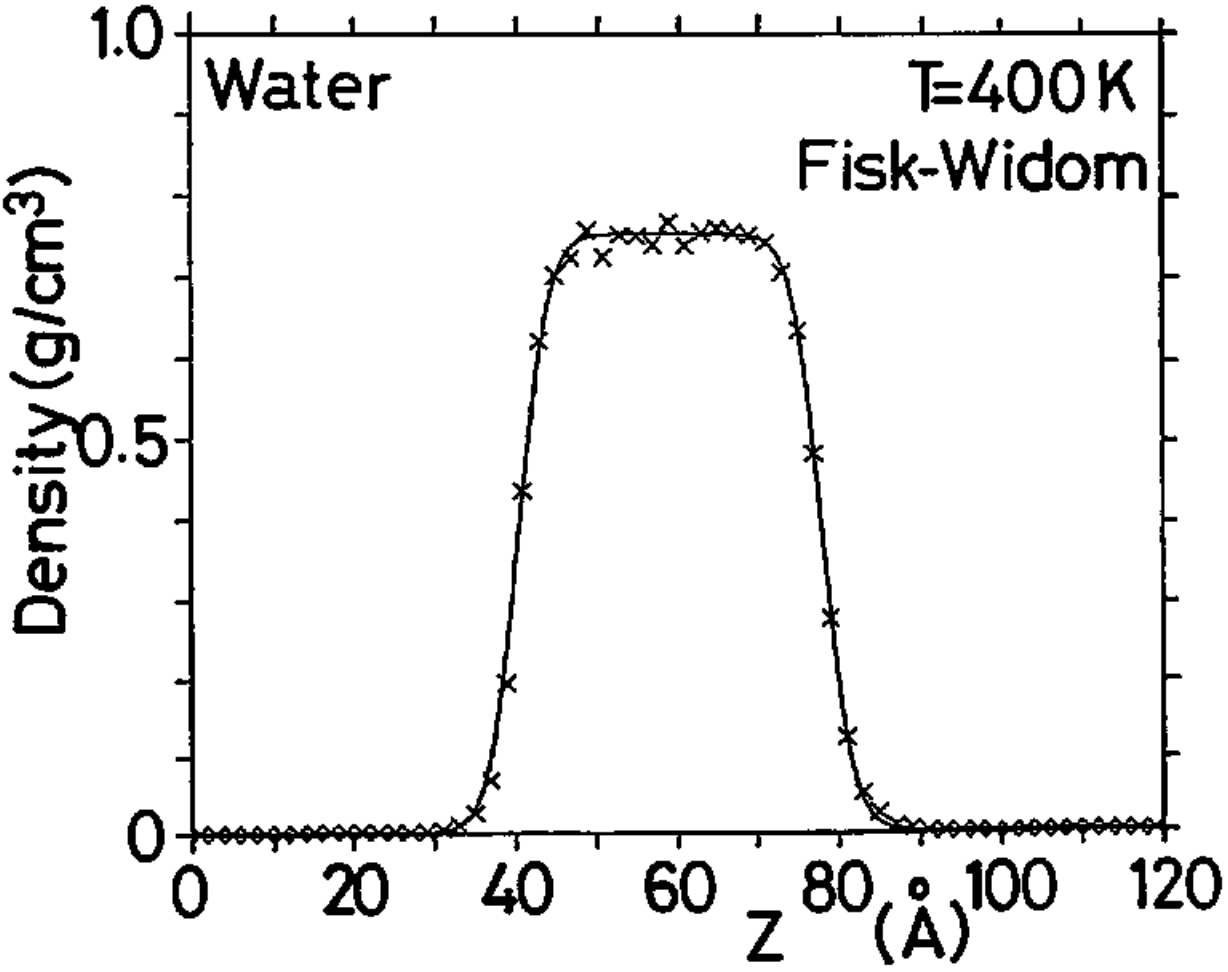

Fig. V-1. (b) Fisk-Widom profile.

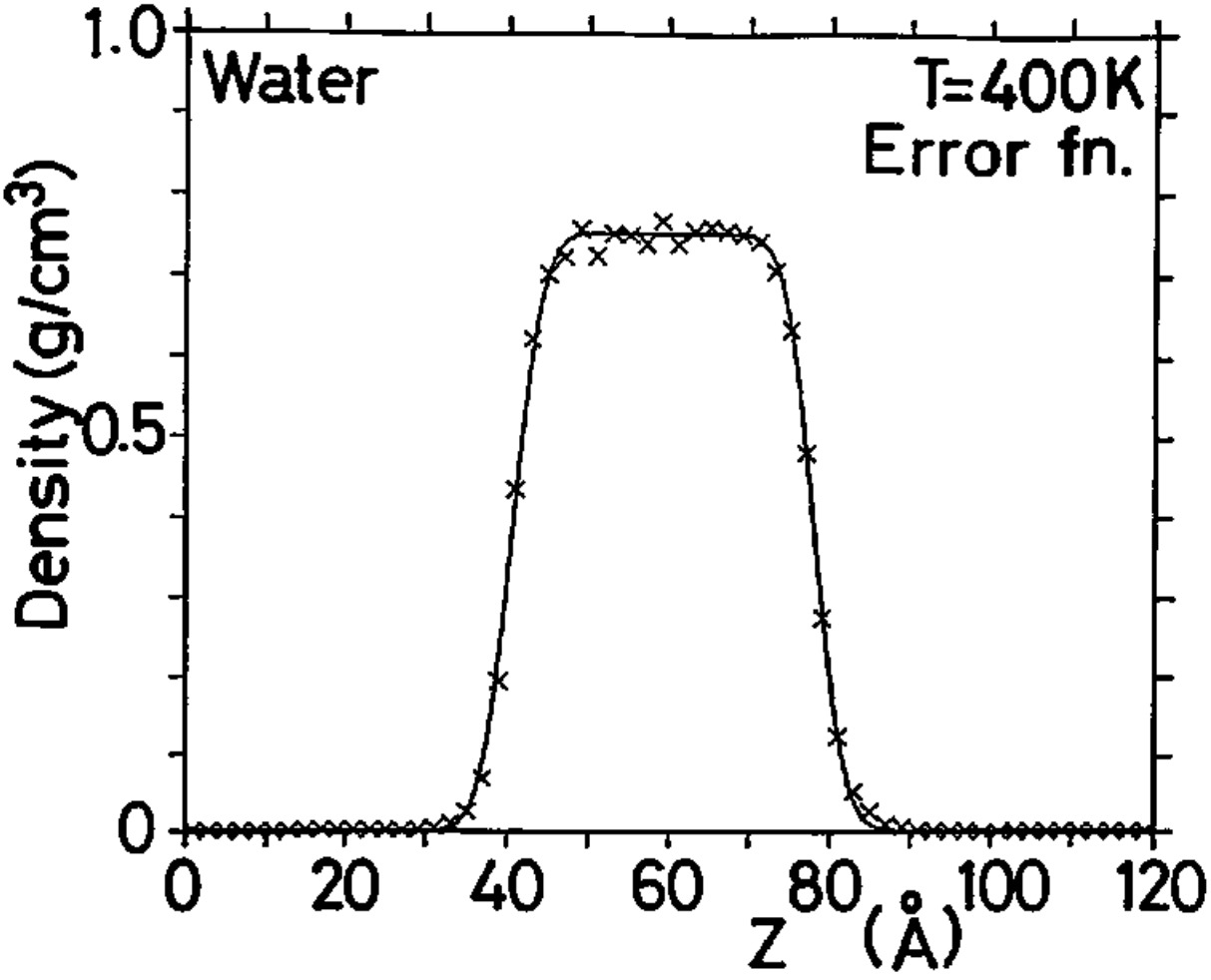

Fig. V-1. (b) Error function profile.

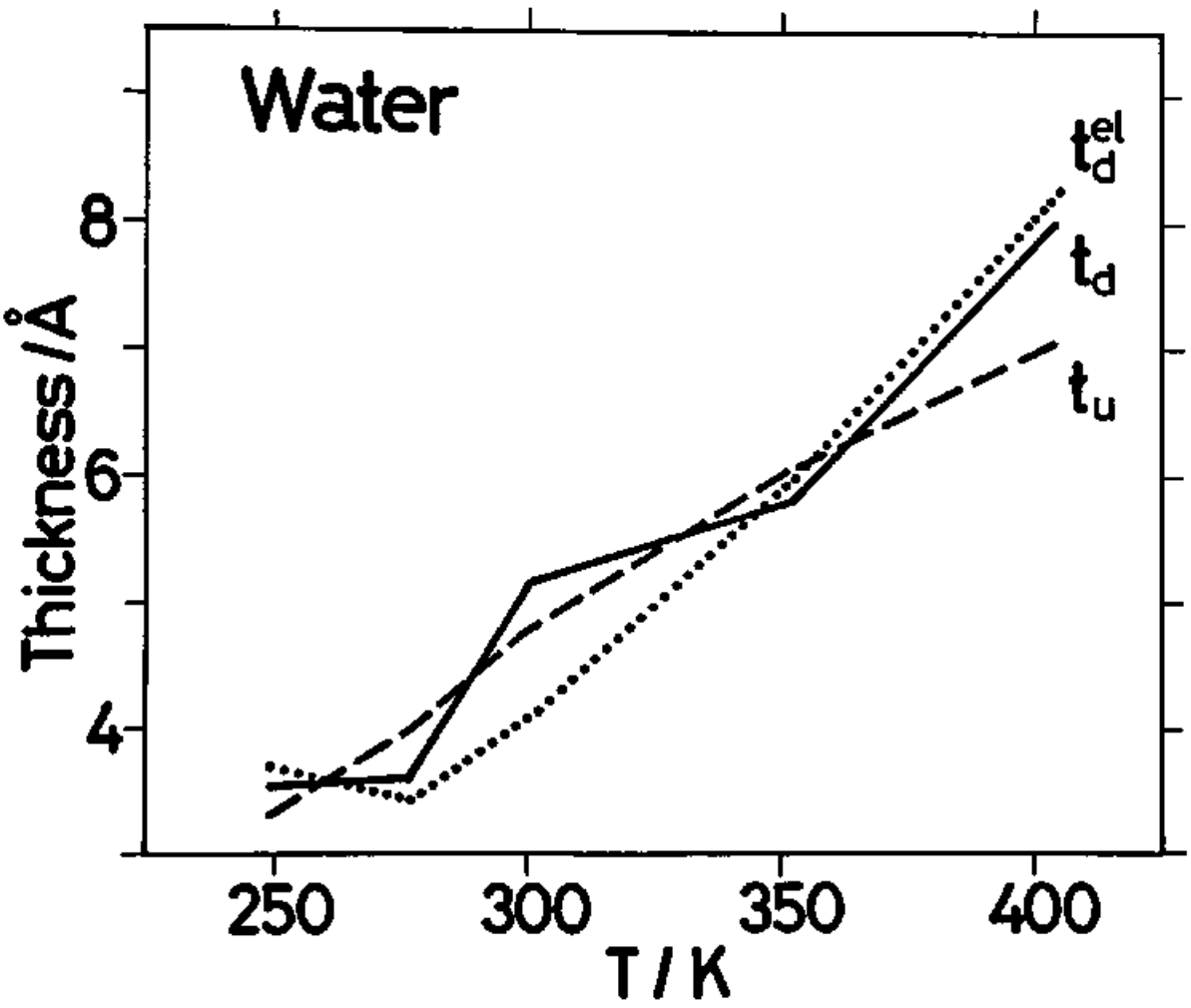

Fig. V-2.

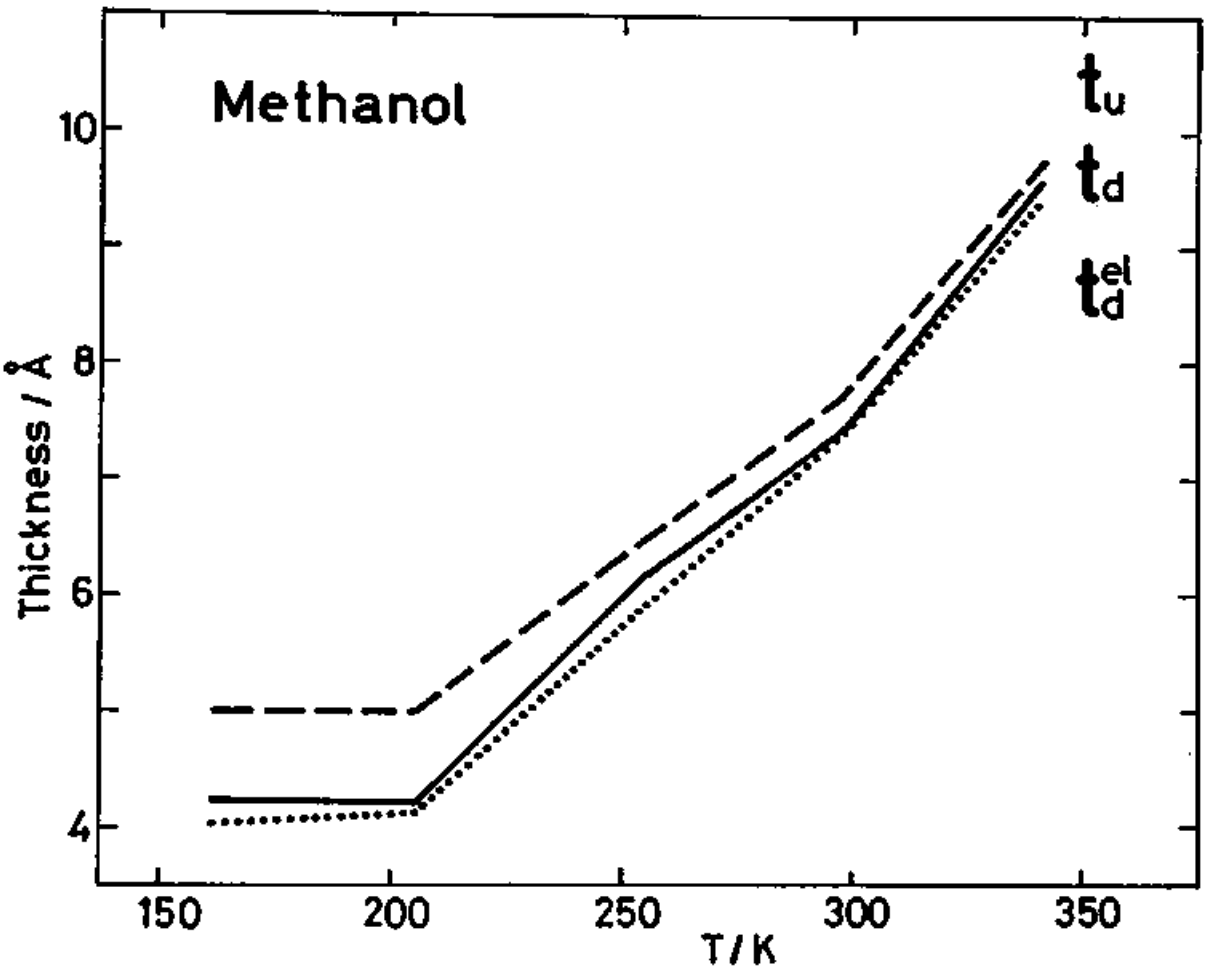

Fig. V-3.

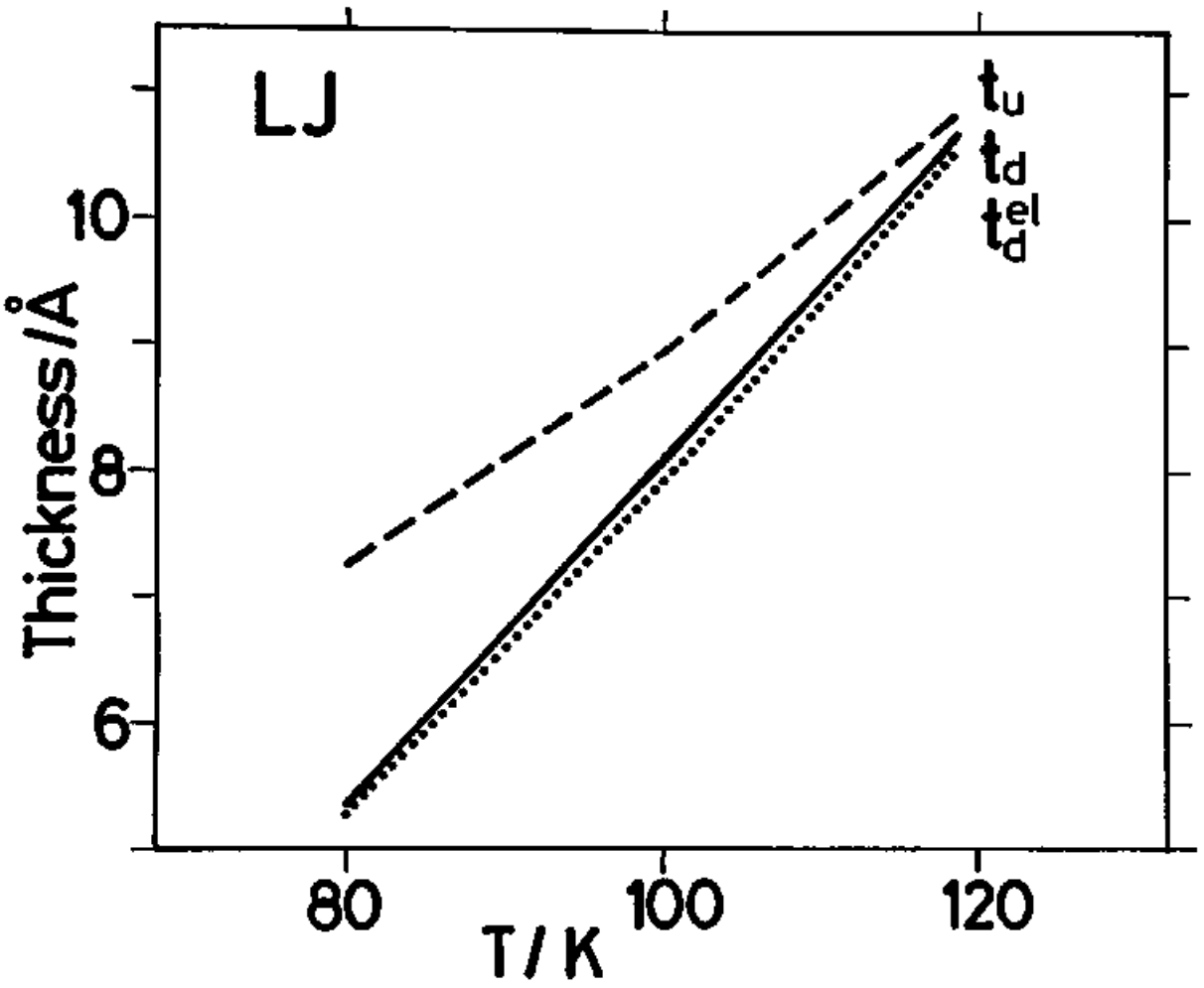

Fig. V-4.

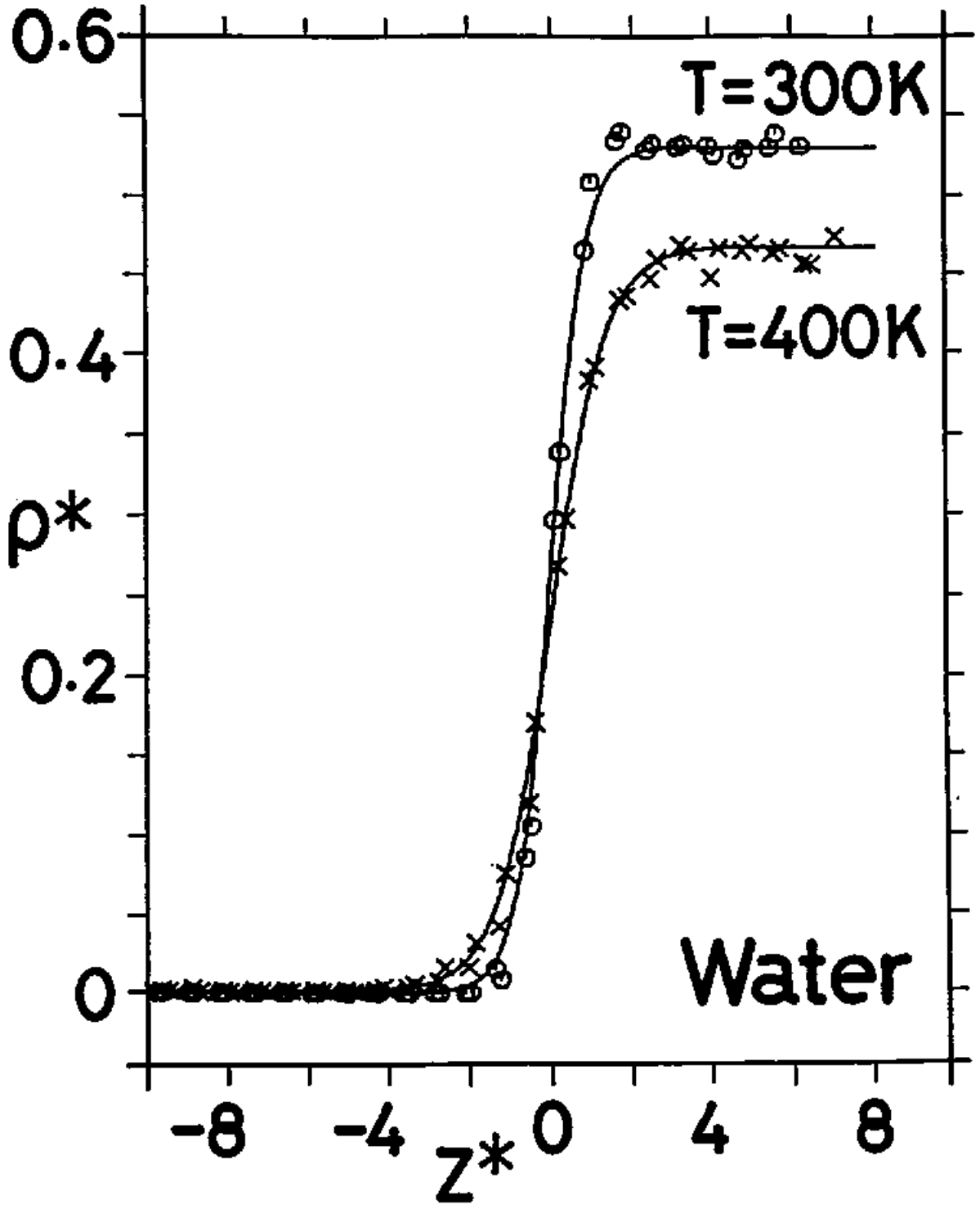

Fig. V-5. (1) Density profiles.

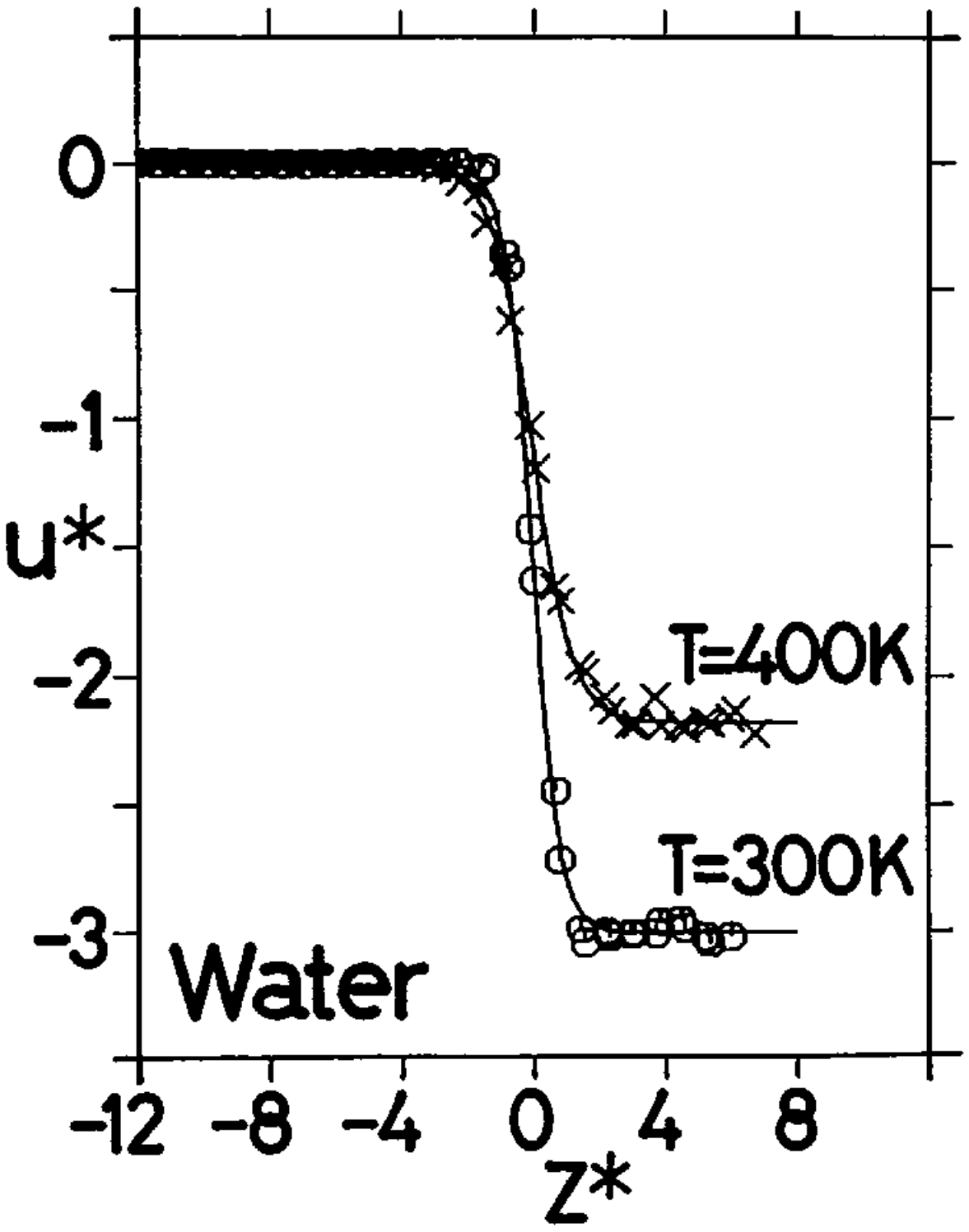

Fig. V-5. (2) Energy profiles.

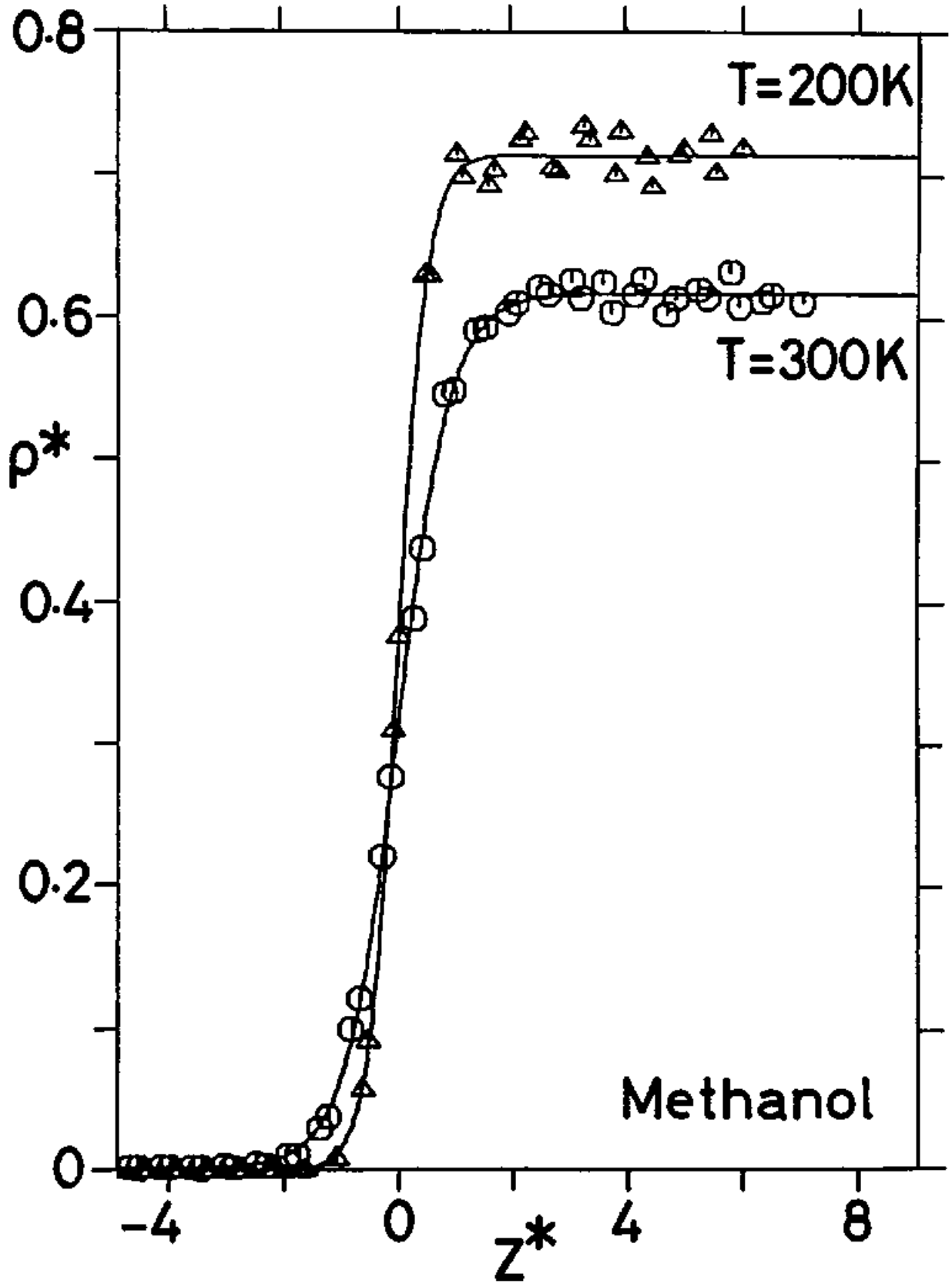

Fig. V-6. (1) Density profiles.

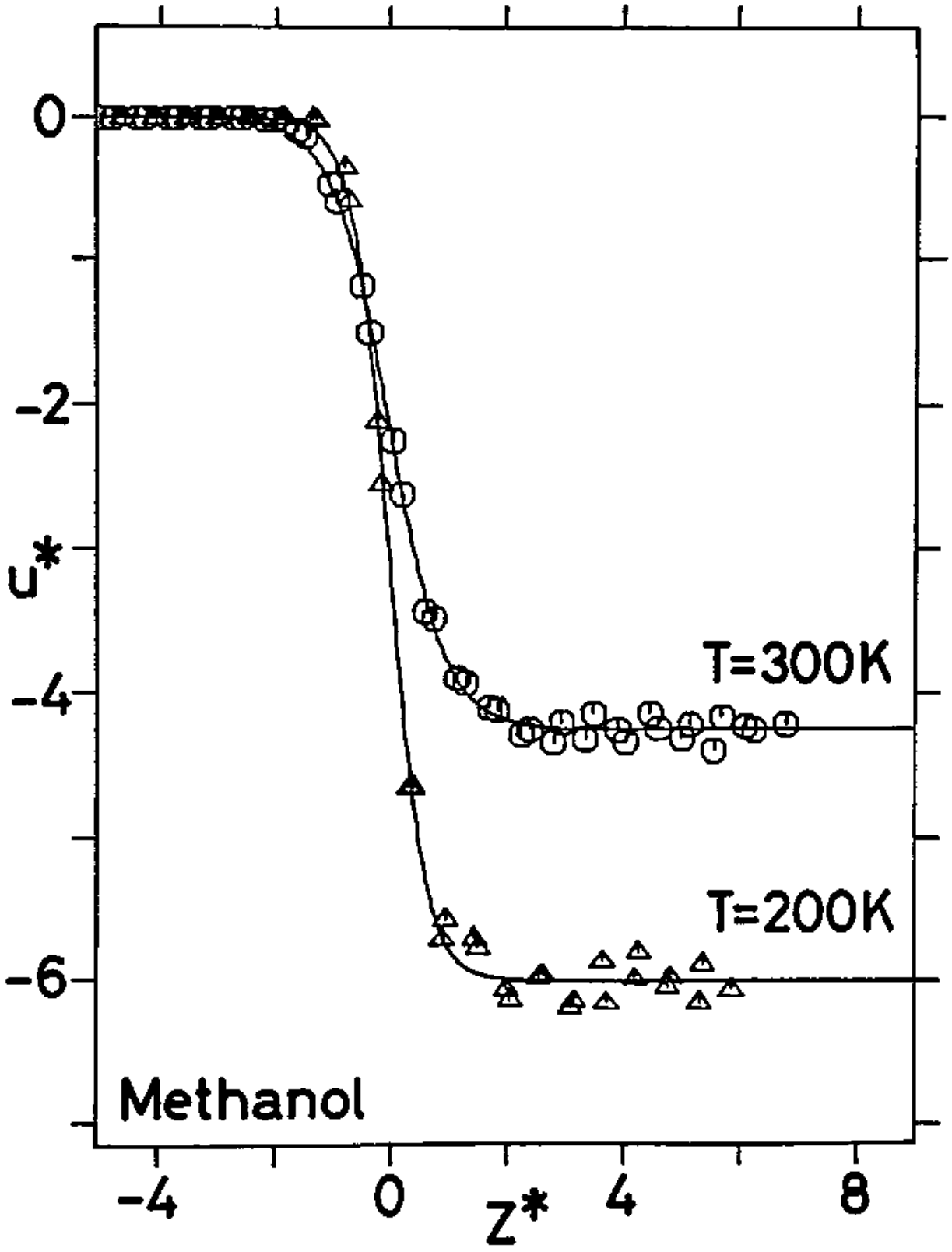

Fig. V-6. (2) Energy profiles.

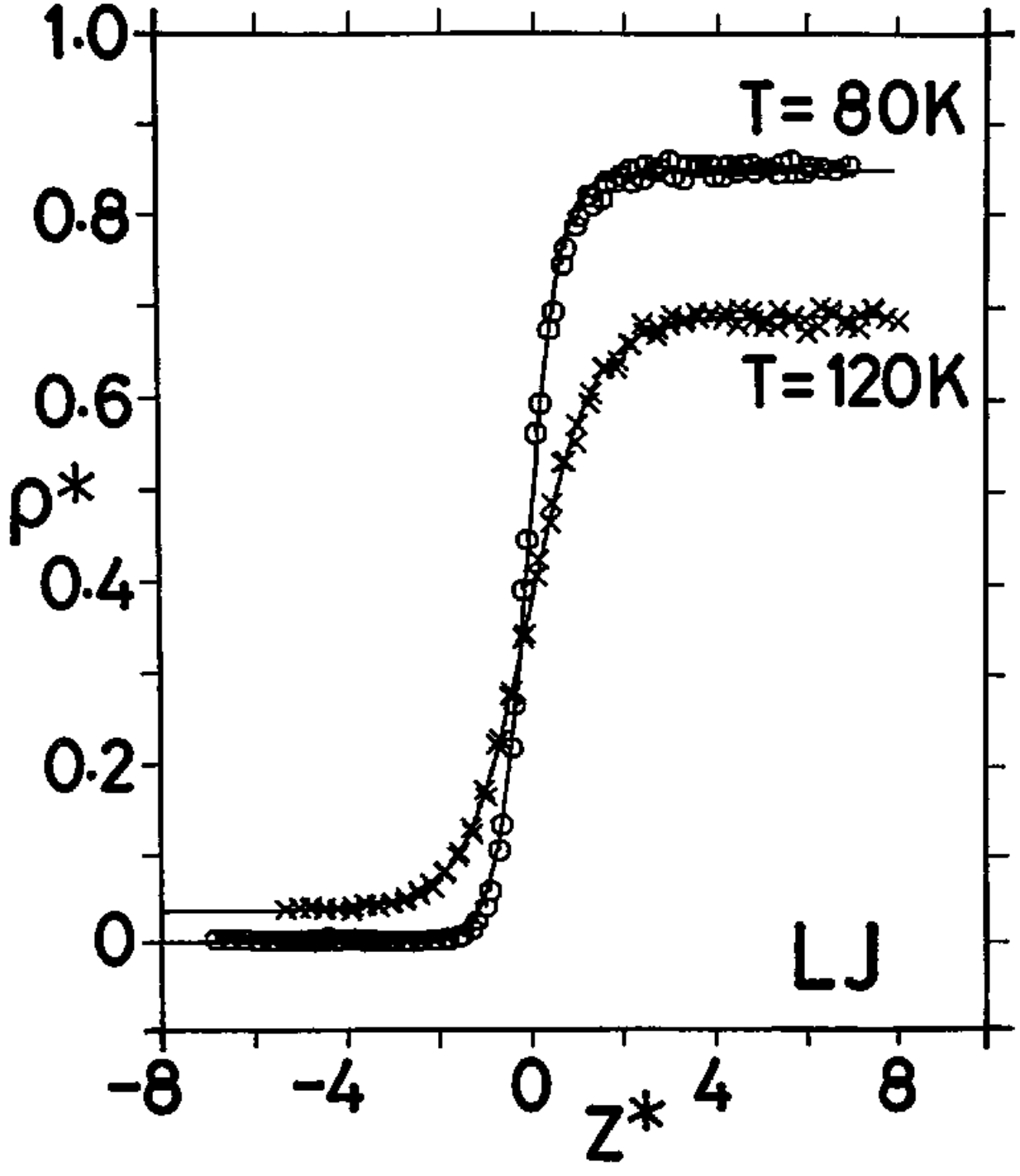

Fig. V-7. (1) Density profiles.

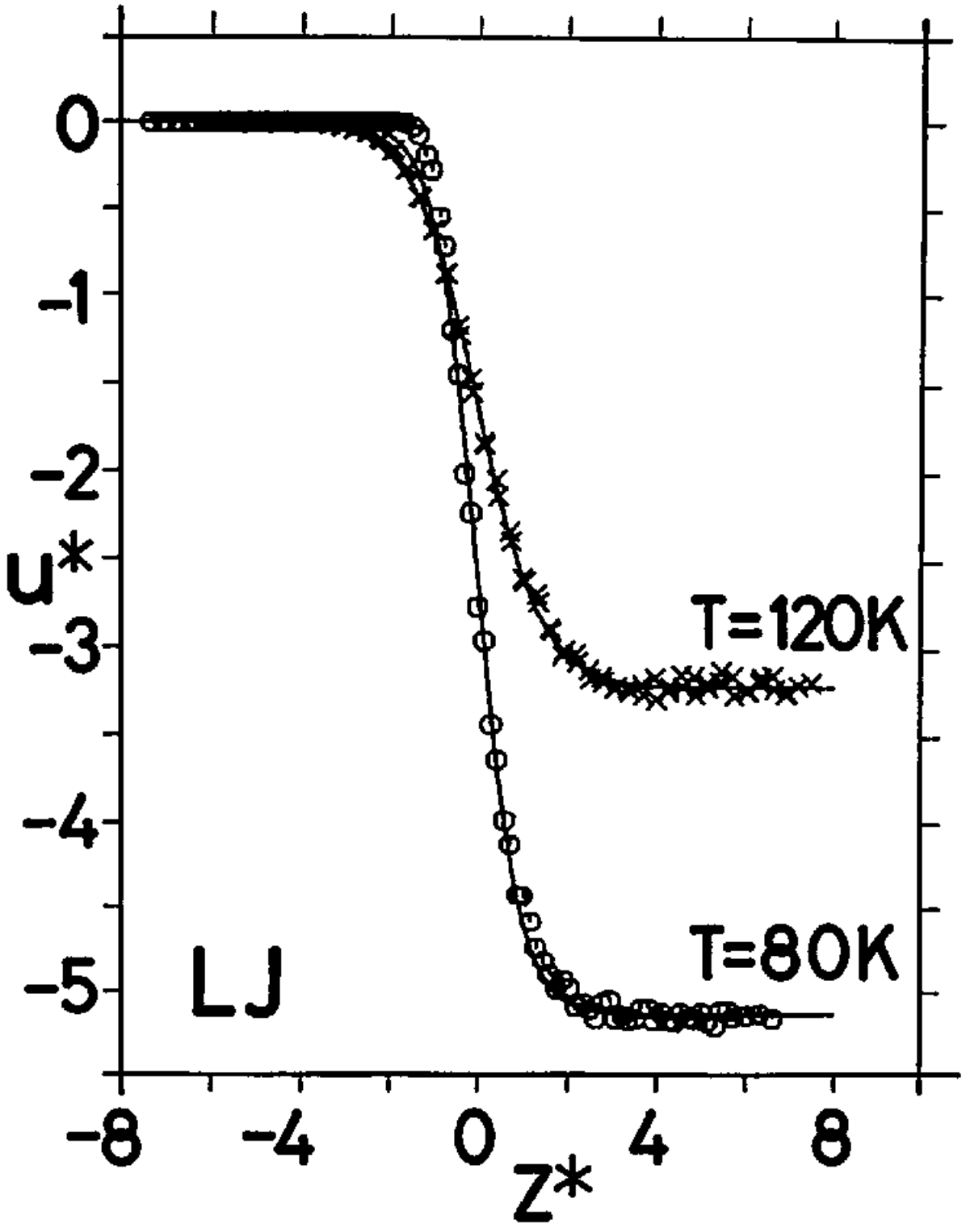

Fig. V-7. (2) Energy profiles.

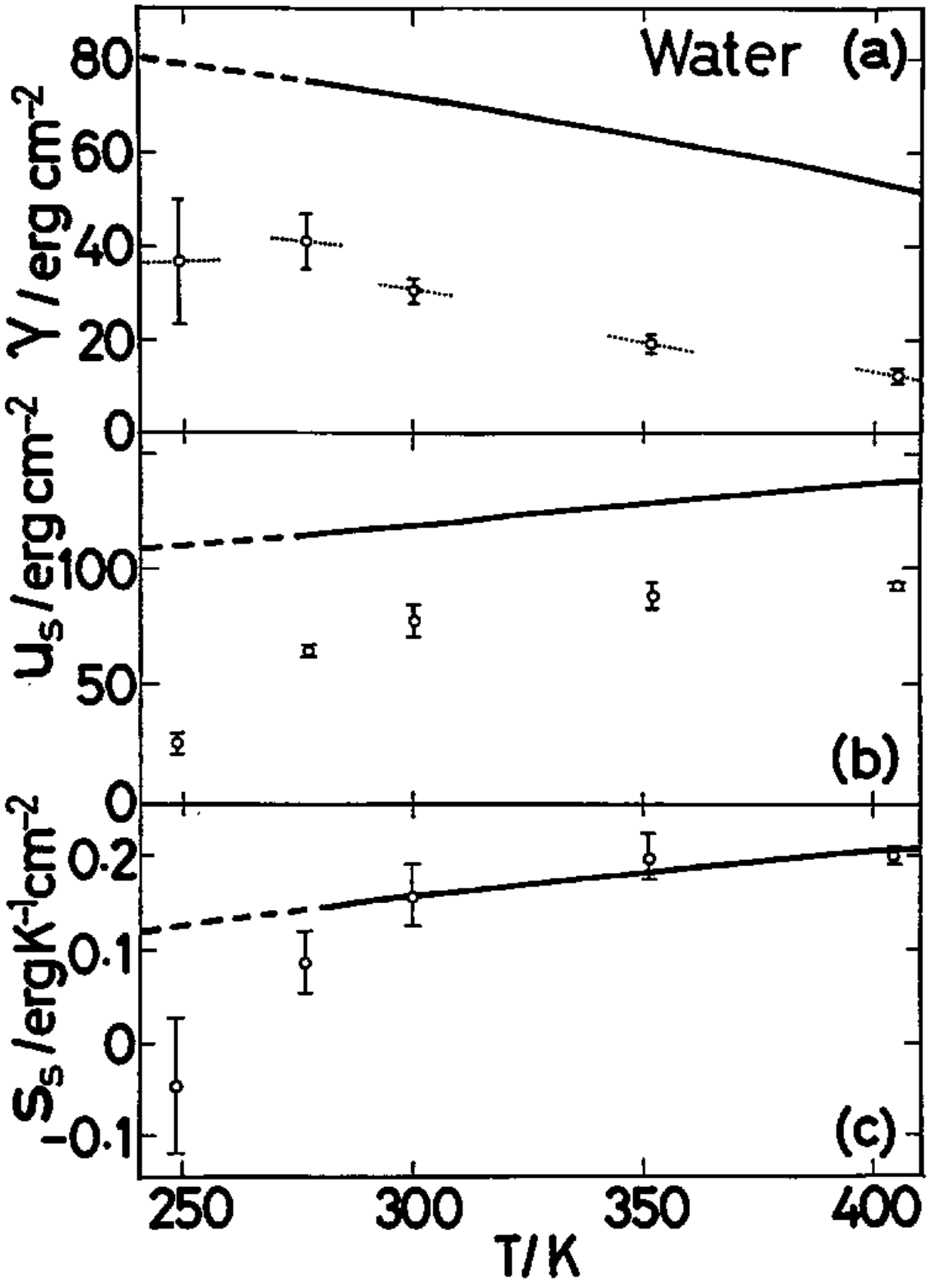
Water (a)
80
60
40
20
0
γ / erg cm⁻²
100
50
0
U_s / erg cm⁻²
(b)
0.2
0.1
0
-0.1
S_s / erg K⁻¹ cm⁻²
(c)
250
300
350
400
T / K

Fig. V-8.

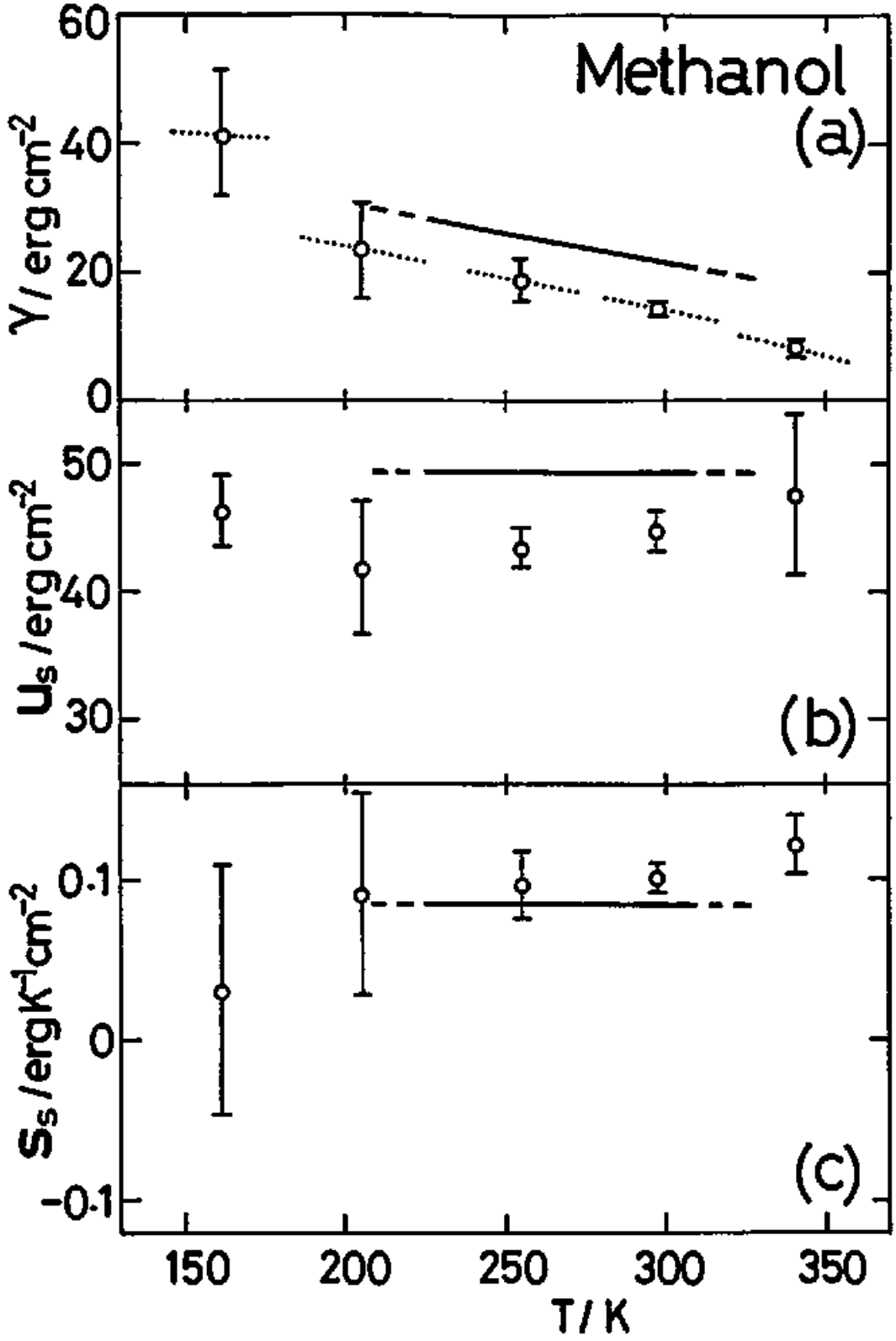
Methanol
(a)
(b)
(c)
γ / erg cm⁻²
Us / erg cm⁻²
Ss / erg K⁻¹ cm⁻²
T / K
60
40
20
0
50
40
30
0.1
0
-0.1
150
200
250
300
350

Fig. V-9.

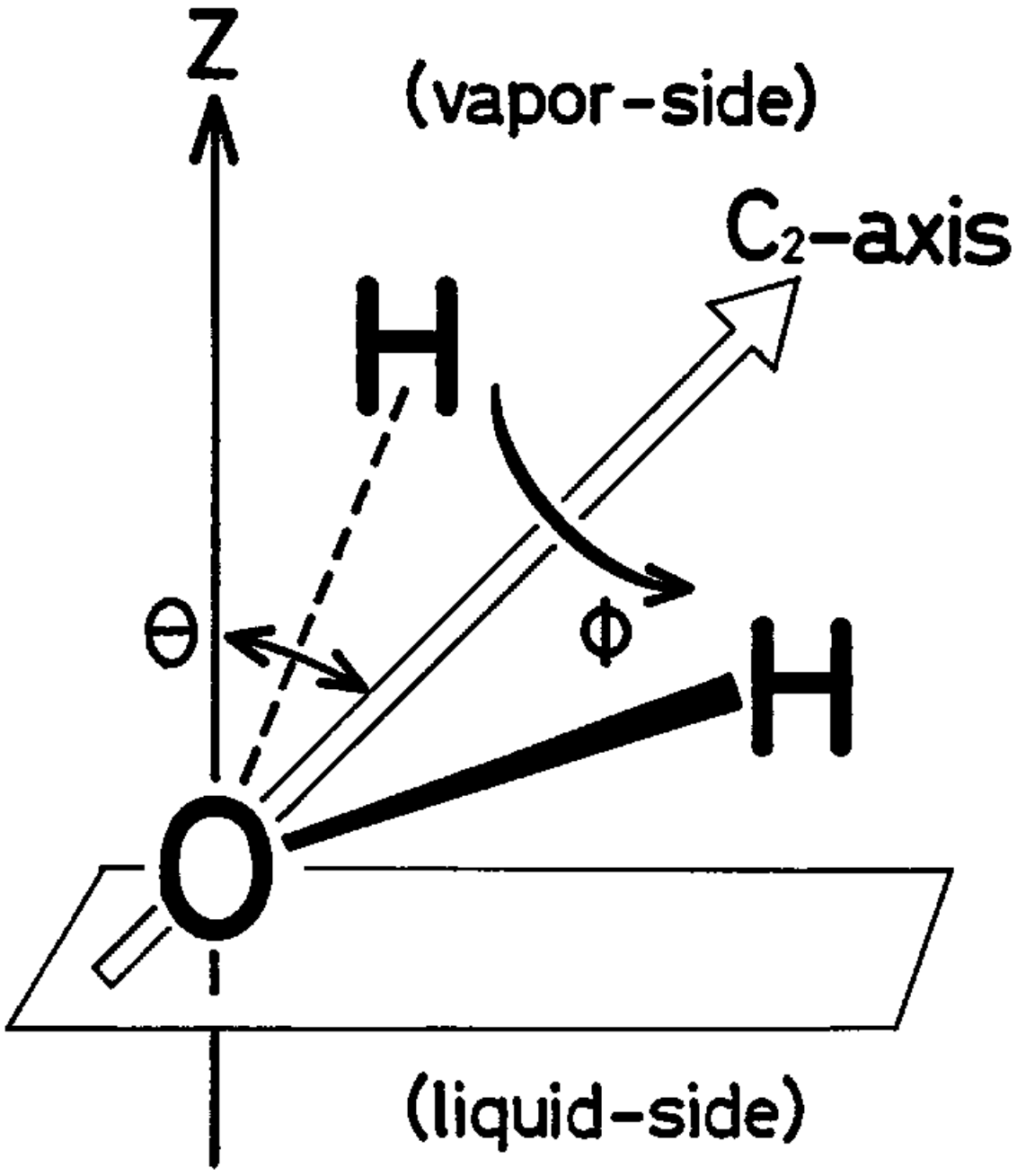

Fig. V-10.

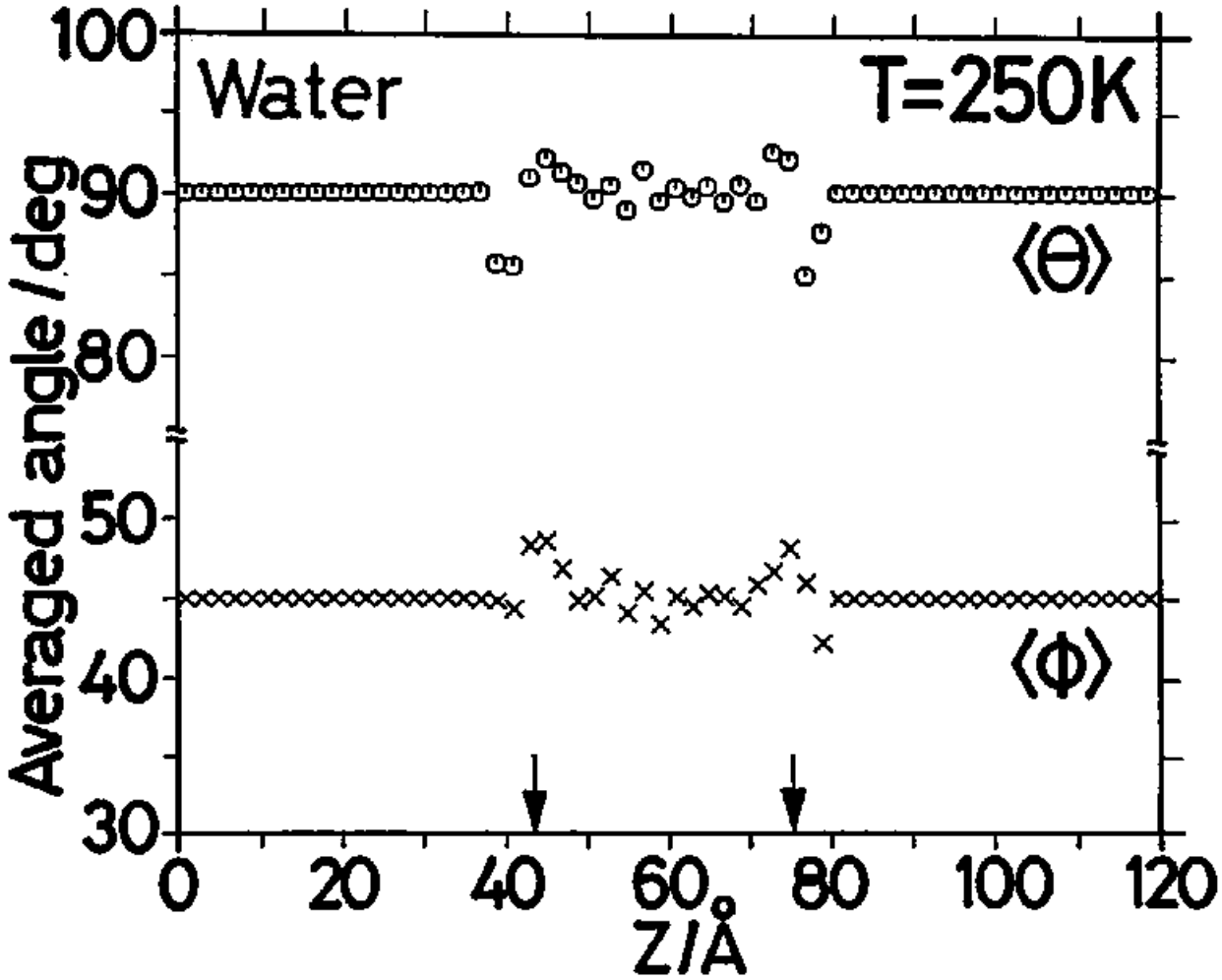

Fig. V-11. (1) T=250 K.

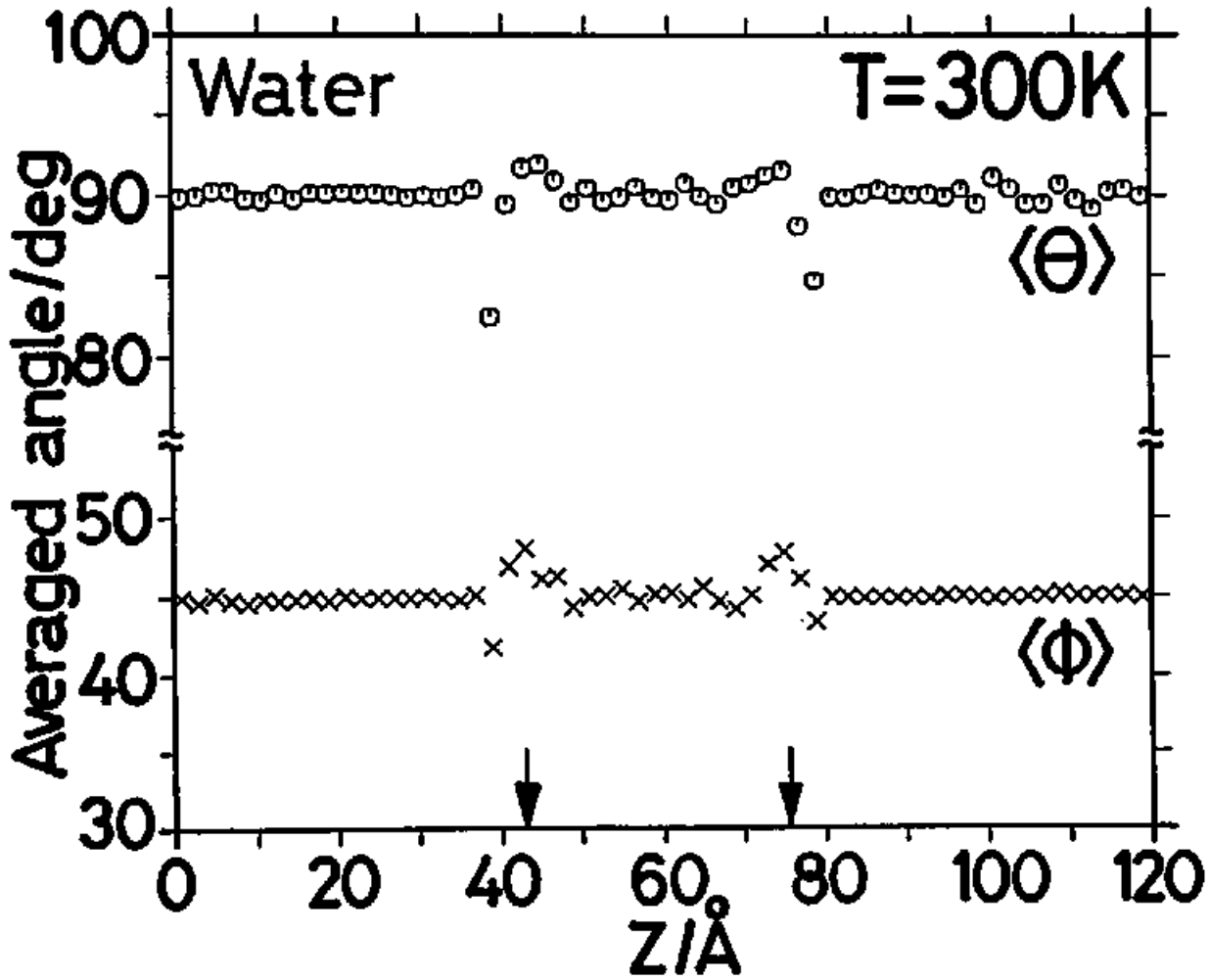

Fig. V-11. (2) T=300 K.

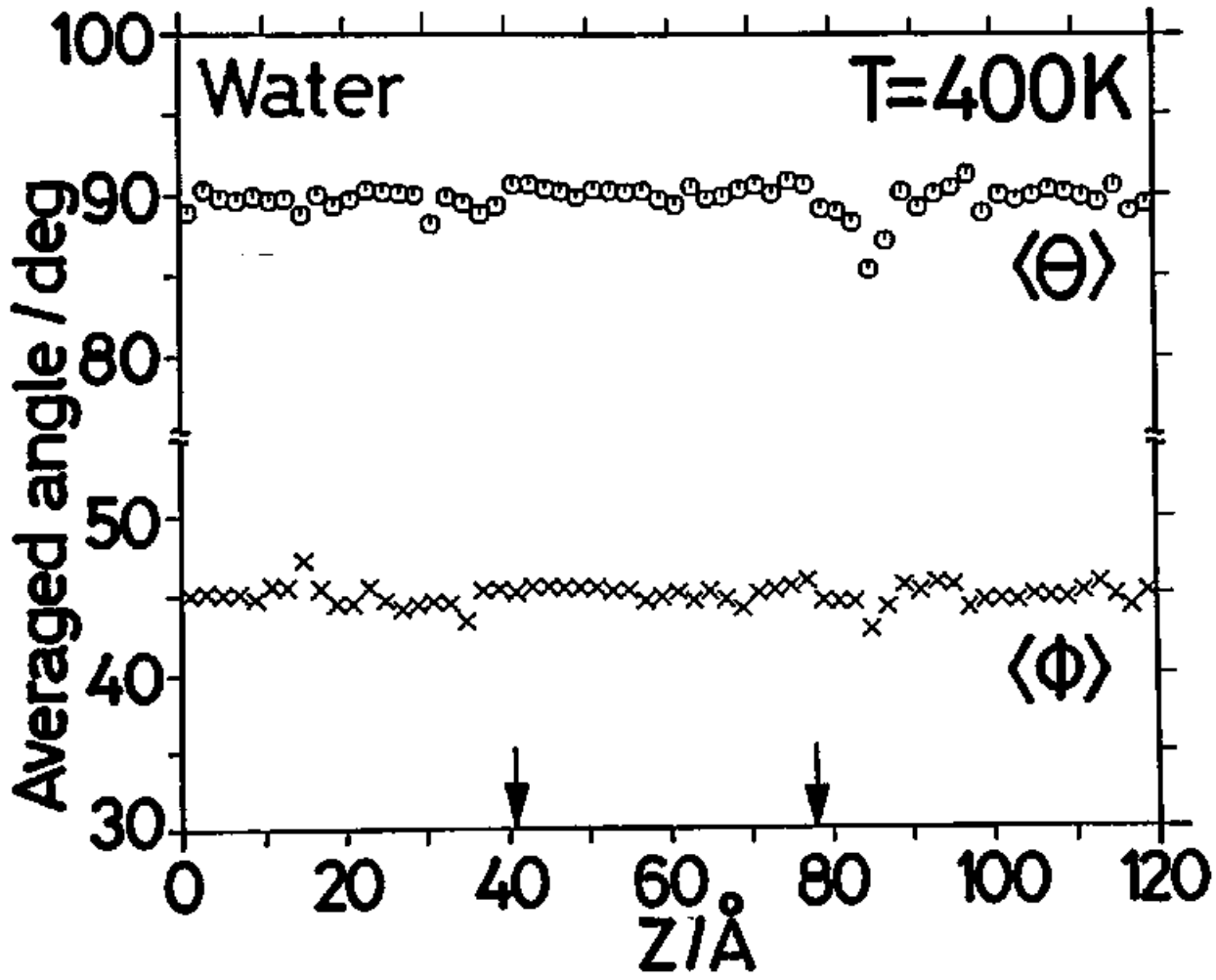

Fig. V-11. (3) T=400 K.

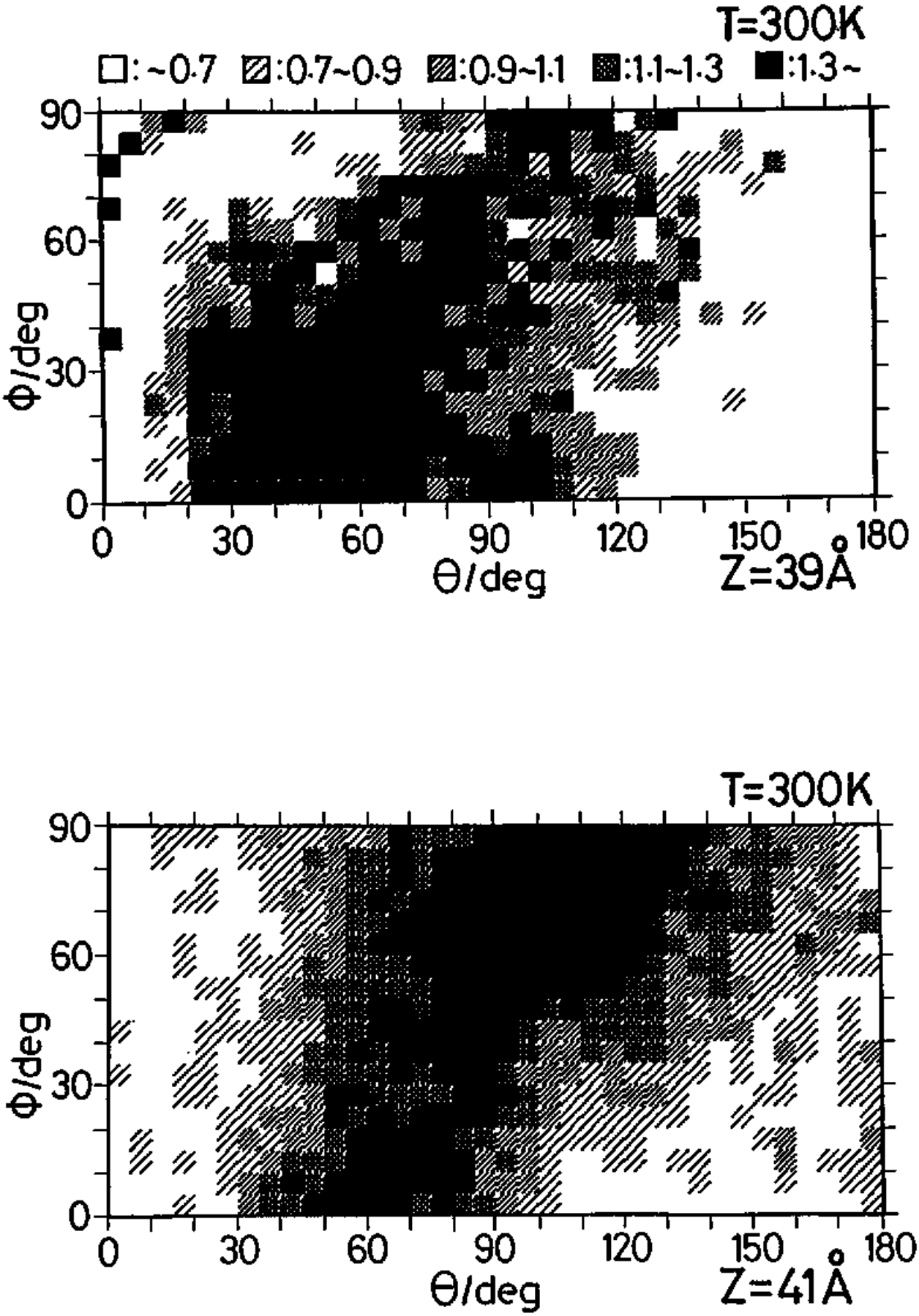

Fig. V-12. to be continued.

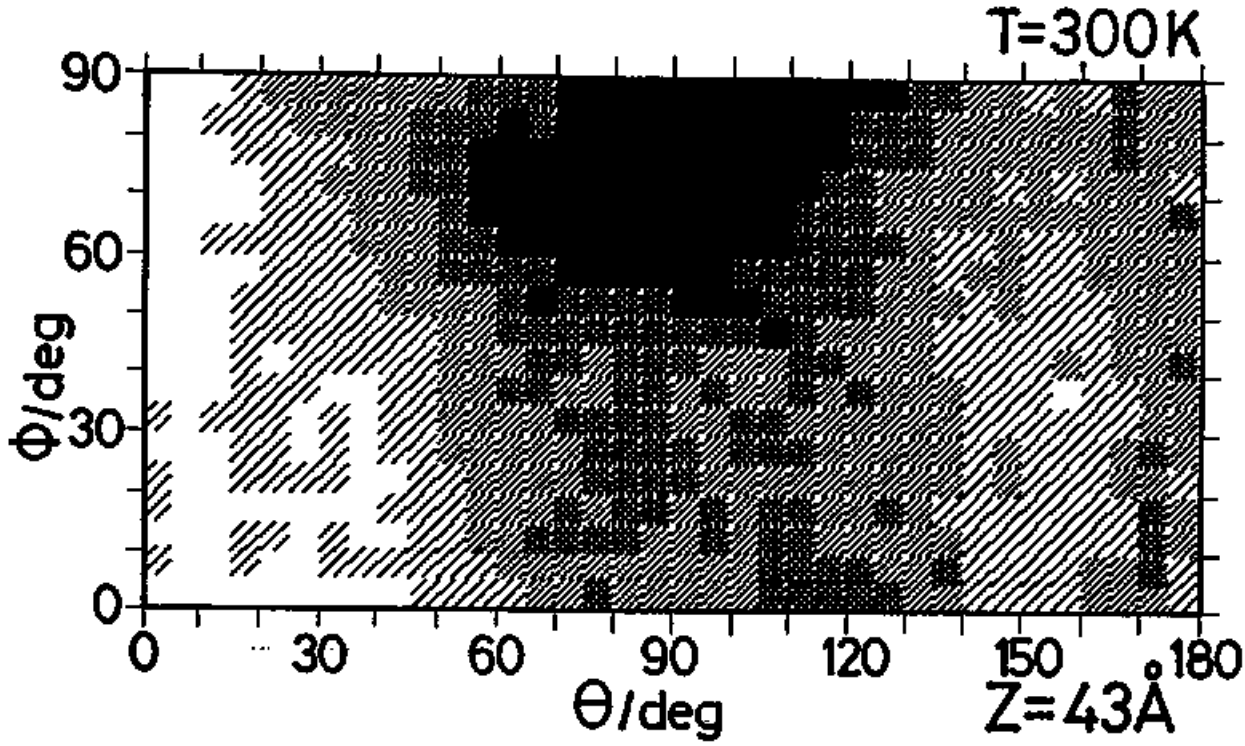

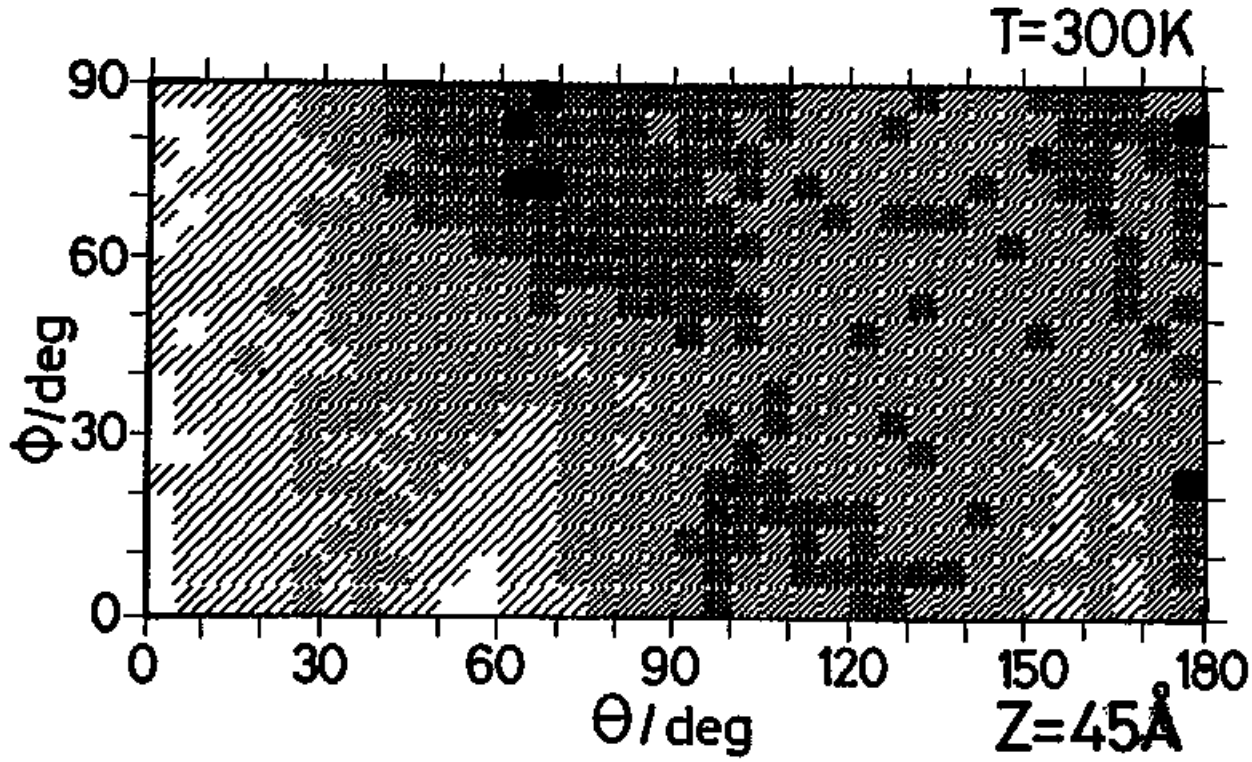

Fig. V-12. continued.

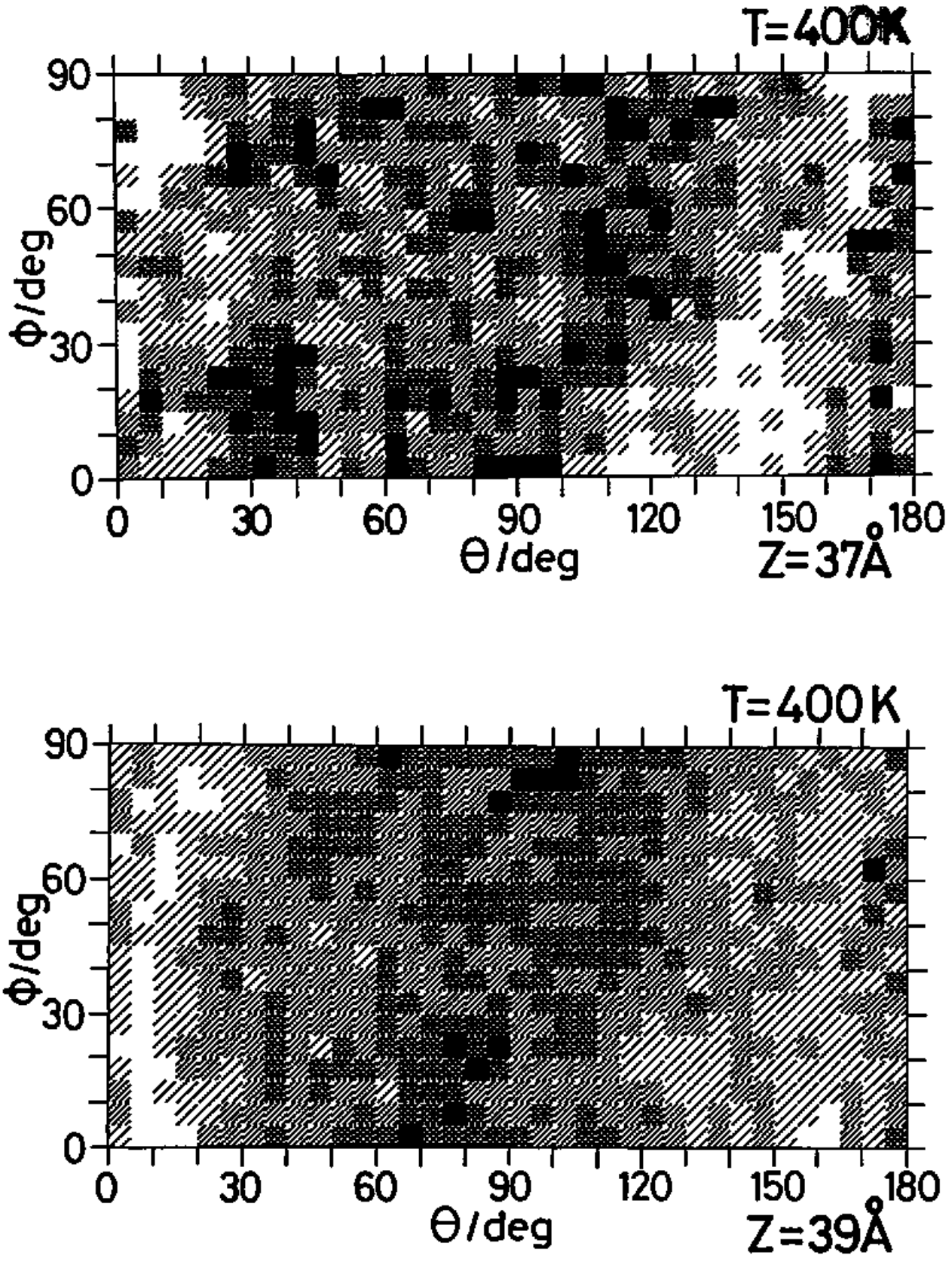

Fig. V-13. to be continued.

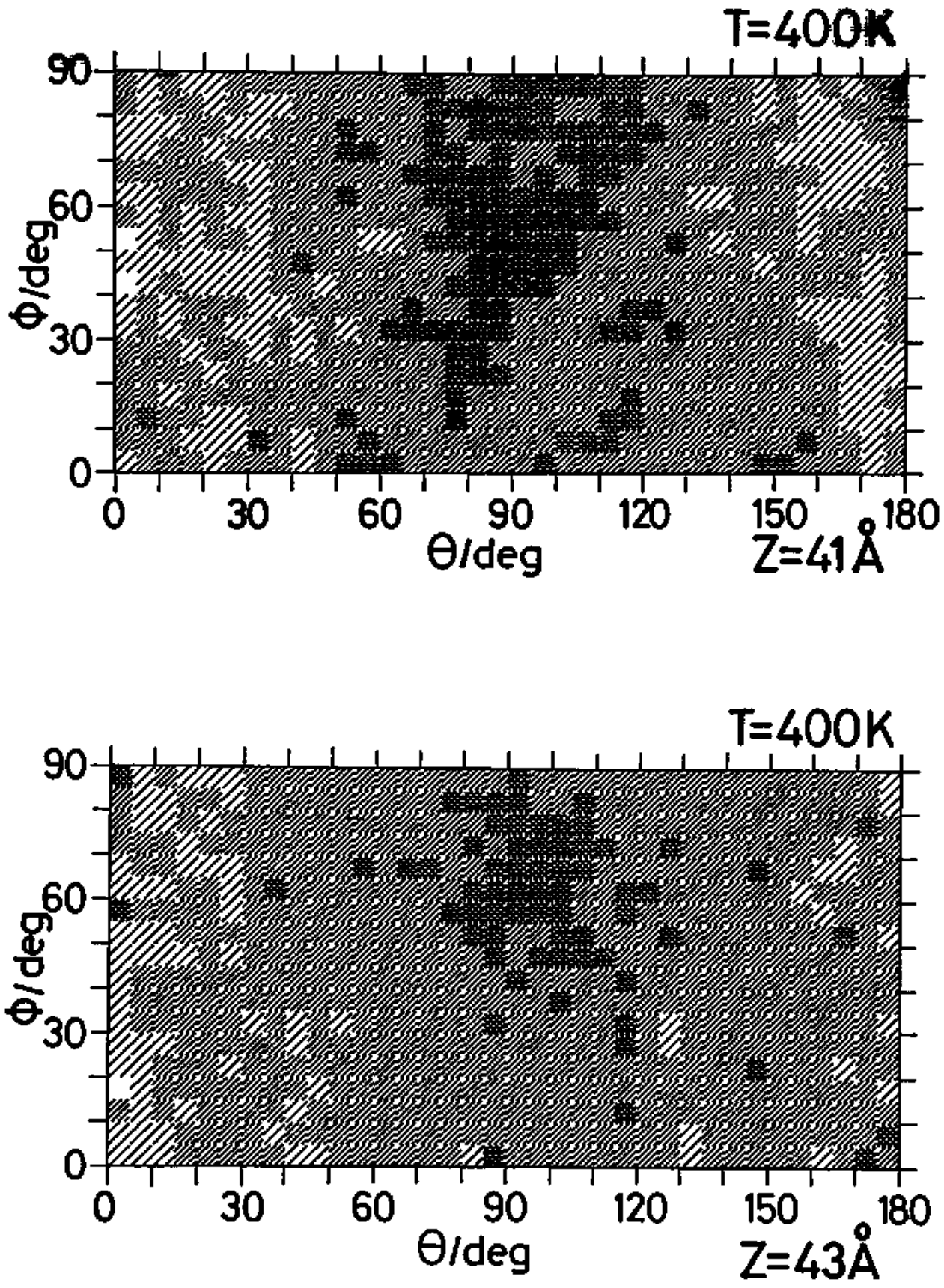

Fig. V-13. continued.

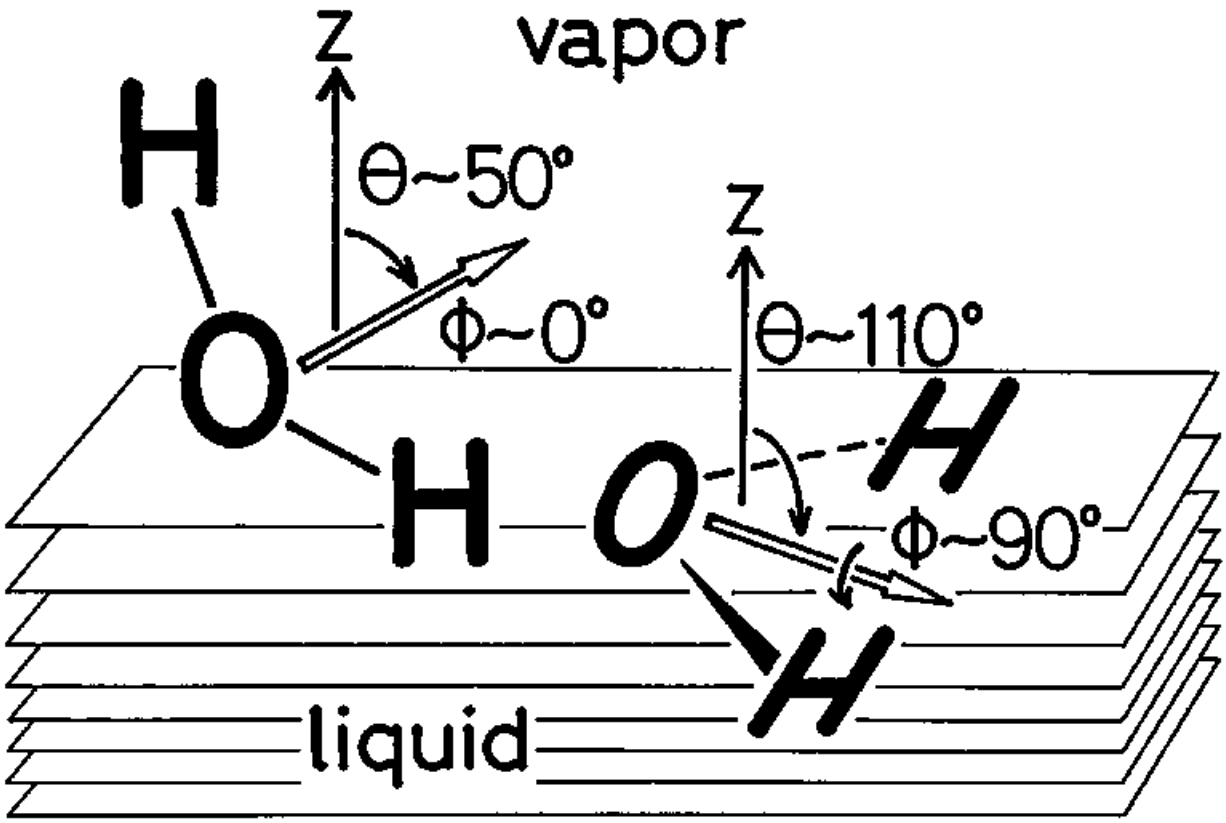

Fig. V-14.

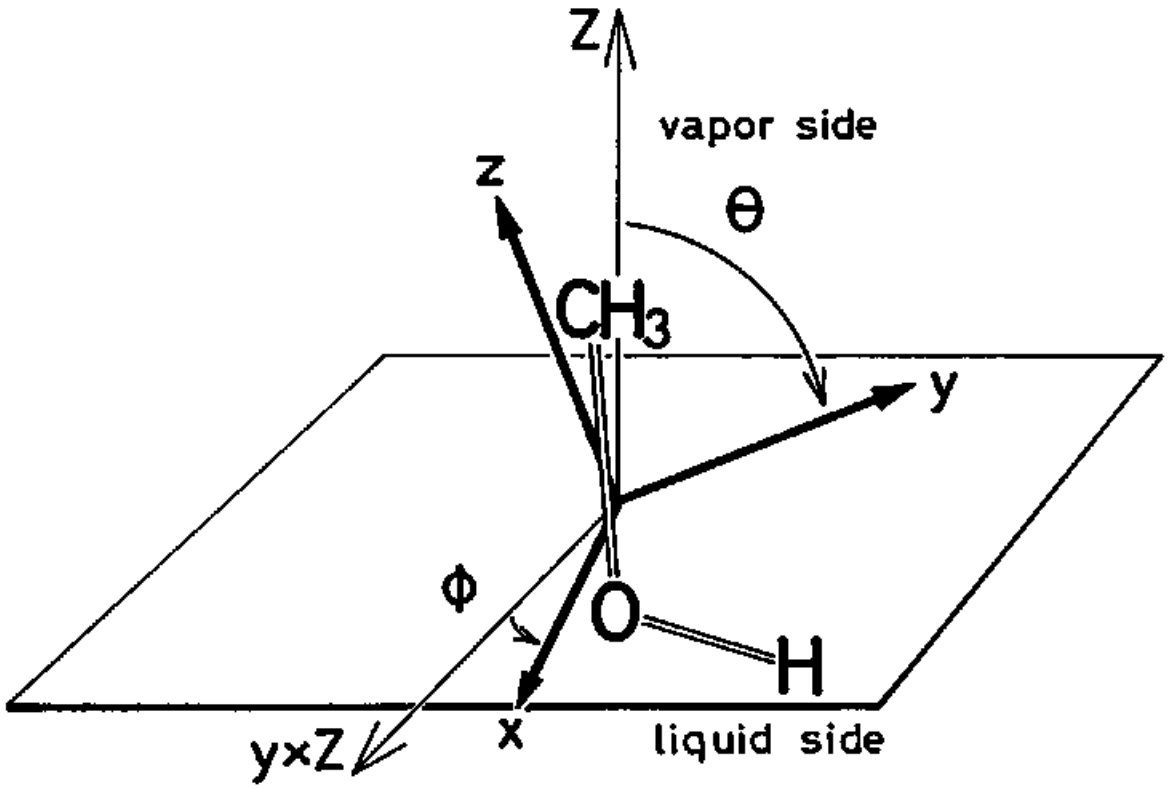

Fig. V-15.

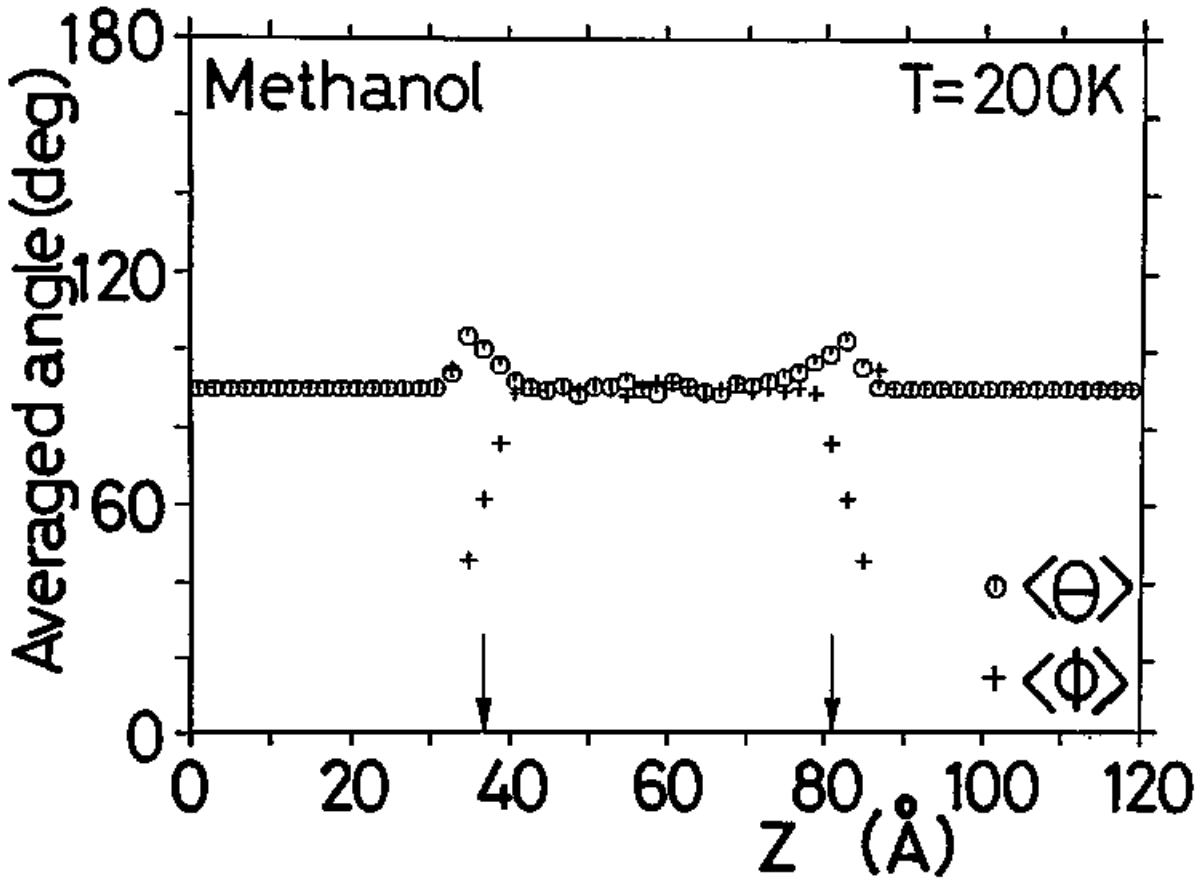

Fig. V-16. (1) T=200 K.

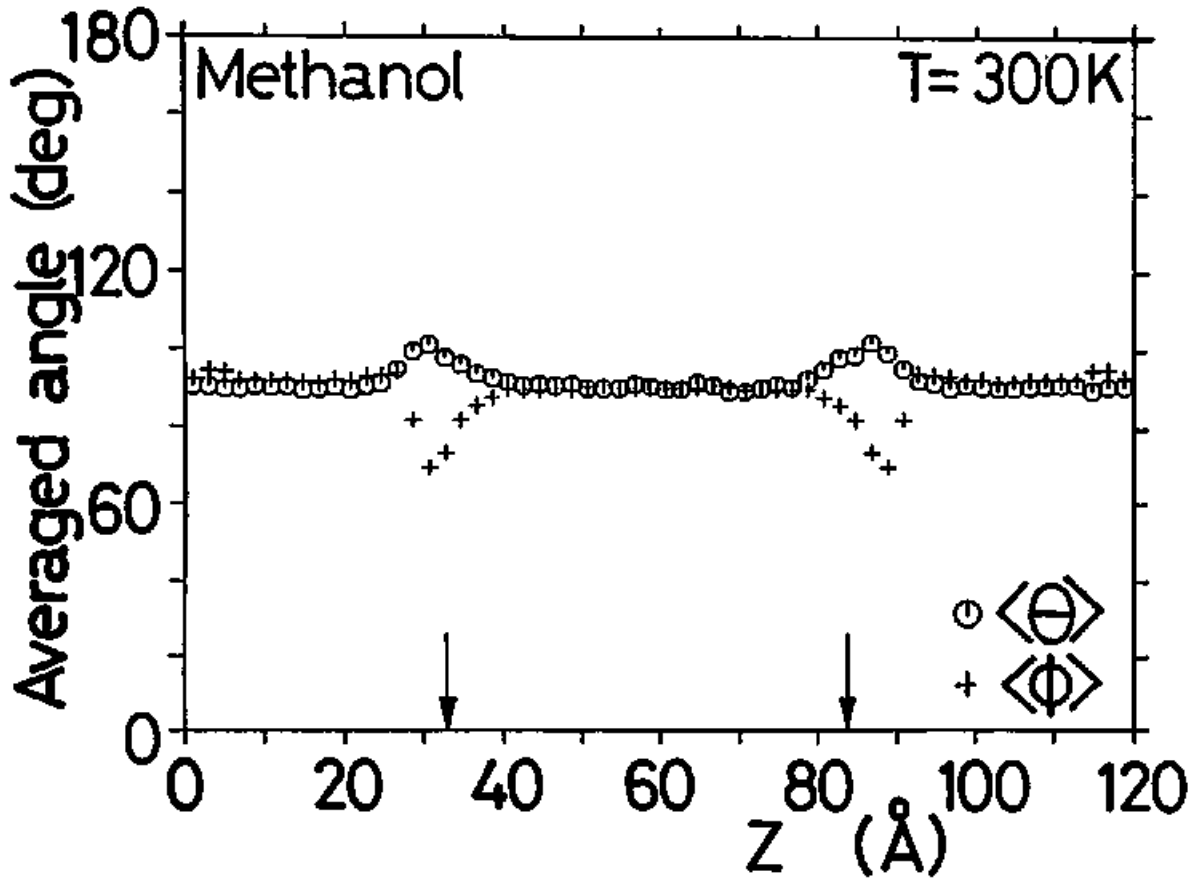

Fig. V-16. (2) T=300 K.

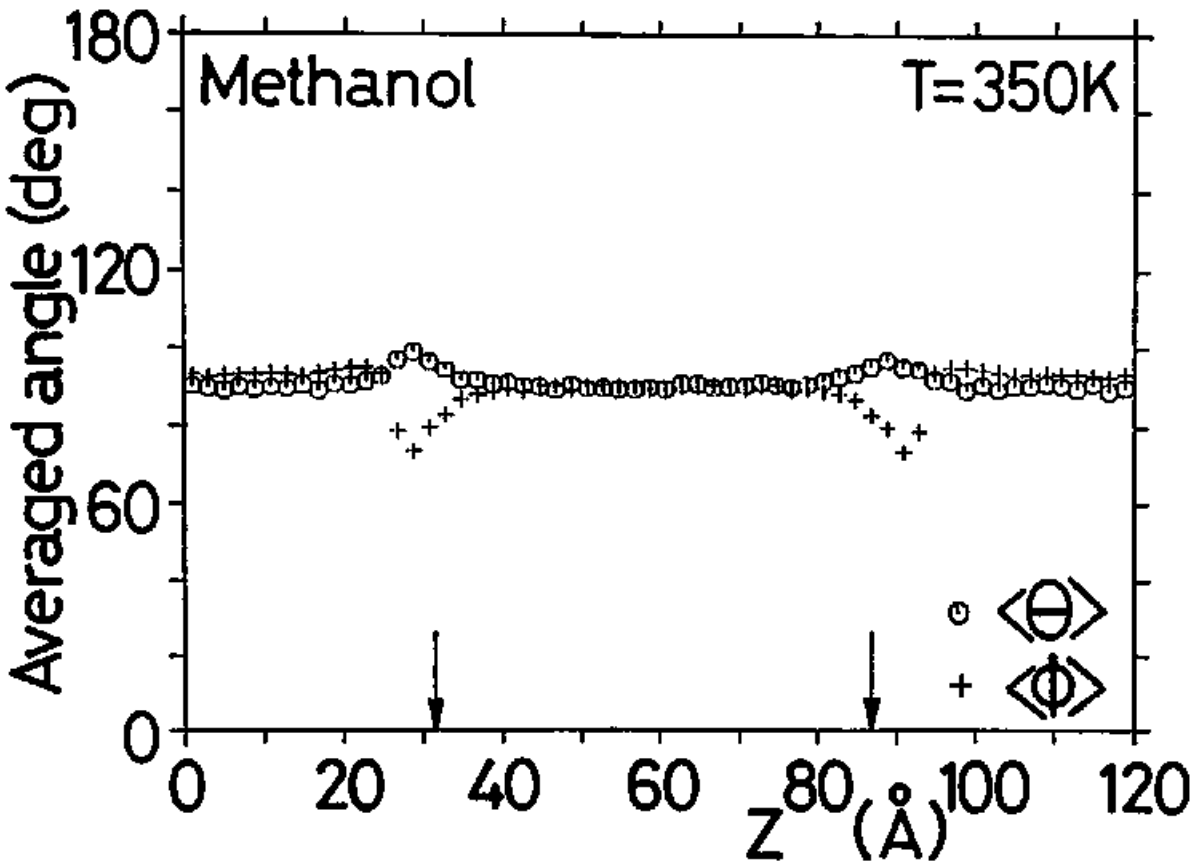

Fig. V-16. (3) T=350 K.

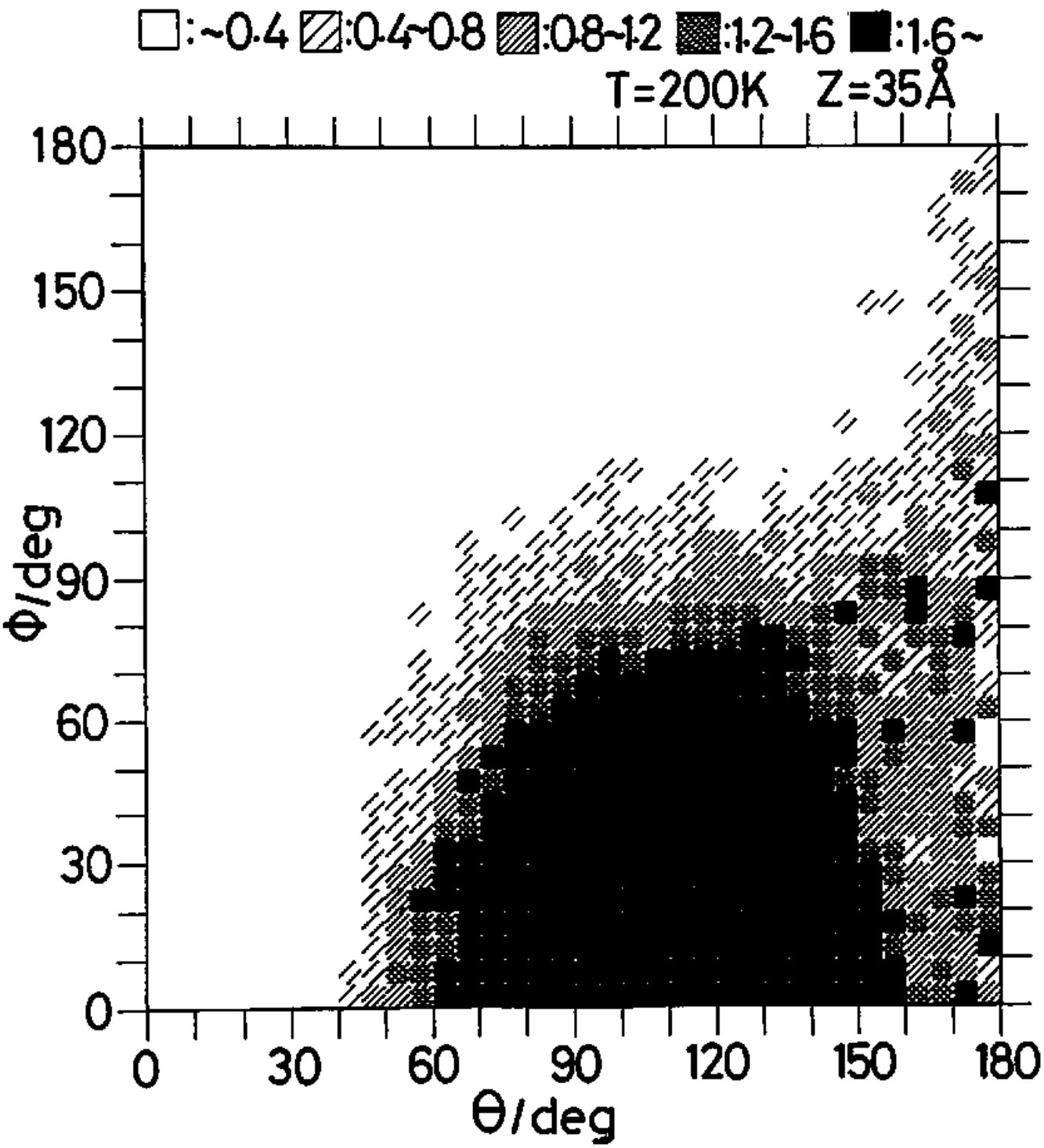

Fig. V-17. to be continued.

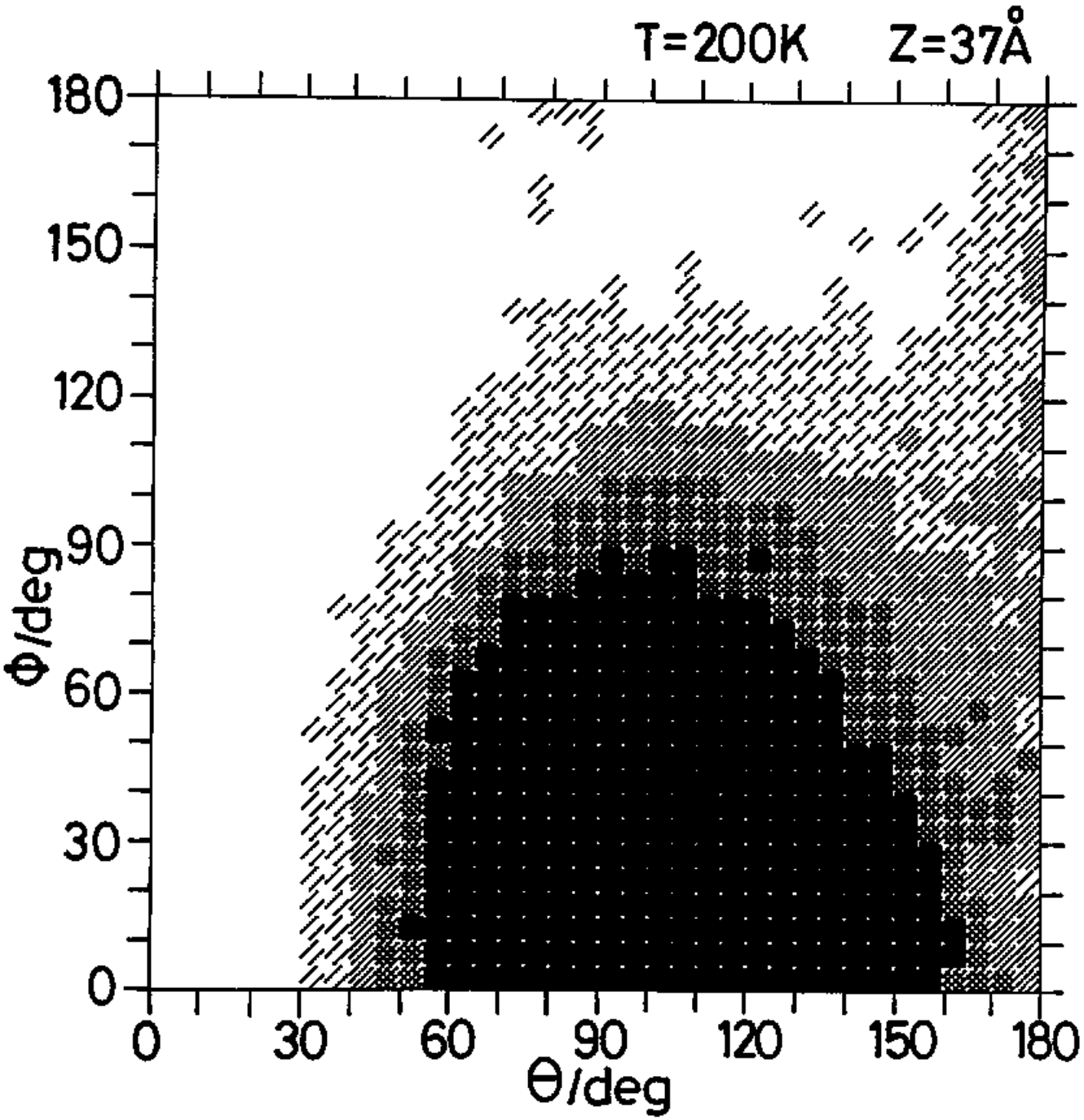

Fig. V-17. continued.

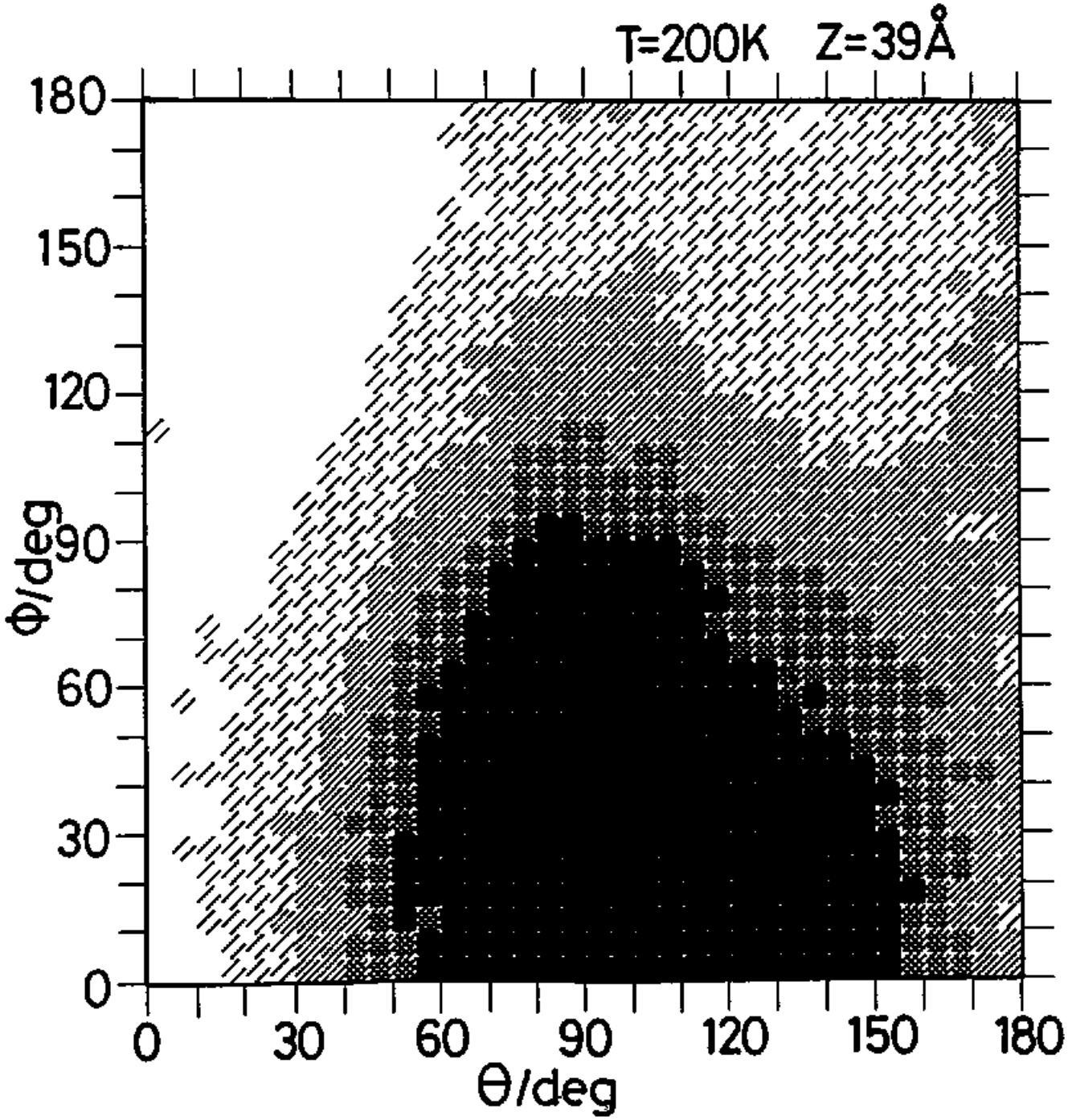

Fig. V-17. continued.

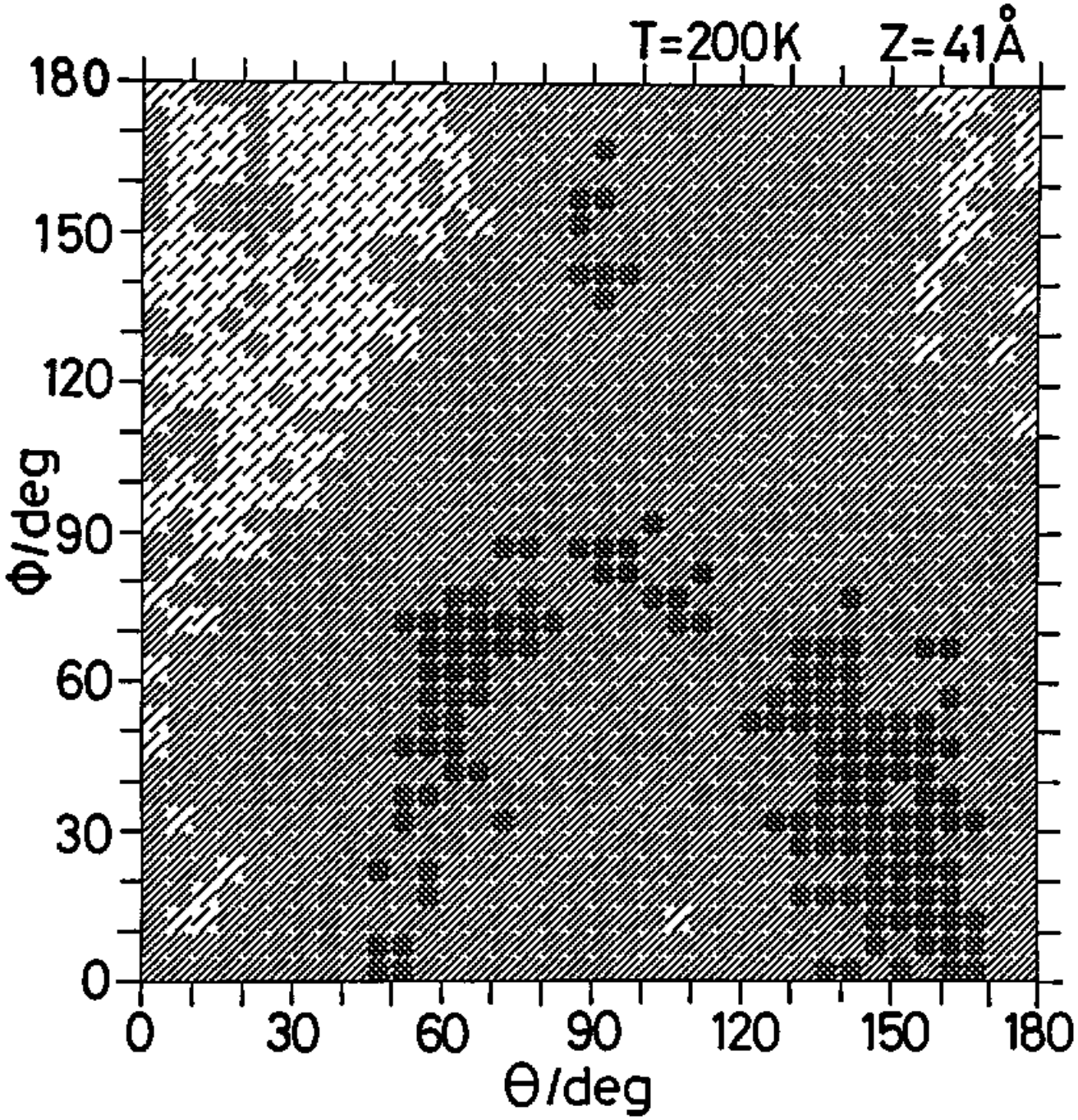

Fig. V-17. continued.

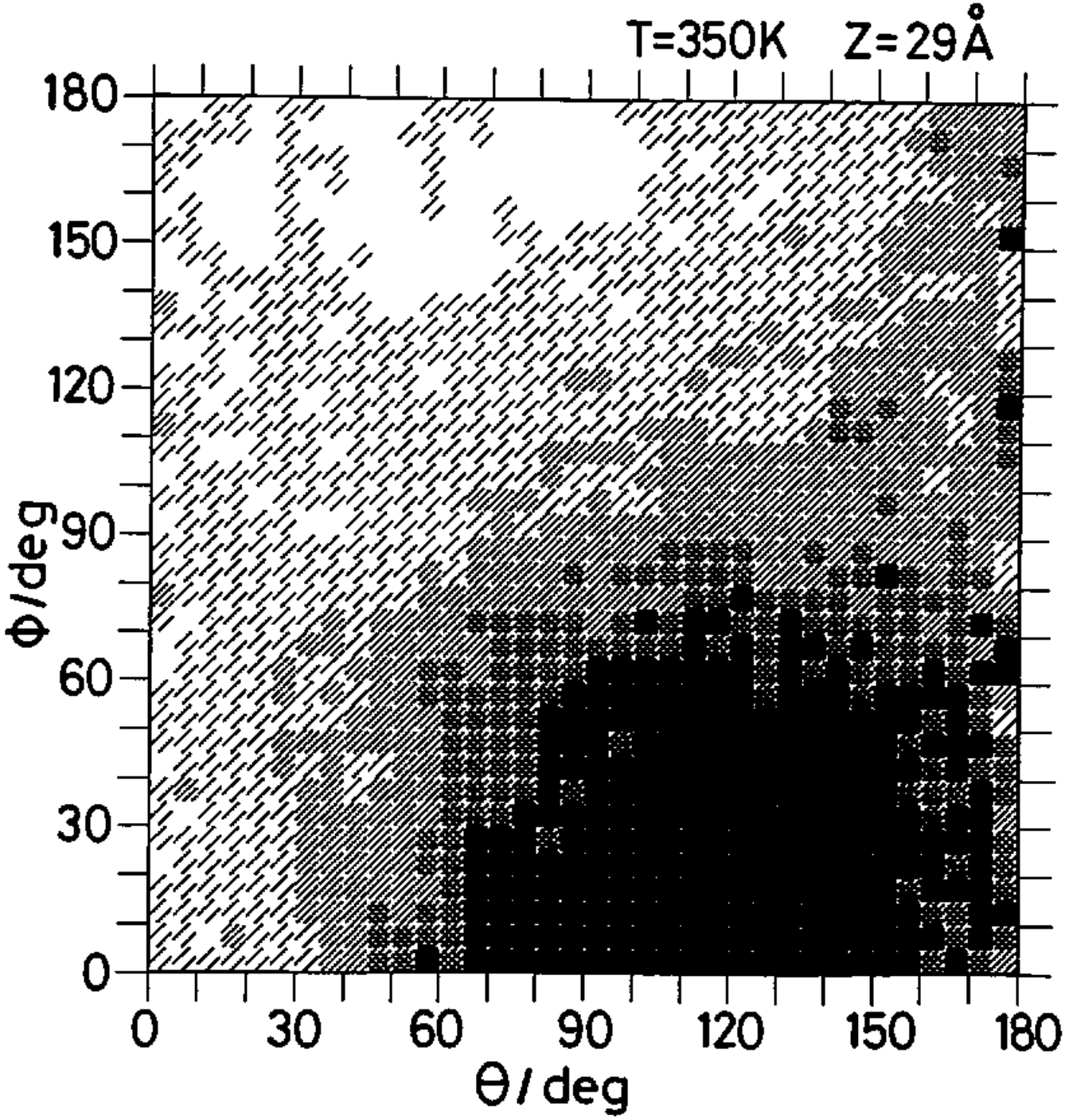

Fig. V-18. to be continued.

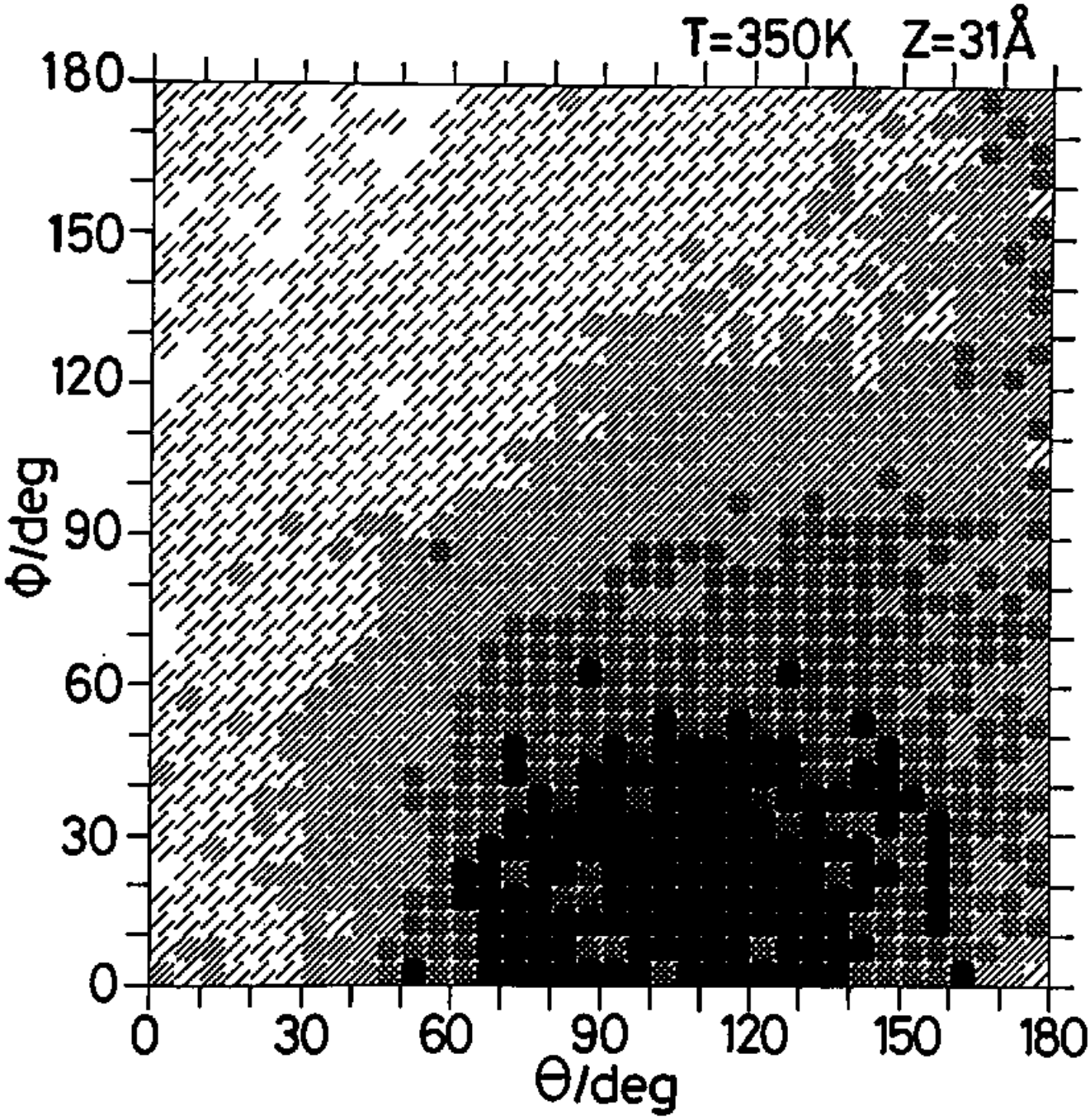

Fig. V-18. continued.

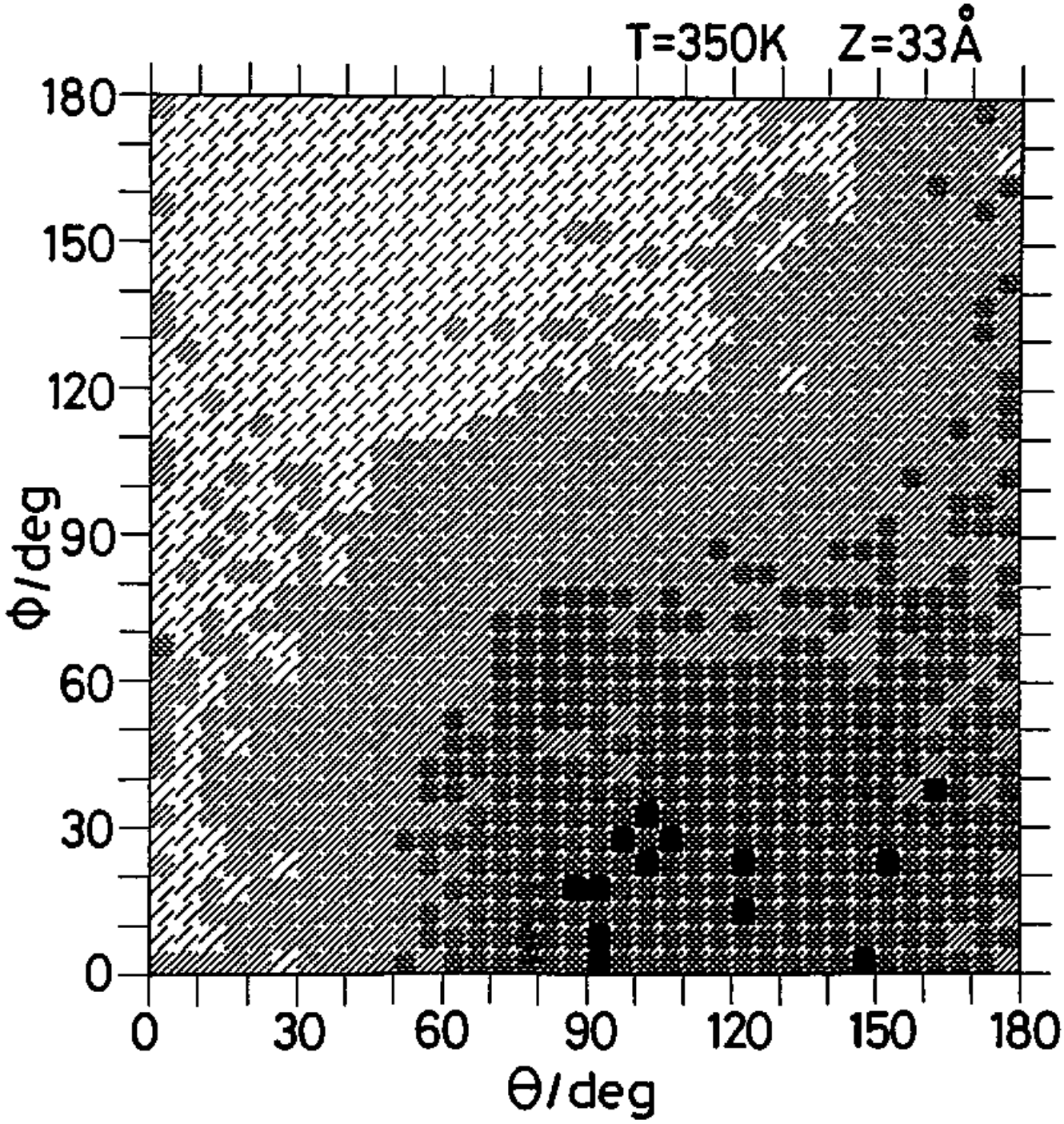

Fig. V-18. continued.

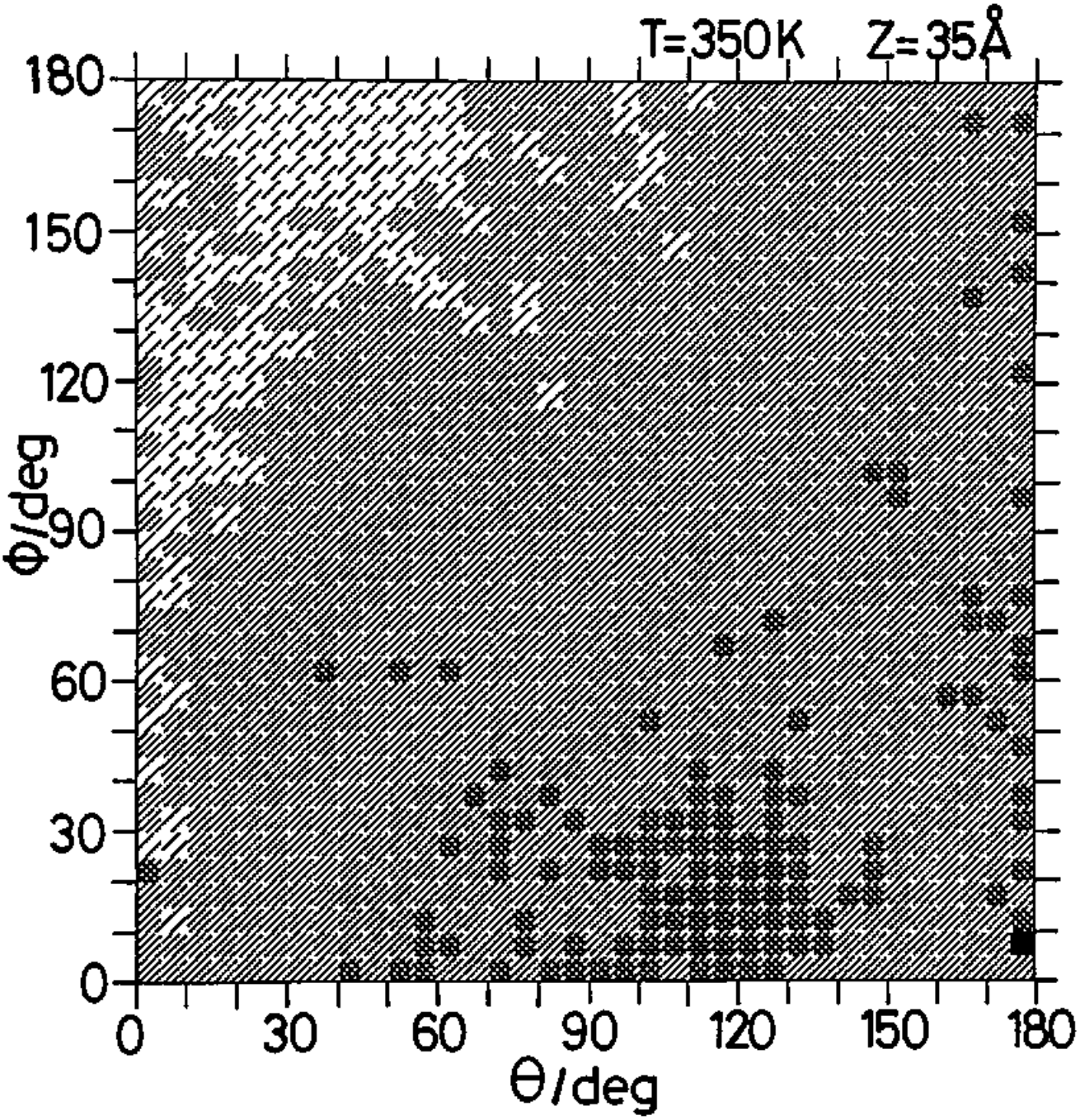

Fig. V-18. continued.

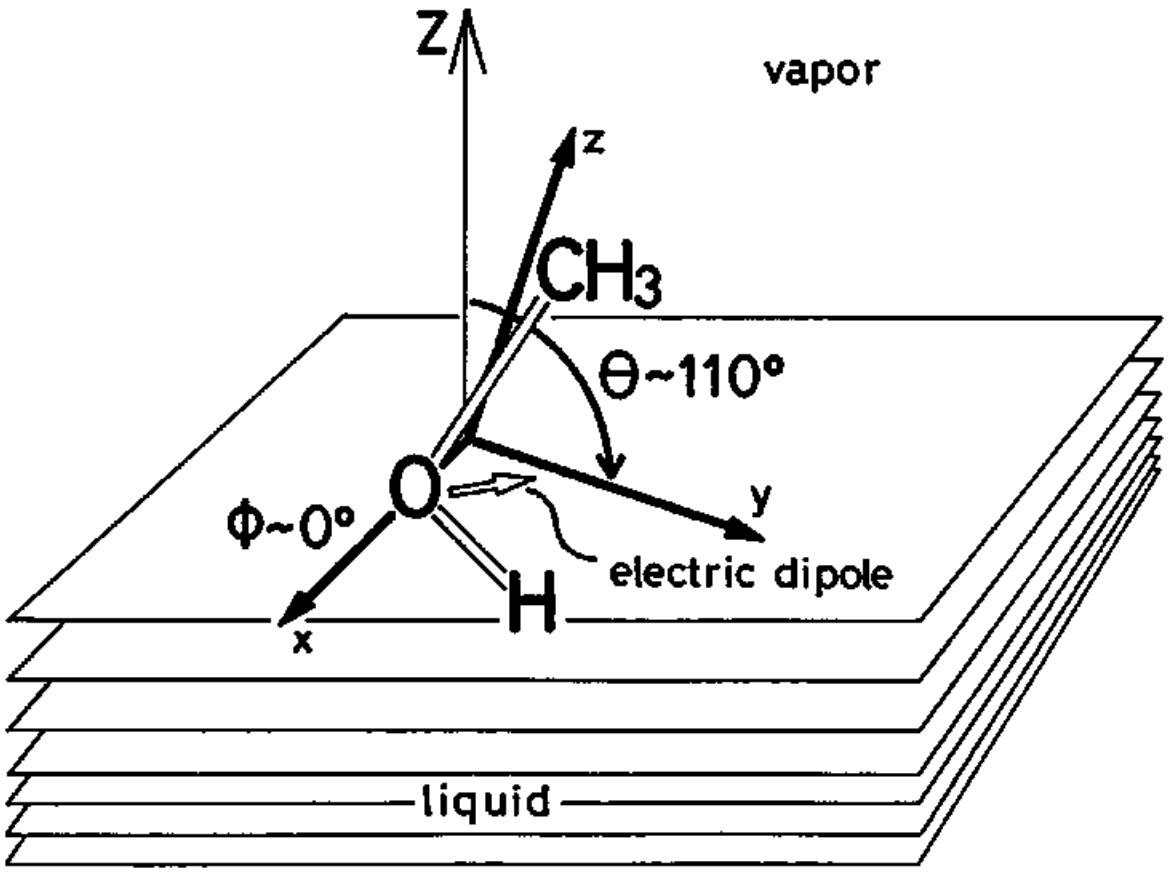

Fig. V-19.

VI

La mer sera très haute cette nuit.
La mer viendra la prendre avant toi...dépêche-toi!
Maurice Maeterlinck, PELLÉAS ET MÉLISANDE

The tide will be much rising this night.
The sea is going to take it away before you...hurry up!

Ⅵ. Discussion

Various discussions concerning the simulational results, including comparison with experimental works, are given in this section.

A. Local pressure tensor

In the previous section we calculated the surface tension γ using the local pressure tensor components P_n (normal) and P_t (tangential), Eq.(Ⅲ-7). One can ask now how the components themselves change as functions of position z. We show in Figs.Ⅵ-1, Ⅵ-2, and Ⅵ-3 some examples of the profiles of the pressure tensor components, $P_n(z)$ and $P_t(z)$. Although statistical fluctuation is rather large especially at high temperatures, $P_n(z)$ is smoother than $P_t(z)$; thermodynamics consideration tells us that $P_n(z)$ is constant because of the equilibrium condition of two phases if the surface is strictly flat. In practice, however, the capillary wave is exited on the surface, so $P_t(z)$ and $P_n(z)$ are a little bit mixed together. As to $P_t(z)$ it is obvious that it shows a deep valley near the surface, which represents the attractive interaction between molecules parallel to the surface and causes the surface tension.

We here defined the surface tension profile, $\gamma(z)$, as follows:

$$\gamma(z) = P_n(z) - P_t(z). \qquad (Ⅵ-1)$$

This $\gamma(z)$ indicates the strain forced near the surface; positive value of $\gamma(z)$ means the existence of attractive interaction between molecules and corresponds to the expanded region.[139] Figs.VI-4, VI-5, and VI-6 shows this $\gamma(z)$ for water, methanol, and LJ system, respectively. The surface of tension, which is the most strained region, lies more toward the liquid phase than does the Gibbs surface.[139] It is already well known that the compression region (negative $\gamma(z)$ region) appears just above the surface (vapor side of the surface) for LJ system, the reason of which is not clarified yet. The similar feature is also observed for water and methanol surface.

B. Surface Invariants

Egelstaff and Widom[158] discussed the possibility that the product of the isothermal compressibility κ and the surface tension γ of a liquid near its triple point is a fundamental length characteristic of the liquid. They showed data of various liquids and concluded that the value L, defined as

$$L = \kappa \gamma / 0.07, \qquad \text{(VI-2)}$$

is about 4 Å, which would correspond to the surface thickness or the core diameter; some examples are listed in Table VI-1. More recently Sanchez[159] developed this theory and presented a new empirical relation as follows:

$$\gamma \, (\kappa / \rho_l)^{1/2} = A_0^{1/2} \approx 0.26 \, (\varepsilon \sigma^2 / M)^{1/2}, \qquad \text{(VI-3)}$$

where ε and σ are the LJ potential parameters for the liquid, M the molecular weight; see Table VI-2 for some examples. We here study the applicability of these relations to our simulational results. For κ, we utilized the analytic formula of the equation of state, for CC water in Ref.141 and for LJ (argon) in Ref.151; as to the detail, see Appendix C. Unfortunately we can not find any available formula for κ of methanol.

The results are listed in Table VI-3. The temperature dependence of L for water is much different from that for LJ; as the temperature decreases to T_t, L of water increases rapidly, but L of LJ decreases slightly to the predicted value σ. The similar difference between water and LJ exists in the behavior of A_0 of Sanchez. Eq.(VI-3) predicts that $A_0^{1/2}$ equals to be 4.19 for water (ε=809.1 K, σ=2.641 Å and M=18.015 amu) and 1.40 for LJ (ε=119.8 K, σ=3.405 Å, and M=39.95 amu). The relation (VI-3) holds well for all simulated temperatures of LJ system, but it is not so good for water and a strong temperature dependence is observed, as moderately stated by Sanchez.[158]

C. Entropy lowering

As described in Sec. II, Good[114] collected surface excess entropy data of various substances near T_t, which include strongly hydrogen-bonding ones such as water and alcohols, and proposed that the small value of the surface entropy of water or methanol is caused by some molecular orientation near the surface probably due to hydrogen bonding. He showed that the averaged molar

surface entropy s^A, defined in Eq.(V-8), of nonpolar compounds is 24.4 J/Kmol (= 2.93 R, where R is the gas constant), that of polar nonhydrogen bonding compounds is 23.8 J/Kmol (=2.86 R), but that of strongly hydrogen bonding ones (water, methanol, etc.) is 10.8 J/Kmol (=1.30 R). From Tables V-4, V-5, and V-6, it is obvious that the results of our simulations agree quite well with the Good's statement; s^A is 1.3 R for water at T=300 K, 0.9 R for methanol at T=250 K, and 2.3 R for LJ system at T=80 K.

Good tried to explain this entropy lowering of 2.9 R - 1.3 R = 1.6 R by considering a deficit of entropy due to the completely oriented n layers as follows:

$$\delta s = nR\ln 2. \qquad \text{(VI-4)}$$

His result of δs=1.6 R gives the number of oriented layers n$\sim$2.3, from which he suggested that the orientational ordering continues at least deep into the third layer. Can this picture explain our simulational results ? In order to estimate the entropy deficit due to the orientational ordering, we calculated one-body excess entropy ΔS^1, statistical mechanically defined with the (θ, ϕ) distribution function, $P(\theta, \phi; z)$, as

$$\Delta S^1 = \int_{-\infty}^{\infty} dz \Delta s^1(z), \qquad \text{(VI-5)}$$

where $\Delta s^1(z)$ is the local excess entropy profile,

$$\Delta s^1(z) = -\frac{\rho(z)}{M} k_B \int\int d\theta\, d\phi \; [P(\theta, \phi; z)\ln P(\theta, \phi; z) - P_0 \ln P_0]$$

$$= -\frac{\rho(z)}{M} k_B[\langle \ln P(\theta, \phi; z)\rangle - \langle \ln P_0\rangle]. \qquad \text{(VI-6)}$$

Here $\rho(z)$ is the mass per unit volume at position z, M is the molecular weight, and P_0 represents the completely random distribution. In Figs. VI-7 and VI-8, some examples of $\Delta s^1(z)$ are shown. The lowering of entropy certainly occurs near the surface, but is also observed in the bulk liquid due to the statistical fluctuation of $P(\theta, \phi; z)$. To remove this fluctuational effect, we further estimated the bulk entropies (of liquid and vapor phase) from the local entropy and subtracted them from the value of the integration. The results are shown in Tables VI-4 and VI-5, where the total deficit of the excess entropy from that of the highest temperature, ΔS, is also listed.

For the case of water one can see that the contribution of the one-body term ΔS^1 is by order of magnitude smaller than the total entropy deficit ΔS. Good's simple explanation of entropy lowering by dipole-orientational ordering, therefore, cannot be accepted for water surface and the importance of many-body effects (more complicated structural ordering due to the hydrogen bonding network, etc.) is suggested. The detail of this is not known yet, but the phenomena analogous to the hydrophobic structure-making[15] probably occur. For example, ΔS_h (the hydration entropy) of apolar solutes at 25 ℃ is about -240 ~ -130 J/Kmol (-29 R ~ -15 R),[15] which is consistent with our result of ΔS^A = -2 R ~ -R (Table VI-4) of the liquid-vapor interface if one regards the vacuum as a "solute" and assumes that about 10 water molecules are in contact with one "solute"; notice that ΔS_h is the

entropy per mole of solute and ΔS^A is per mole of water.

It is quite different for the case of methanol. As pointed out in the previous section, the tendency of orientational ordering of methanol is so strong that the value of ΔS^1 is by an order of magnitude larger than that of water, and even at higher temperatures its magnitude does not decrease so much. When one consider the fact that the molar surface excess entropy s^A of methanol is by about R smaller than that of LJ, the value of $\Delta S^1{}^A \sim -0.5$ R (at T=200 K) suggests that the main cause of entropy deficit is this orientational ordering of molecules. In this sense water and methanol are quite different in surface properties, although they are both considered in a bunch as strongly hydrogen-bonding substances and they actually show similarly anomalous properties as bulk liquid. Comparison of $\Delta s^1(z)$ between methanol and water (Figs.VI-7 and VI-8) will make the difference more clear; the valley of entropy deficit is five times deeper for methanol than for water.

We showed in the former section that the surface profiles (density or energy profile) of methanol have no significant difference from those of simple fluids but its thermodynamic properties of surface are nearly as abnormal as water. From the above estimation of ΔS^1 we can attribute this unique feature of methanol to the molecular orientational ordering near the surface, as Good suggested. On the other hand the origin of the anomaly of water surface becomes more puzzling; in principle one have to take account of many body correlations, but the formulation and estimation are not so easy to be executed.

D. Ellipsometry and surface thickness

Apart from the recently developing x-ray reflectivity measurement,[153] ellipsometry is almost the only experimental approach to evaluate the surface thickness. In this technique one measures the polarization of the light reflected at the interface and estimates the surface thickness under some model assumption of dielectric constant (refractive index) profile, $\varepsilon(z)$, of the transition layer. A brief description is given in Appendix D. The problem is that one cannot exactly know $\varepsilon(z)$, which depends on the frequency of the incident light. Usually two step assumption is made as follows; (1) the density profile $\rho(z)$ takes some analytic form, i.e., hyperbolic tangent or error function etc., and (2) the Clausius-Mossotti formula is applicable for this transition layer:

$$\varepsilon(z)/\varepsilon_0 = \left[1+\frac{8\pi}{3}\frac{\rho(z)}{M}\alpha\right] \Big/ \left[1-\frac{4\pi}{3}\frac{\rho(z)}{M}\alpha\right], \qquad \text{(VI-7)}$$

where α is the molecular polarizability and ε_0 is the dielectric constant of the vacuum. How appropriate are these assumptions? While it is impossible to investigate the applicability of the Clausius-Mossotti formula with computer simulation, it is a easy task to look into the assumption of $\rho(z)$ because we know "exact" density profile from simulation.

Another problem is the possibility to detect experimentally the anisotropy of $\varepsilon(z)$ due to the molecular orientational ordering near the surface. If molecular polarizability tensor α_{ij} is known, components of the anisotropic $\varepsilon(z)$, $\varepsilon_{\parallel}$ (parallel component) and $\varepsilon_{\perp}$ (normal component), can

be in principle expressed with the orientation distribution $P(\theta, \phi; z)$; see Appendix D.

As to the case of water, the molecular polarizability is measured by Murphy[160] for the light of wave length λ=5145 Å:

$$\alpha_{xx} = 1.528\times10^{-24}\ \text{cm}^3 \quad \text{in electrostatic unit,}$$
$$\alpha_{yy} = 1.415\times10^{-24}\ \text{cm}^3, \qquad \text{(VI-8)}$$
$$\alpha_{zz} = 1.468\times10^{-24}\ \text{cm}^3,$$

which suggests that the anisotropy of water molecules is not so strong in view of the polarizability. We calculated the coefficient of ellipticity $\bar{\rho}$ in three different manners; (1)to assume that $\rho(z)$ is tanh form and that $\varepsilon(z)$ is isotropic, (2) to assume that $\varepsilon(z)$ is isotropic but to use the simulation data of $\rho(z)$, and (3) to use the simulation data of $\rho(z)$ and $P(\theta, \phi; z)$ so that $\varepsilon(z)$ is anisotropic. The results are listed in Table VI-6. The calculated ε_l, the dielectric constant (refractive index for light of λ=5145 Å) of liquid phase, is a little smaller than the experimental value, which reflects the fact that the simulated density of bulk liquid is lower than that of the real water. Three $\bar{\rho}$'s, named Iso.+Tanh, Iso., and Aniso., according to the assumptions described above, give almost the same value; Iso.+Tanh, however, shows a slightly larger value near the room temperature. The last tree columns of Table VI-6 show the 10-90 surface thickness t_d^{el} evaluated from these $\bar{\rho}$'s under the tanh assumption:

$$\bar{\rho} = \frac{\pi}{\lambda}\,\frac{t_d^{el}}{4.394}\sqrt{\varepsilon_v + \varepsilon_l}\,\ln\frac{\varepsilon_l}{\varepsilon_v}. \qquad \text{(VI-9)}$$

While Iso. and Aniso. give almost the same thicknesses, Tanh. again gives a larger result near the room temperature. Since the usual experimental approach is similar to this Iso. calculation, we compare t_d^{el} (Iso.) with t_d (thickness of density profile) and t_u (thickness of energy profile) in Fig. V-2. It is obvious that t_d^{el} is much smaller than t_d, which suggests that the usual experimental analysis under the assumption of tanh form, Eq.(VI-9), may fail for water surface due to the misfit of $\rho(z)$ to the tanh function, as previously stated. The anomalous smallness of the thickness which Beaglehole suggests[1] may be explained in this way. As to the anisotropic effect, it is probably impossible to experimentally detect it because t_d^{el} of Aniso. and that of Iso. are nearly the same. Another fact one can notice is the increase of $\overline{\rho}$ near T=250K. Kizel'[161] studied various organic compounds by the ellipsometric technique and found the similar peculiar raise of $\overline{\rho}$ near the freezing point for several types of liquid. He considered this phenomenon as "preparation for solidification", which may hold true in this case. Concerning the experimental values of $\overline{\rho}$, readers may refer to Ref.162 and references therein (Table VI-7); the agreement with our result seems good.

For methanol, reliable values of α_{ij} are not known yet, so we use orientational averaged value of Bridge and Buckingham,[163]

$$\overline{\alpha} = 3.31\times10^{-24}\ \mathrm{cm}^3 \text{ for } \lambda = 6328\ \text{Å}. \qquad \text{(VI-10)}$$

The results of ε_1, ρ, and t_d^{el} are listed in Table VI-8. The t_d^{el} is almost

equal to t_d, see Fig. V-8. This fact suggests that the assumption of tanh type $\rho(z)$ is quite good, which is already expected from the fitting result of $\rho(z)$, Fig. V-6. Kizel' experimentally obtained $\overline{\rho}=4.6\times10^{-4}$ for methanol near room temperature, which does not differ so much from our estimation.

We used the value[12] $\alpha=1.642\times10^{-24}$ cm^3 for the LJ (argon) system. The results are listed in Table VI-9. The good agreement between calculated and observed values of ε_l suggests the applicability of the Clausius-Mossotti formula. Both thicknesses, t_d and t_d^{el}, are in good agreement (Fig. V-4), which shows the tanh function is well fitted to $\rho(z)$. For experimental values, see Table VI-10; larger values than our result suggests the effect of capillary wave.

E. Surface potential

When molecules having electric dipole take some orientational ordering near the surface, we can expect that they make an electrical double layer and induce electrostatic potential difference between liquid and vapor phases, which is called the surface potential. Assume that molecules with dipole moment μ exist in a layer of thickness Δ. When the number density is n and the averaged orientation is $\langle\cos\theta\rangle$ (θ is defined as described in Sec. V-C), the following electric potential difference between both sides of the layer is generated:

$$\chi_\Delta = (\Delta\mu/\varepsilon_0)\, n \langle\cos\theta\rangle, \qquad \text{(VI-11)}$$

where ε_0 is the dielectric constant of the vacuum. The summation, or the integral of χ_Δ gives the surface potential χ, the potential of liquid phase ($z=+\infty$) relative to its bulk vapor phase ($z=-\infty$) is expressed as follows:

$$\chi = \mu / \varepsilon_0 \int_{-\infty}^{\infty} dz \, [\rho(z)/M] \langle \cos\theta \rangle_z, \qquad \text{(VI-12)}$$

where $\rho(z)$ is the mass per unit volume and M is the molecular weight, so $\rho(z)/M$ represents the number density profile. A more detailed and general derivation of χ is given in Appendix E.

The μ of CC water is evaluated to be 7.082×10^{-30} Cm = 2.12 D from the charges and molecular shape; one of experimental values is 1.855 D.[12] The result of the calculation is listed in Table VI-11. The positive values of χ mean that the dipole of water tends to point inwards (into liquid phase). The detail is, however, more complicated because there exist two different orientational tendencies, as described in Sec. V-C. It is shown in Fig. VI-9, examples of the electric potential profile $\chi(z)$ defined as

$$\chi(z) = \mu / \varepsilon_0 \int_{-\infty}^{z} dz \, [\rho(z)/M] \langle \cos\theta \rangle_z. \qquad \text{(VI-13)}$$

The inner (liquid) phase is certainly positive (relative to the vapor phase), but, as expected, the slight negative part exists in the vapor side of the transition layer, which corresponds to the orientation with one hydrogen atom projecting towards the vapor. The temperature dependence of χ is as expected from the result of orientational ordering described in Sec. V-C,

i.e., χ decreases rapidly with increase of the temperature, and at T<300K χ seems to be saturated.

The experimental evaluation of χ is an important problem in analytical chemistry and electrochemistry when one tries to divide the free energy of hydration of ions into "chemical" contribution due to short-range interactions and electrostatic long-range contribution. The χ is not a directly measurable quantity since one can only estimate it through subtracting the chemical free energy change, calculated from theoretical consideration based upon various solvation models, from the free energy change measured by such as the Kenrick-Frumkin method[165] (measurement of total work needed to put a test charge from one phase to another). As a result of such model calculation, even the sign of χ has long been controversial[166] since Frumkin et al.[167] gave the conclusion of $\chi \sim +0.1 - +0.2$ V. Schiffrin[168] evaluated the temperature derivative of χ and found $d\chi/dT = -0.39 \pm 0.04$ mV/K at T=25 ℃, which suggests χ is positive because χ is expected to approach to zero as temperatures rise to T_c. Their estimation qualitatively agrees with our result. Conversely saying, the result of computer simulation can be used to estimate the validity of assumptions in calculating the chemical contribution of the ionic hydration. More recent experiments seem to support our result ($\chi \sim +0.1$ V).[169]

For methanol the dipole moment μ evaluated from partial charges of TIPS model is 7.36×10^{-30} Cm; one of experimental values[12] is 5.67×10^{-30} Cm. The result of calculation is listed in Table VI-12. The negative value of χ means that the dipole of methanol tends to point outwards (into vapor phase), but its absolute value is much smaller than that of water, which suggests

that the dipole is almost parallel to the surface. Even at higher temperatures ($T \gtrsim 300$ K) χ remains nonzero, which reflects the strong orientational tendency due to the hydrophobic groups, as already discussed. We show in Fig.VI-10 examples of potential profile $\chi(z)$, which is almost monotonic for methanol since there exists only one typical orientation.

Unfortunately we could not find any experimental studies of the surface potential measurement of methanol to be compared with our simulational results. It will be of great interest to compare the temperature dependence of χ between water and methanol, although we expect that the absolute value of χ of methanol is very small and measurement of it will be rather difficult.

F. Effect of free ions on surface potential

In liquid water there exist free ions, H^+ (H_3O^+) and OH^-, produced by the dissociation as

$$2H_2O \rightleftharpoons H_3O^+ + OH^-,$$

the concentration of which is $[H_3O^+]=[OH^-] \approx 10^{-7}$ mol/l. Since the electrostatic potential is screened by these ions, surface potential χ will become smaller, which is schematically shown in Fig.VI-11. In this subsection we roughly estimate the effect of ions.

The electrostatic potential made by free ions, $\phi(z)$, is related to the number density of free ions, $n_+(z)$ and $n_-(z)$, by the Poisson equation:

$$d^2\phi/dz^2 = -[e/\varepsilon(z)][n_+(z)-n_-(z)], \qquad \text{(VI-14)}$$

where e is the elementary charge and $\varepsilon(z)$ is the static dielectric constant. Total potential is the sum of the original $\chi(z)$ and this $\phi(z)$, which is related to the density $n_\pm(z)$ by the Boltzmann distribution,

$$n_\pm(z) = \alpha n(z)\exp[\mp(e/k_BT)\{\phi(z)+\chi(z)\}], \qquad \text{(VI-15)}$$

where n(z) is the number density of molecules and α is the dissociation rate. Coupling Eqs.(VI-14) and (VI-15) together one obtains the Poisson-Boltzmann equation:

$$d^2\phi/dz^2 = [2e/\varepsilon(z)]\alpha n(z)\sinh[(e/k_BT)\{\phi(z)+\chi(z)\}]. \qquad \text{(VI-16)}$$

Given $\varepsilon(z)$, n(z), and $\chi(z)$, we can solve this equation for $\phi(z)$ under the following boundary condition:

$$d\phi/dz\,|_{z\to-\infty} = d^2\phi/dz^2\,|_{z\to-\infty} = 0. \qquad \text{(VI-17)}$$

The real surface potential χ_{total} is expressed as

$$\chi_{total} = \phi(\infty) + \chi(\infty). \qquad \text{(VI-18)}$$

We need some assumption of $\varepsilon(z)$, for which we adopt simple linear

combination of ε of bulk phases.

The result of numerical integration, which is executed with the leap-frog method, is shown in Table VI-13, from which it is concluded that we can completely neglect the effect of free ions on χ. When one considers the phenomena such as surface adsorption of other ions, however, these screening effect cannot be neglected, of course.

G. Origin of the orientational structure

The origin of the orientational ordering near the surface, in principle a result of the anisotropic interaction between molecules, can be sought in two different ways; one is the picture where the electric multipoles are interacting, and the other is the one where the hydrogen bonding plays an important role. For the former, Gubbins and his co-workers,[111,112] and Tarazona and Navascués[113] have developed the perturbation theory and the integro-differential theory for liquid-vapor interface of simple polar fluids (e.g., the Stockmayer model), and found that dipoles (and quadrupoles also) have the effect to align the molecules; the preferred orientation is the one parallel to the surface at its liquid side and the one perpendicular at the vapor side. This conclusion qualitatively agrees with our result of water, though the effect of more higher-order multipoles will not be estimated so easily in these approaches. For the hydrogen-bonding picture, Lee et al.[170] executed MD simulation of water (ST2 model) near flat hydrophobic walls and proposed the picture of "dangling" hydrogen bonds; i.e., a water molecule prefers to take the orientation with one potentially hydrogen-bonding group

toward the wall to balance the minimization of the energy and the maximization of the density. The similar result (formation of an aligned ice structure) is obtained by Valleau et al.[171] for TIPS2 water model[172] near inert hard walls. Linse[173] reported the Monte Carlo simulation of benzene-water liquid-liquid interface and found the preferred alignment of water dipoles parallel to the surface and the reinforcement of the hydrogen bonding. We have not studied the detailed character of hydrogen bonding network in this work, but believe that the similar explanation holds true for the liquid-vapor interface, contrary to the expectation[170] that the orientational preference would not be observed for these less regular surfaces.

The picture of hydrogen bonding can better explain the origin of orientational ordering of methanol. The fact that the methyl group can not take part in hydrogen bonding causes the orientation that the methyl group is put out to vapor phase to be energetically stabilized. One question arises now why two different orientations exist for water case; both the lying-down orientation (liquid side) and the standing orientation (vapor side) are the one which three hydrogen bonds are possible at the sacrifice of one hydrogen bond, but the standing orientation makes the electric double layer and becomes energetically less stabilized than lying-down orientation. Although the detailed analysis has not been done yet, we feel that the key is the entropy. It is well known[16] that the interaction potential changes more mildly for oxygen side than for hydrogen side; in other words, a slight change of direction of a hydrogen bond causes a drastic potential rise for hydrogen, but does not for oxygen. In order to show it we make a minimum

potential surface (Fig.VI-12); it is the surface at the distance proportional to the value of interaction potential minimum when one put another molecule at a position toward the direction from the center of mass. It is obvious that the surface is more sharp-pointed near the hydrogen atoms than near the oxygen atom (lone pair), which suggests that it is entropically preferable for a water molecule to make a hydrogen bond using its oxygen site than using its hydrogen site. In bulk phases, of course, this is not true because one must consider the fact that the companion molecule uses its hydrogen site. When we consider the preferable orientation at the interface, however, it may be enough to look at the entropy of one molecule; the standing orientation, which sacrifices one hydrogen bond with its hydrogen atom, is entropically more favorable than the lying-down one, which sacrifices a bond with its lone pair.

Table VI-1. Values of the product of isothermal compressibility κ and surface tension γ for various liquids at or near T_t. The data are taken from Ref 158.

	γ (dyn/cm)	κ ($10^{-10}Pa^{-1}$)	$\gamma\kappa/0.07$ (Å)
Ar	13.1	21.2	3.97
Xe	18.7	16.6	4.43
N_2	11.8	21.1	3.56
O_2	18.4	12.0	3.15
Water	76	5.0	5.43
Ethanol	23	11.2	3.68
Benzene	29	9.4	3.89
Aniline	43	4.5	2.76

Table VI-2. Values of $A_0^{1/2}=\gamma(\kappa/\rho_l)^{1/2}$ and $0.26(\varepsilon\sigma^2/M)^{1/2}$ for various liquids according to Eq.(VI-3). The data are taken from Ref.159.

Substance	T (℃)	$A_0^{1/2}$ [10^{-4}(erg cm^2/g)$^{1/2}$]	$0.26(\varepsilon\sigma^2/M)^{1/2}$ [10^{-4}(erg cm^2/g)$^{1/2}$]
Ar	-188	1.38	1.28
H_2	-255	3.18	3.64
N_2	-196	1.78	1.58
O_2	-183	1.76	1.50
CO_2	0	1.90	1.97
NH_3	-140	3.97	3.95
Water	20	4.94	4.19
	120	4.21	
Methane	-163	3.15	2.70
Methanol	0	2.76	3.33
	50	2.80	
Benzene	20	2.99	2.91

Table VI-3. Invariants of the liquid-vapor interface of water and LJ system; L is defined by Egelstaff and Widom[158] as $L=\kappa\gamma/0.07$, and $A_0^{1/2}$ is defined by Sanchez[159] as $A_0^{1/2}=\gamma(\kappa/\rho_l)^{1/2}$. where κ is the isothermal compressibility (here calculated from the equation of state), γ the surface tension, and ρ_l the bulk liquid density. For water there are two types of the equation of state[141]. G-EOS (general type) and L-EOS (for liquid state).

system	T (K)	κ (10^{-10}Pa^{-1})	γ (dyn cm^{-1})	ρ_l (10^{-4}g cm^{-3})	L (Å)	$A_0^{1/2}$ (erg cm^{2}g^{-1})$^{1/2}$
water	400	16.2 (G-EOS)	11.7	0.756	2.71	1.71
		17.4 (L-EOS)			2.86	1.78
	350	12.1 (G-EOS)	18.7	0.820	3.23	2.27
		12.4 (L-EOS)			3.31	2.30
	300	11.2 (G-EOS)	30.5	0.860	4.88	3.48
		13.0 (L-EOS)			5.66	3.75
	275	11.0 (G-EOS)	41.0	0.868	6.44	4.62
		17.3 (L-EOS)			10.13	5.79
	250	11.3 (G-EOS)	36.7	0.874	5.92	4.17
		81.5 (L-EOS)			42.73	11.21
LJ	120	68.5	5.89	1.15	5.76	1.44
	100	33.5	9.59	1.29	4.59	1.55
	80	17.5	14.34	1.42	3.59	1.59

Table VI-4. Decrease of entropy due to the orientational ordering of a water molecule. ΔS^1 is the one-body excess entropy defined by Eq.(VI-5), and ΔS is the entropy deficit, the difference between s_g at that temperature and s_g at the highest temperature T=400 K. A is the molar area similar to the one in Eq.(V-9).

T (K)	ΔS^1 (erg $K^{-1}cm^{-2}$)	$\Delta S^1 A$ (R)	ΔS (erg $K^{-1}cm^{-2}$)	ΔSA (R)
400	-0.0025±0.0005	-0.023	0	0
350	-0.0038±0.0001	-0.033	-0.001	-0.10
300	-0.0085±0.0002	-0.072	-0.043	-0.52
270	-0.0058±0.0002	-0.049	-0.114	-1.12
250	-0.0030±0.0003	-0.025	-0.246	-2.23

Table VI-5. The same as Table VI-4 for methanol.

T (K)	ΔS^l (erg $K^{-1}cm^{-2}$)	ΔS^l_A (R)	ΔS (erg $K^{-1}cm^{-2}$)	ΔS_A (R)
350	-0.0069±0.0002	-0.106	0	0
300	-0.0143±0.0003	-0.207	-0.021	-0.11
250	-0.0262±0.0005	-0.359	-0.025	-0.10
200	-0.0356±0.0003	-0.466	-0.031	-0.11
160	-0.0333±0.0002	-0.421	-0.091	-0.69

Table VI-6. The dielectric constant of bulk liquid ε_l, the ellipticity coefficient $\overline{\rho}$, and the surface thickness t_d^{el}. The calculated ε_l is from the Clausius-Mossotti formula, Eq.(VI-7). The experimental value of ε_l is estimated with third order extrapolation of the data (for λ =5893 Å) in Ref.53. ε_0 is the dielectric constant of the vacuum. Three different ways of calculation of $\overline{\rho}$ and t_d^{el} are described in the text.

	$\varepsilon_l/\varepsilon_0$		$\overline{\rho}$			t_d^{el}(Å)		
T(K)	Calc.	Obs.	Iso.+Tanh	Iso.	Aniso.	Tanh	Iso.	Aniso.
400	1.553	1.716	7.80×10^{-4}	8.03×10^{-4}	8.00×10^{-4}	7.99	8.23	8.11
350	1.609	1.750	6.15×10^{-4}	6.32×10^{-4}	6.27×10^{-4}	5.77	5.93	5.87
300	1.645	1.774	5.79×10^{-4}	4.71×10^{-4}	4.63×10^{-4}	5.15	4.19	4.11
275	1.653	1.780	4.51×10^{-4}	3.88×10^{-4}	3.81×10^{-4}	3.97	3.42	3.35
250	1.658	1.780	4.08×10^{-4}	4.24×10^{-4}	4.18×10^{-4}	3.56	3.70	3.65

Table VI-7. Some experimental values of ellipticity coefficient $\overline{\rho}$ and surface thickness t_d^{el} at T=20 ℃. Data are taken from Ref.182.

	$\overline{\rho}$	t_d^{el} (Å)
Rayleigh (1892)	4.2×10^{-4}	3.0
Raman and Ramdas (1927)	7.5×10^{-4}	5.0
Bouhet (1927)	4.2×10^{-4}	
Bacon (1939)	4.2×10^{-4}	3.07
Bruce (1939)	3.3×10^{-4}	2.26
Kinoshita (1965)	10.4×10^{-4}	7.1

Table VI-8. The same as in Table VI-6. for methanol.

	$\varepsilon_1/\varepsilon_0$	$\overline{\rho}$		t_d^{el}(Å)	
T(K)	Calc.	Tanh	Iso.	Tanh	Iso.
350	1.580	7.81×10^{-4}	7.78×10^{-4}	9.52	9.42
300	1.657	6.61×10^{-4}	6.87×10^{-4}	7.41	7.39
250	1.723	5.98×10^{-4}	6.01×10^{-4}	6.14	5.91
200	1.790	4.39×10^{-4}	4.55×10^{-4}	4.20	4.13
160	1.844	4.75×10^{-4}	4.72×10^{-4}	4.21	4.04

Table VI-9. The same as in Table VI-6 for LJ system. The observed ε_1 is from Ref 13.

	$\varepsilon_1/\varepsilon_0$		$\overline{\rho}$		t_d^{el}(Å)	
T(K)	Calc.	Obs.	Tanh	Iso.	Tanh	Iso.
120	1.406	1.414	6.17×10^{-4}	5.95×10^{-4}	10.67	10.51
100	1.463	1.475	5.55×10^{-4}	5.30×10^{-4}	8.15	7.95
80	1.517	1.526	4.13×10^{-4}	3.92×10^{-4}	5.45	5.27

Table VI-10. Experimental results of ellipsometry for argon (Beaglehole, 1980, Ref.164.); wave length of the light is λ=6328 Å.

T(K)	ε_v	ε_l	$\overline{\rho}$	t_d^{el}(Å)
120	1.0183	1.4137	8.8×10^{-4}	15.2
110	1.0103	1.4450	7.5×10^{-4}	11.9
100	1.0056	1.4750	6.5×10^{-4}	9.5
90	1.0025	1.5026	5.7×10^{-4}	7.9
85	1.0015	1.5147	4.7×10^{-4}	6.33

Table Ⅵ-11. Surface potential χ of water, which is the electrostatic potential of liquid phase relative to its vapor. There are two surfaces (left and right) in our simulation cell (see Fig.Ⅳ-1), and the average of these values is given in the last column.

	χ (V)		
T(K)	(left)	(right)	(average)
400	0.043	-0.026	0.009
350	0.092	0.111	0.102
300	0.171	0.153	0.162
275	0.153	0.166	0.160
250	0.138	0.196	0.167

Table VI-12. Surface potential χ of methanol.

T(K)	χ(V) (left)	(right)	(average)
350	-0.0392	-0.0210	-0.030
300	-0.0243	-0.0403	-0.032
250	-0.0211	-0.0427	-0.032
200	-0.0602	-0.0493	-0.055
160	-0.0941	-0.0604	-0.077

Table VI-13. Effect of free ions upon surface potential. α is the dissociation rate of water (Ref.13).

T (K)	α	correction ϕ (V) (left)	(right)	χ (V) (left)	(right)
250	4.0×10^{-10}	-1.92×10^{-6}	-4.56×10^{-6}	0.137	0.197
275	8.8×10^{-10}	-3.89×10^{-6}	-4.14×10^{-6}	0.153	0.166
300	19.3×10^{-10}	-25.89×10^{-6}	-13.01×10^{-6}	0.172	0.153
350	81×10^{-10}	-4.48×10^{-6}	-10.04×10^{-6}	0.093	0.111
400	200×10^{-10}	-3.31×10^{-6}	0.53×10^{-6}	0.004	-0.027

[Figure captions in Sec. VI]

Fig. VI-1. Pressure tensor profiles of water, normal component $P_n(z)$ and tangential component $P_t(z)$. The arrows show the position of Gibbs surfaces.

Fig. VI-2. The same as Fig. VI-1 for methanol.

Fig. VI-3. The same as Fig. VI-1 for LJ system.

Fig. VI-4. Surface tension profiles of water. The arrows show the position of Gibbs surfaces.

Fig. VI-5. The same as Fig. VI-4 for methanol.

Fig. VI-6. The same as Fig. VI-4 for LJ system.

Fig. VI-7. Local one-body excess entropy profiles $\Delta s^{1}(z)$ of water. The arrows show the position of the Gibbs surfaces.

Fig. VI-8. The same as Fig. VI-7 for methanol.

Fig. VI-9. Electric potential profile $\chi(z)$ of water; the value at z=60Å is defined to be zero. The arrows show the position of the Gibbs surfaces.

Fig. VI-10. The same as Fig. VI-9 for methanol.

Fig. VI-11. Schematic figure of screening effect of electrostatic potential by free ions.

Fig. VI-12. Minimum potential surface of CC water.

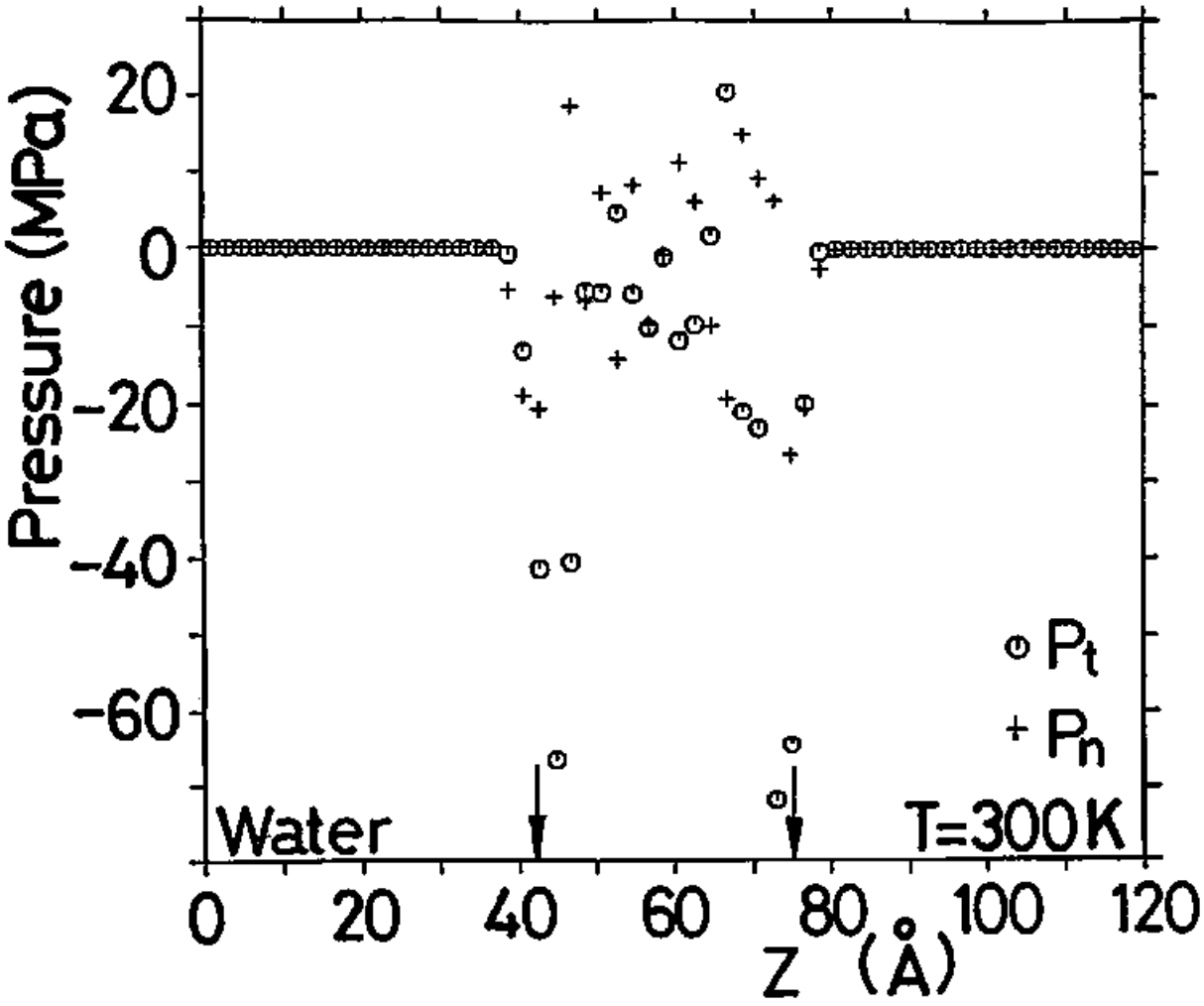

Fig. VI-1. (1) T=300 K.

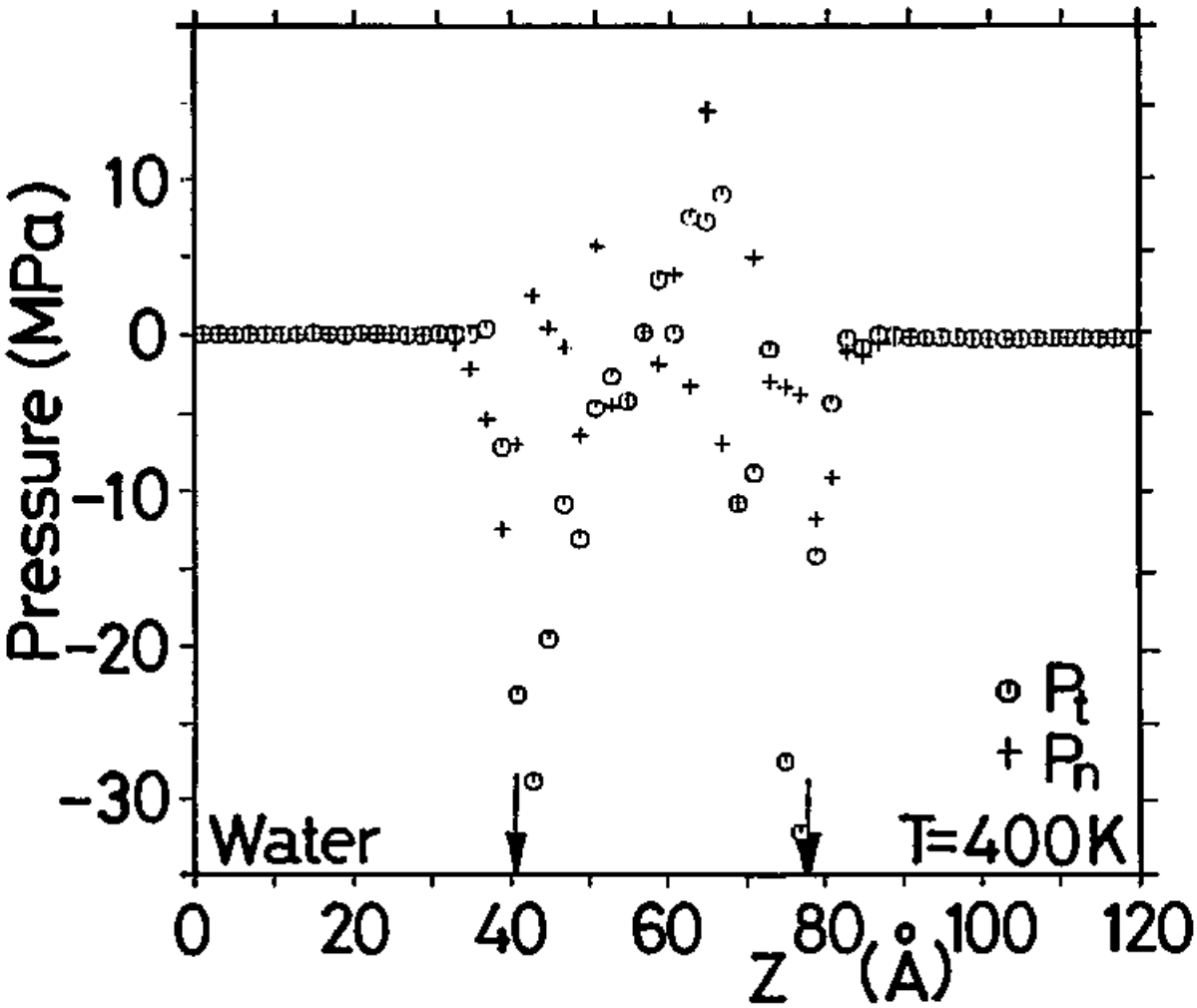

Fig. VI-1. (2) T=400 K.

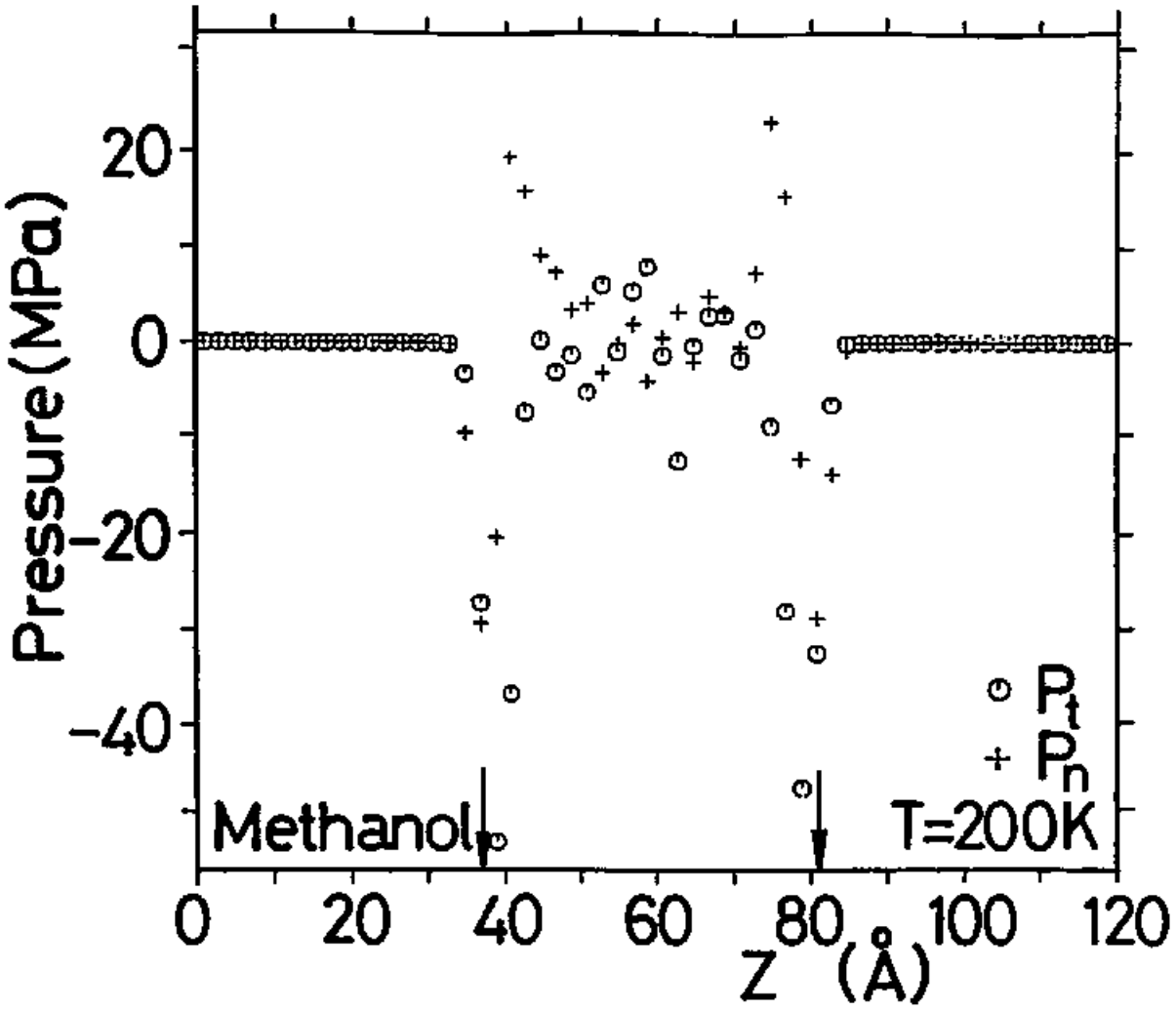

Fig. VI-2. (1) T=200 K.

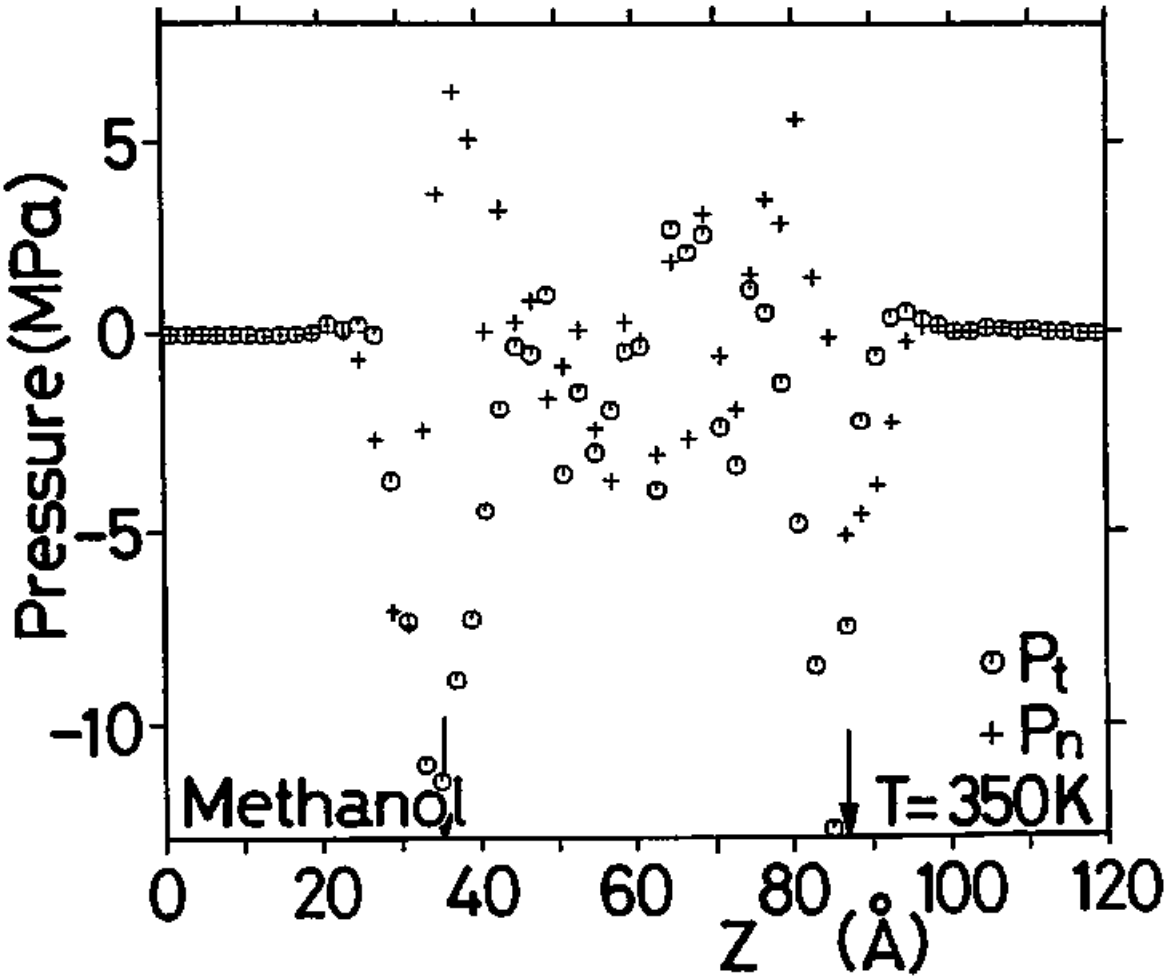

Fig. VI-2. (2) T=350 K.

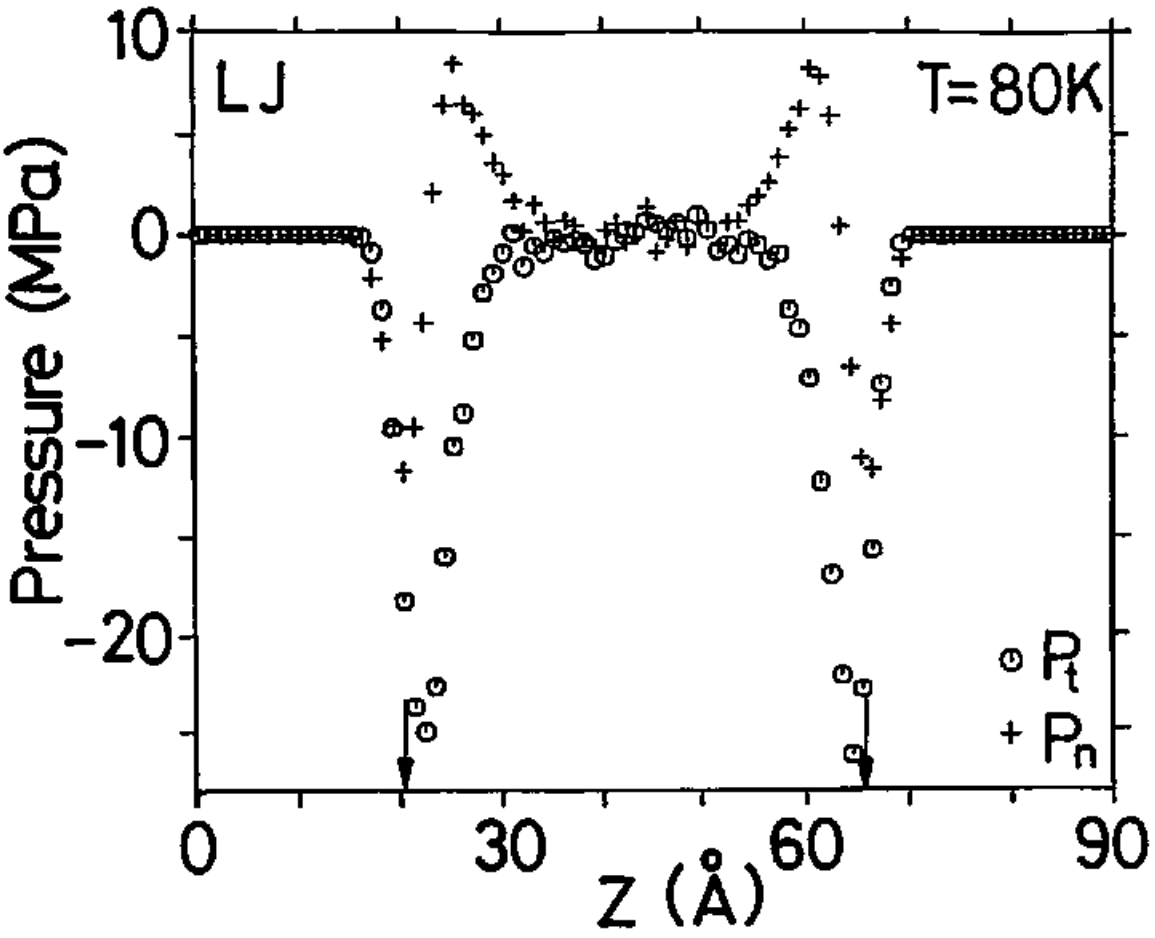

Fig. VI-3. (1) T=80 K.

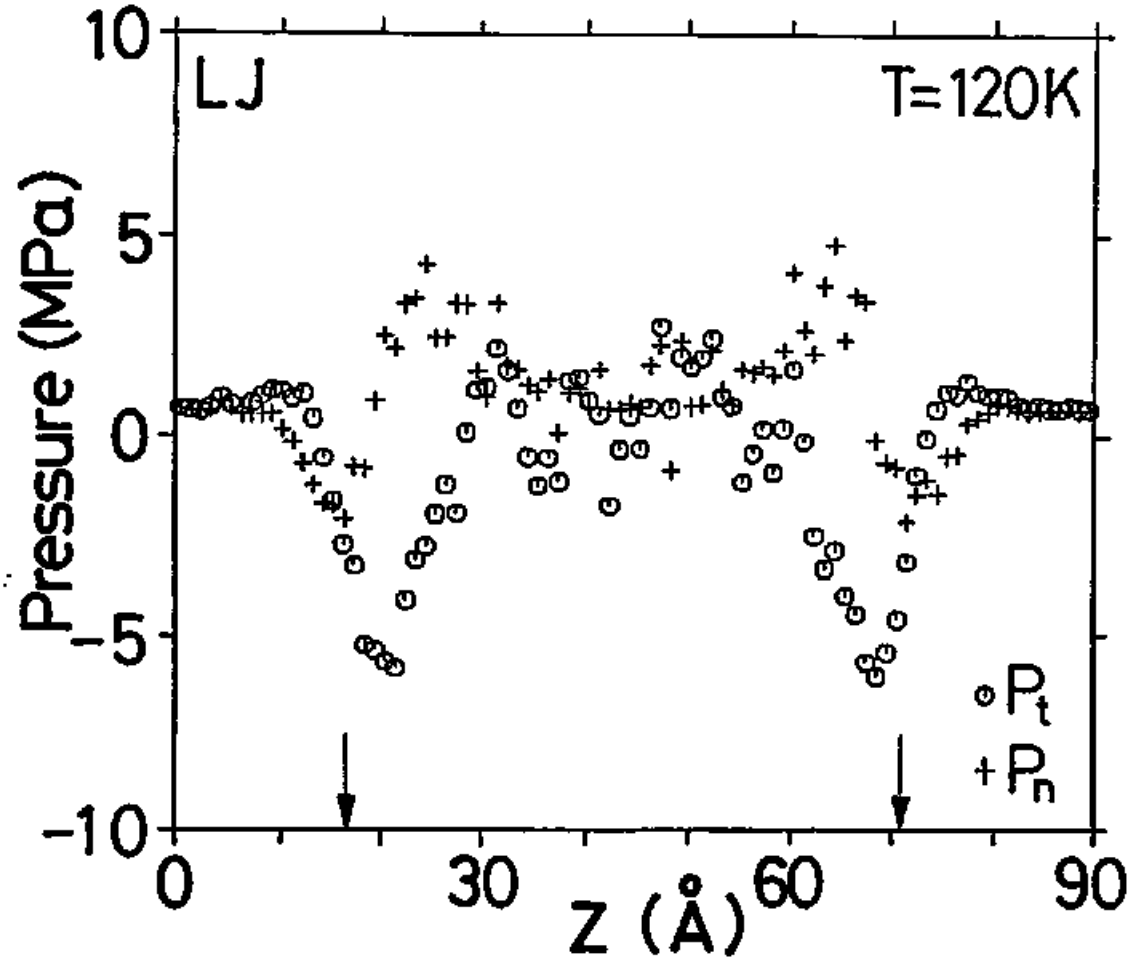

Fig. VI-3. (2) T=120 K.

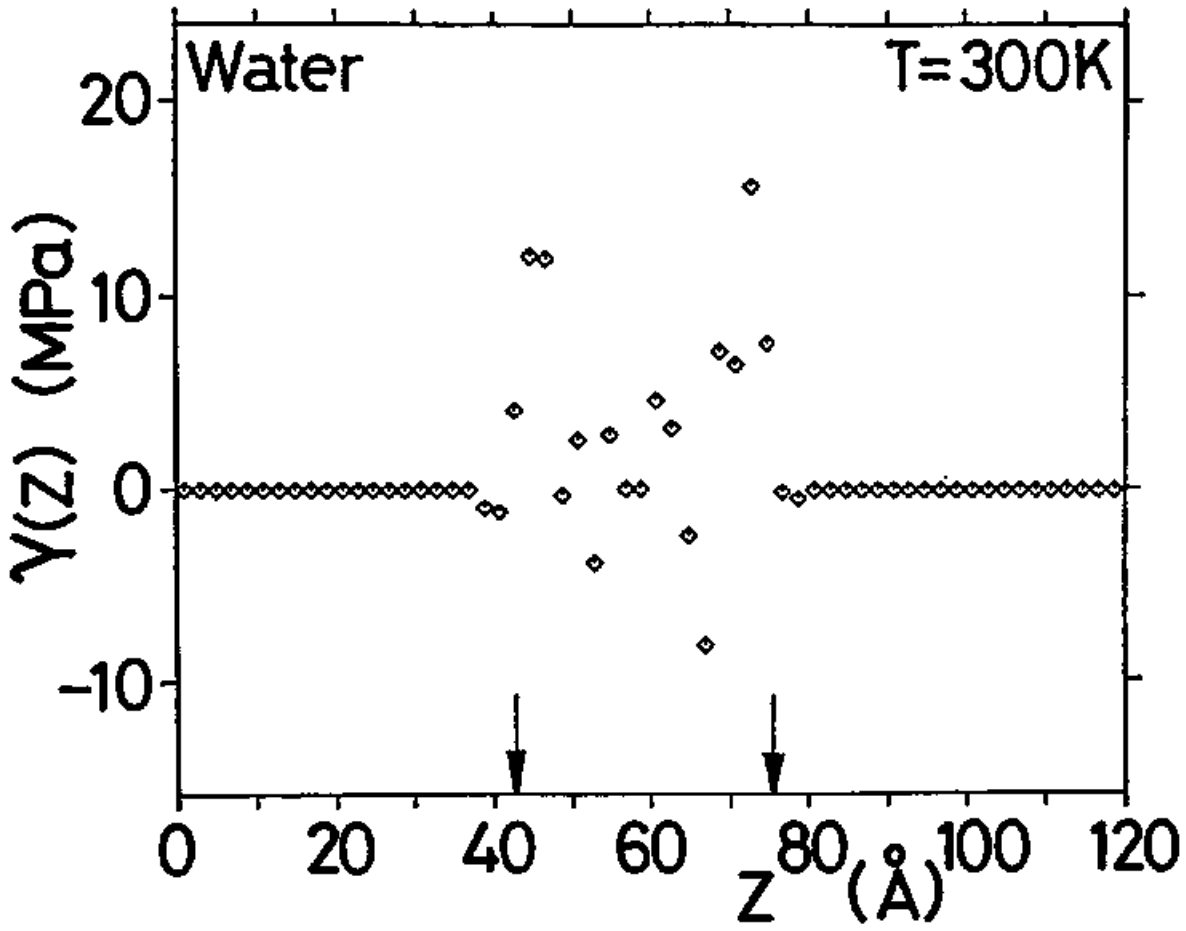

Fig. VI-4. (1) T=300 K.

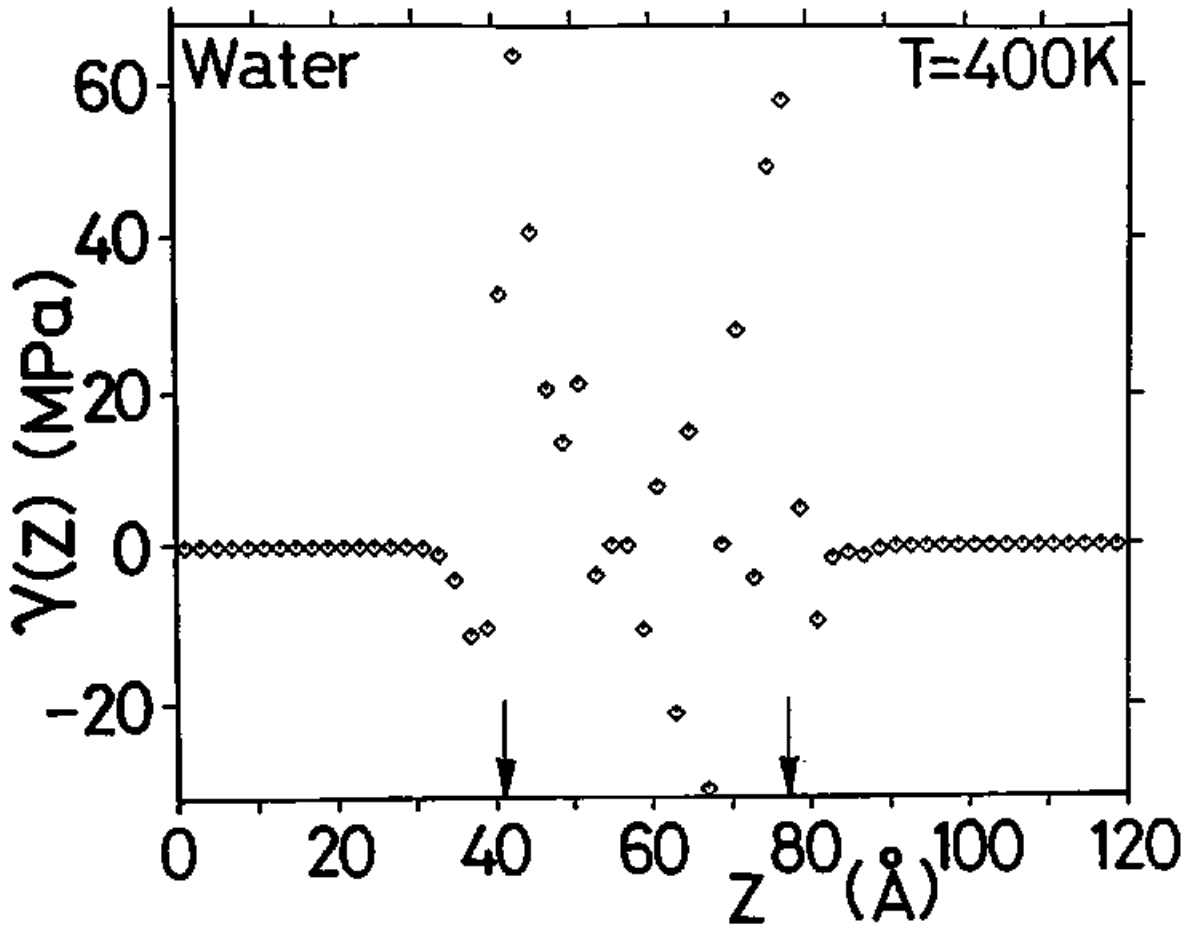

Fig. VI-4. (2) T=400 K.

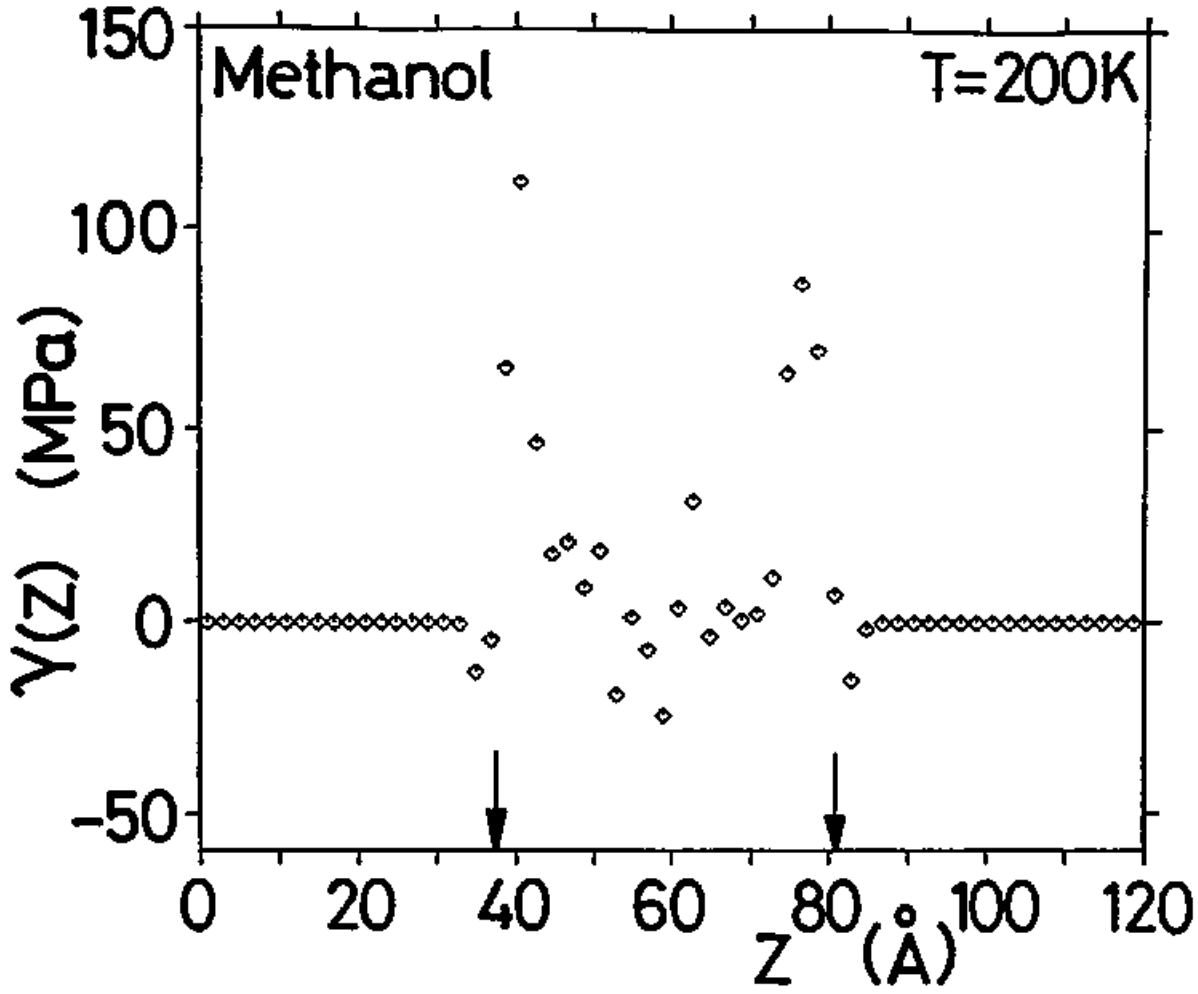

Fig. VI-5. (1) T=200 K.

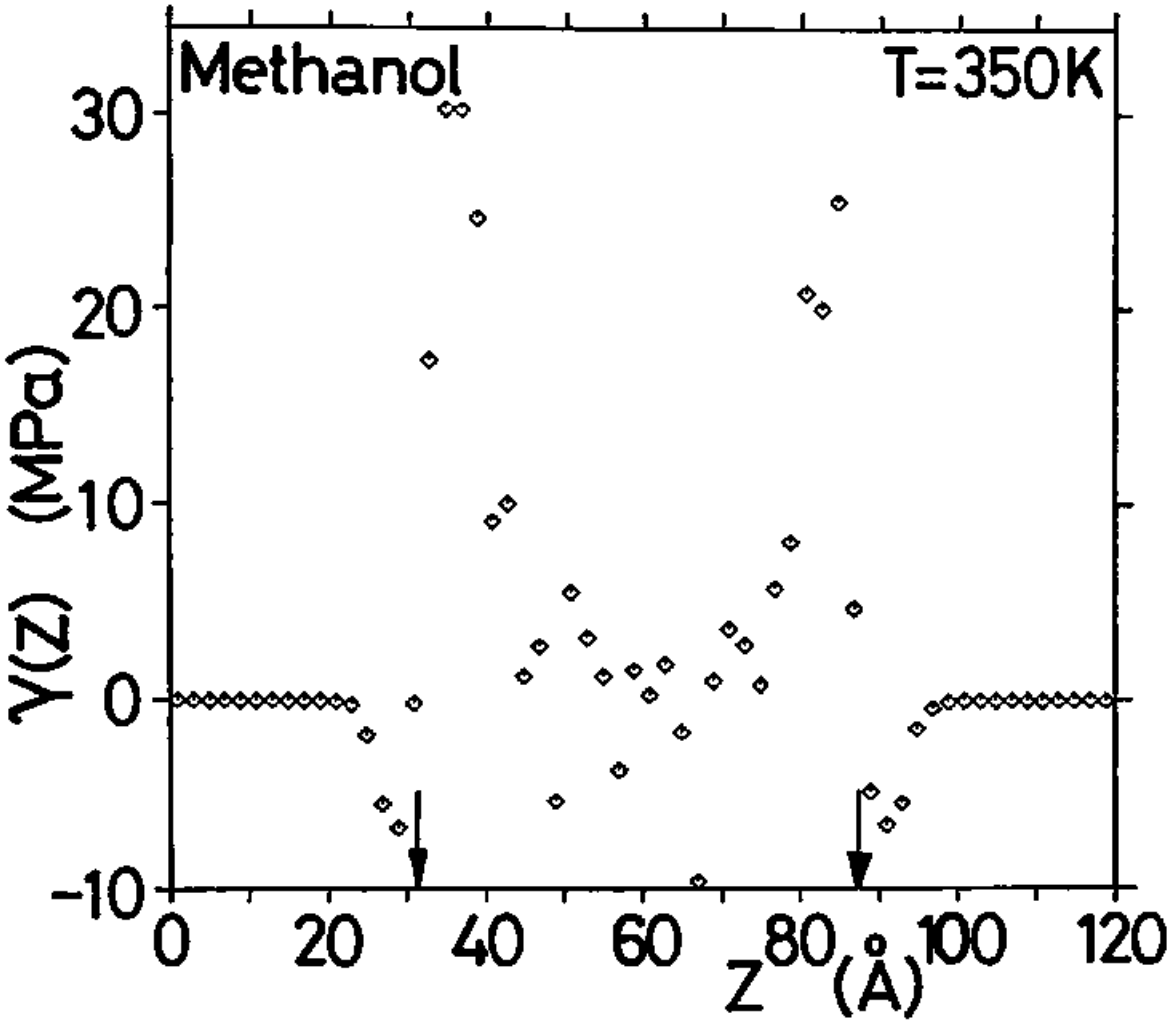

Fig. VI-5. (2) T=350 K.

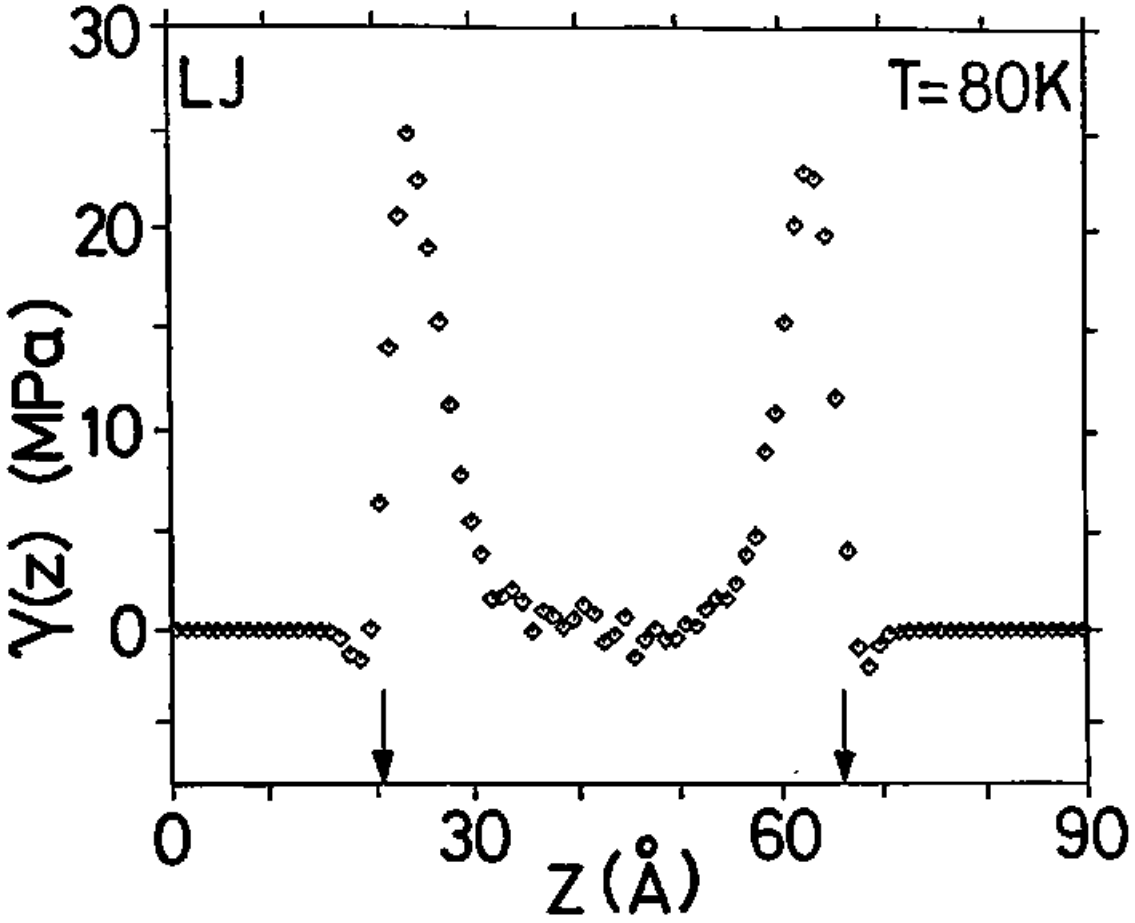

Fig. VI-6. (1) T=80 K.

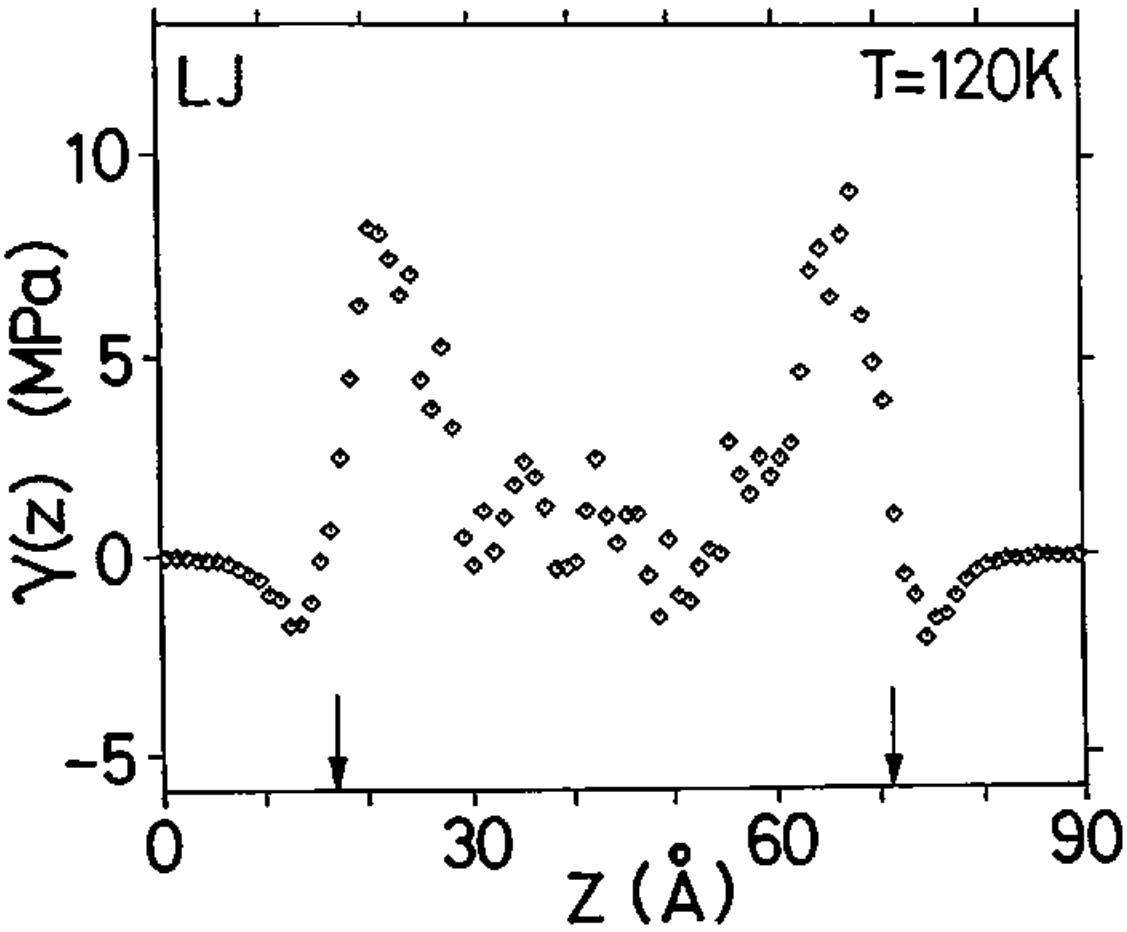

Fig. VI-6. (2) T=120 K.

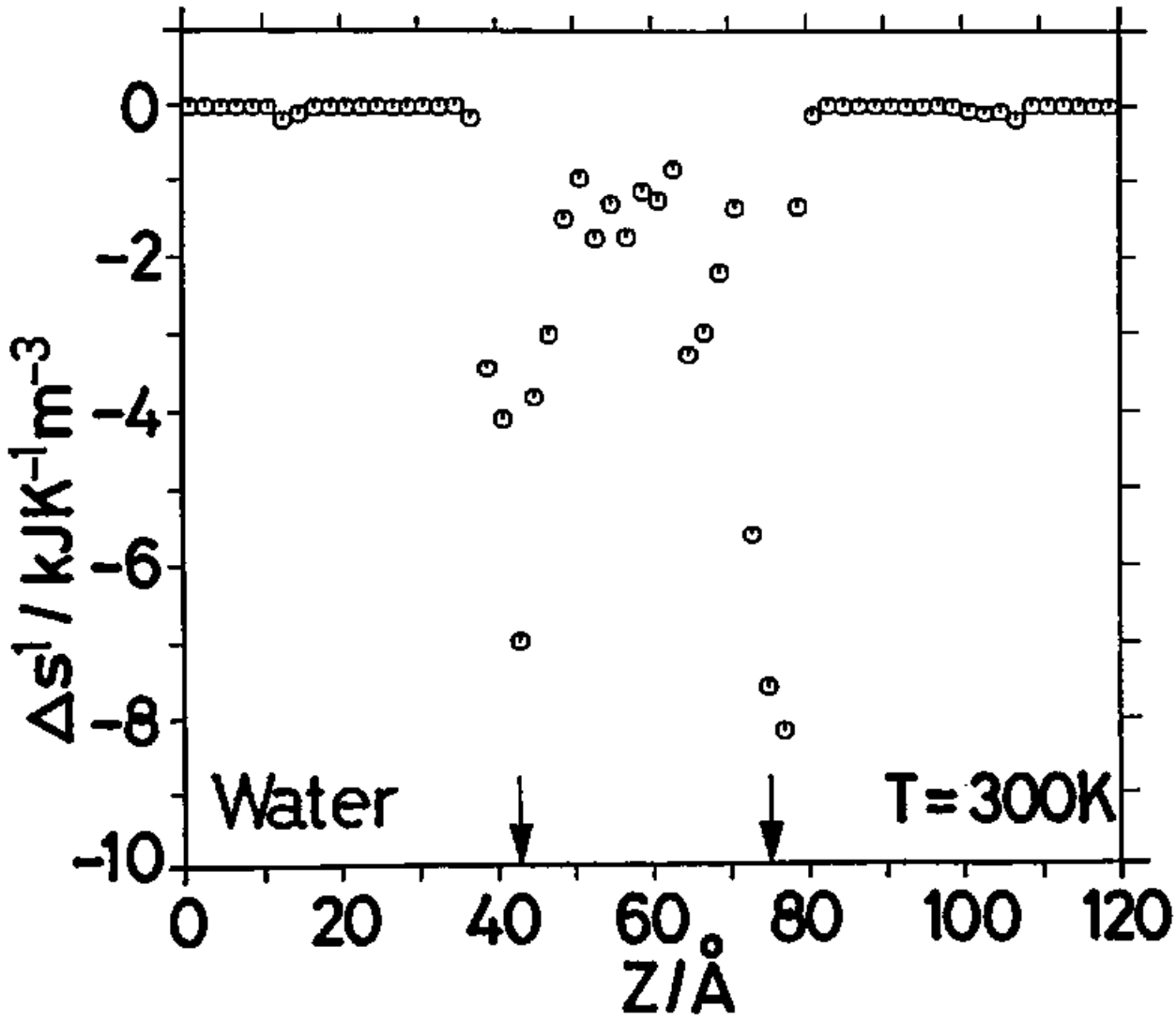

Fig. VI-7. (1) T=300 K.

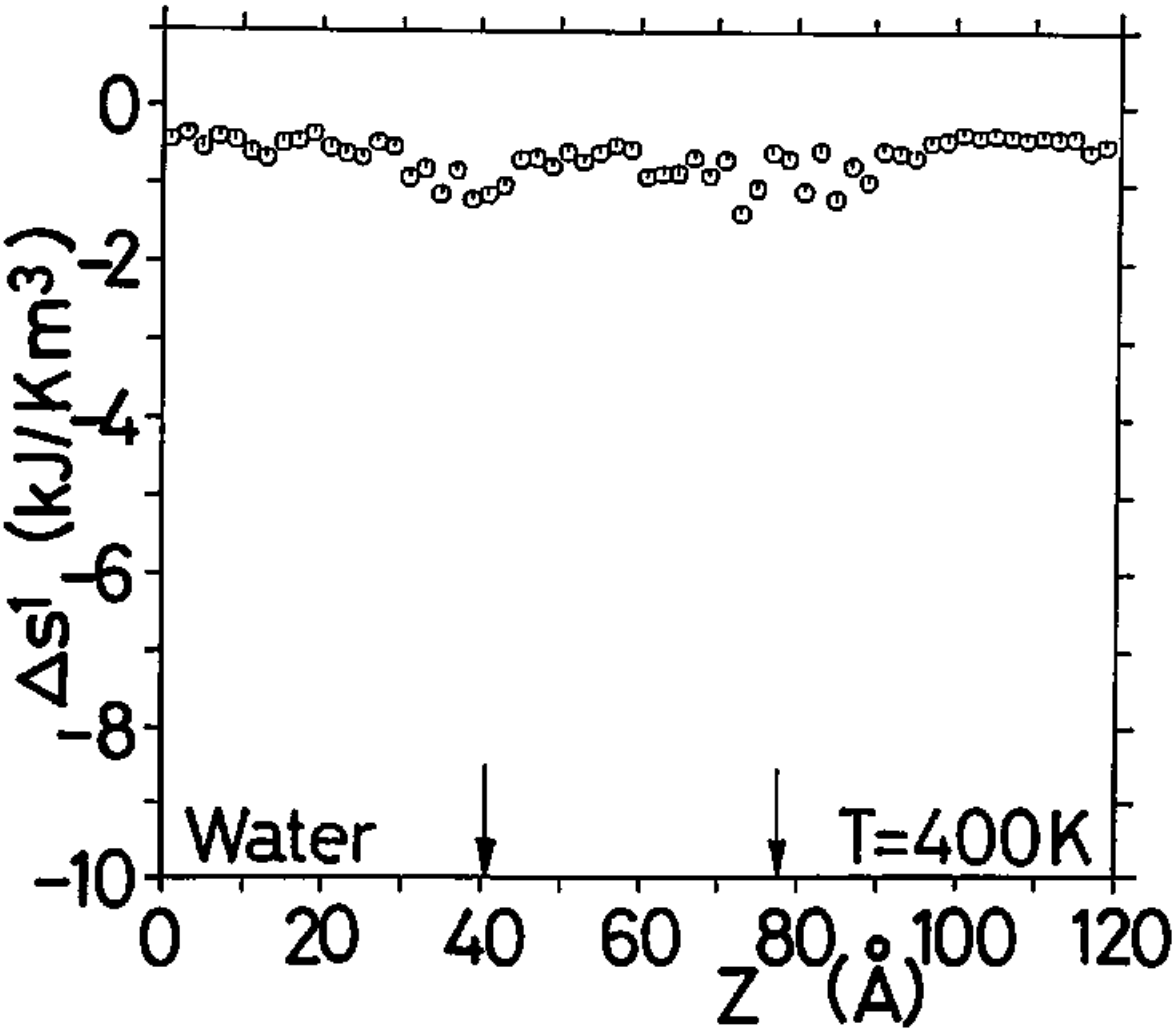

Fig. VI-7. (2) T=400 K.

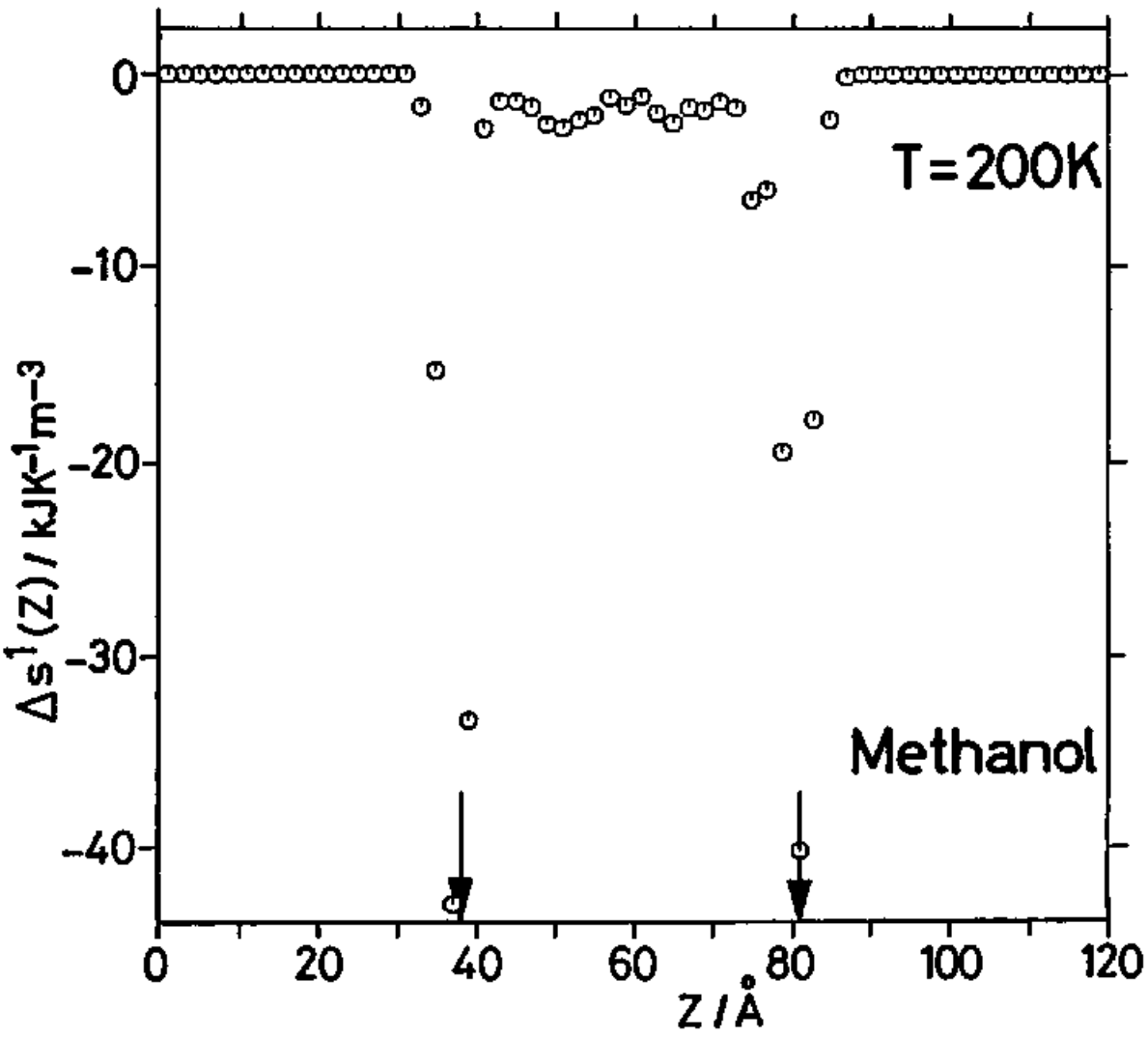

Fig. VI-8. (1) T=200 K.

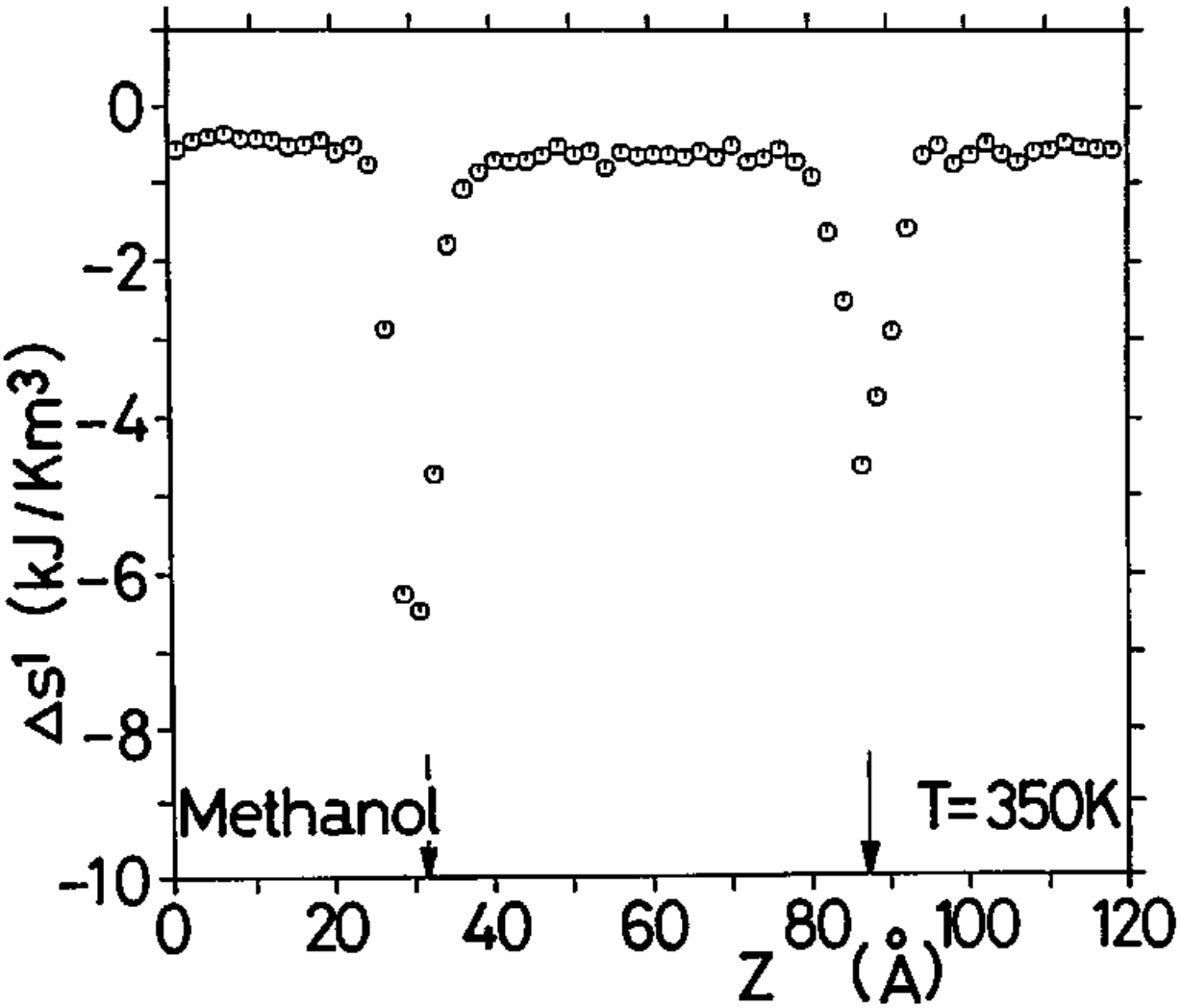

Fig. VI-8. (2) T=350 K.

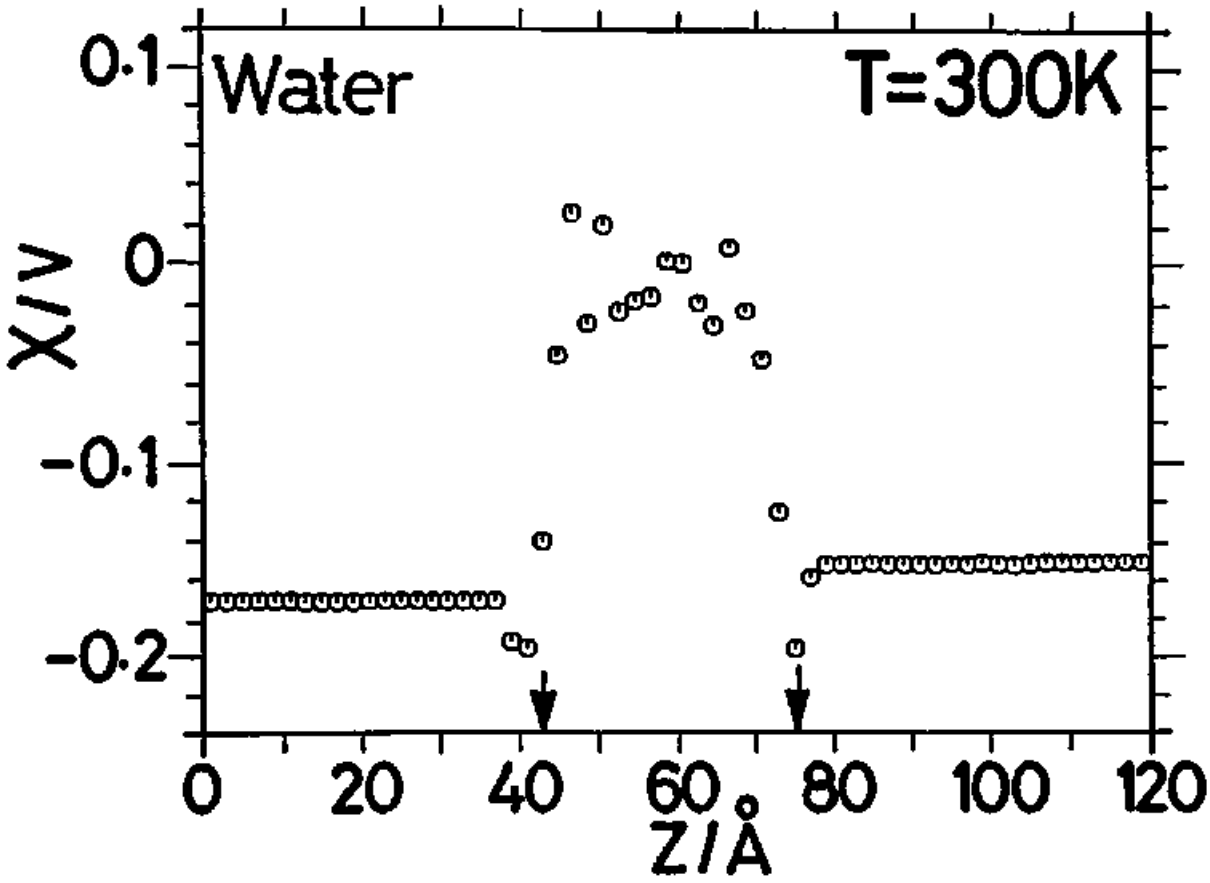

Fig. VI-9. (1) T=300 K.

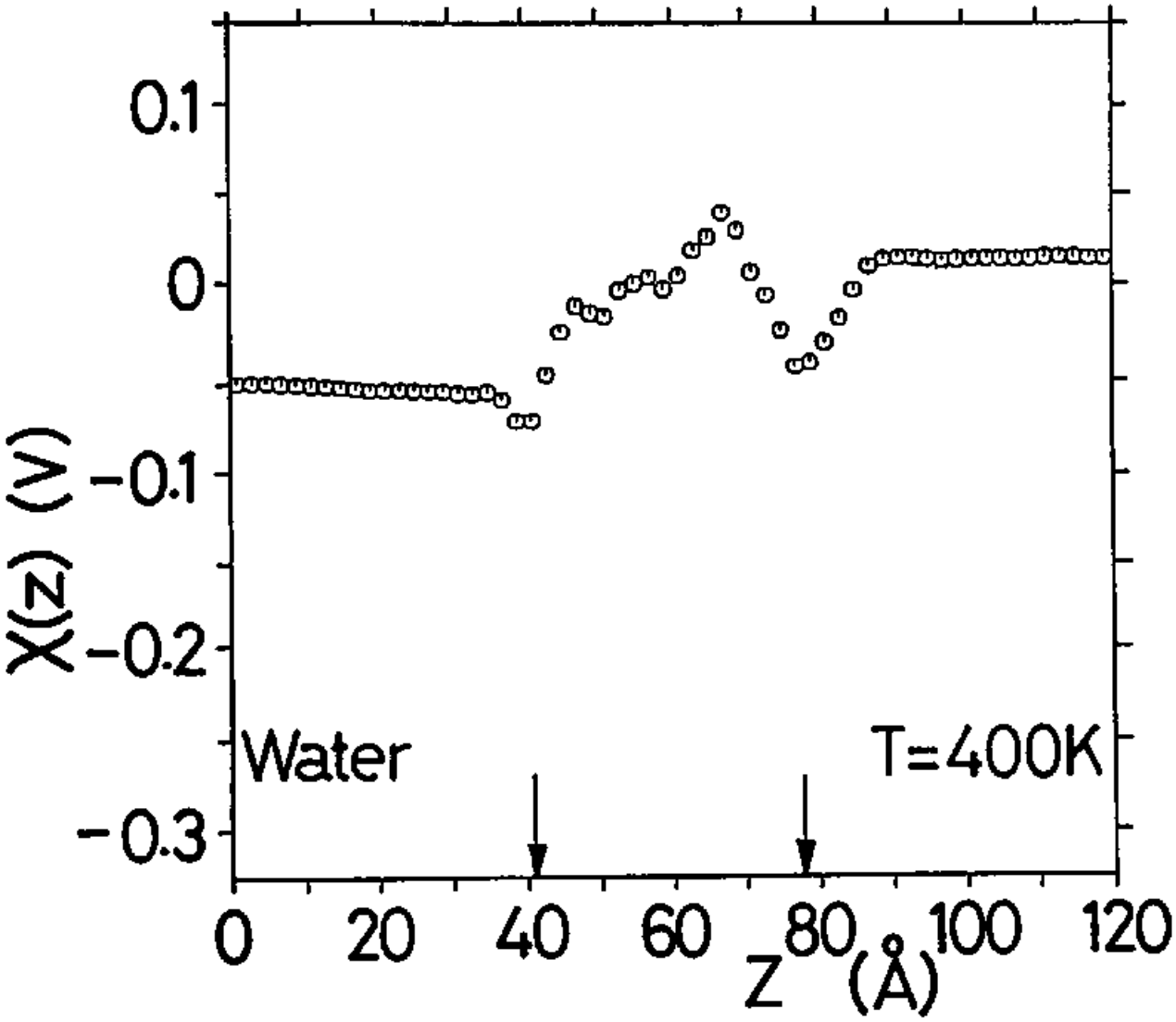

Fig. VI-9. (2) T=400 K.

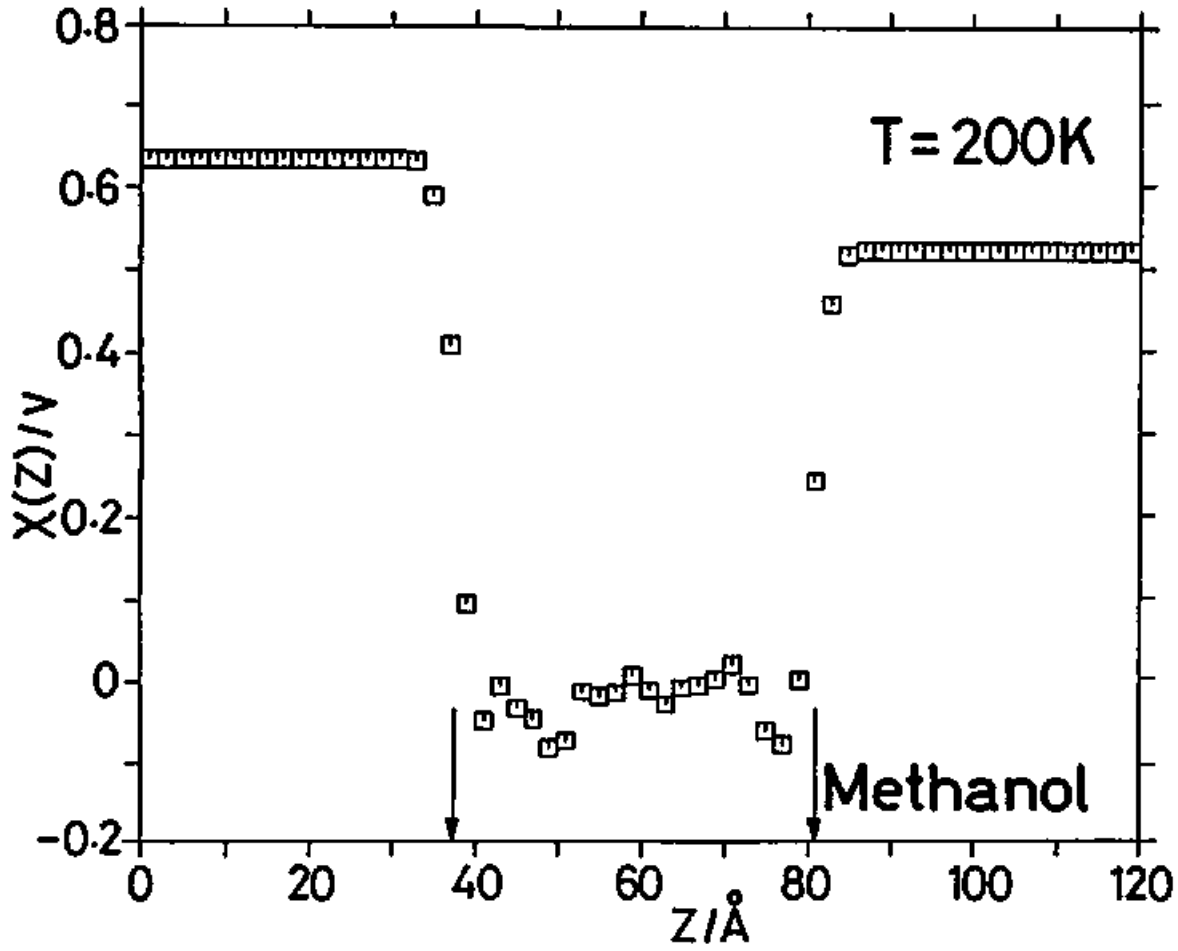

Fig. VI-10. (1) T=200 K.

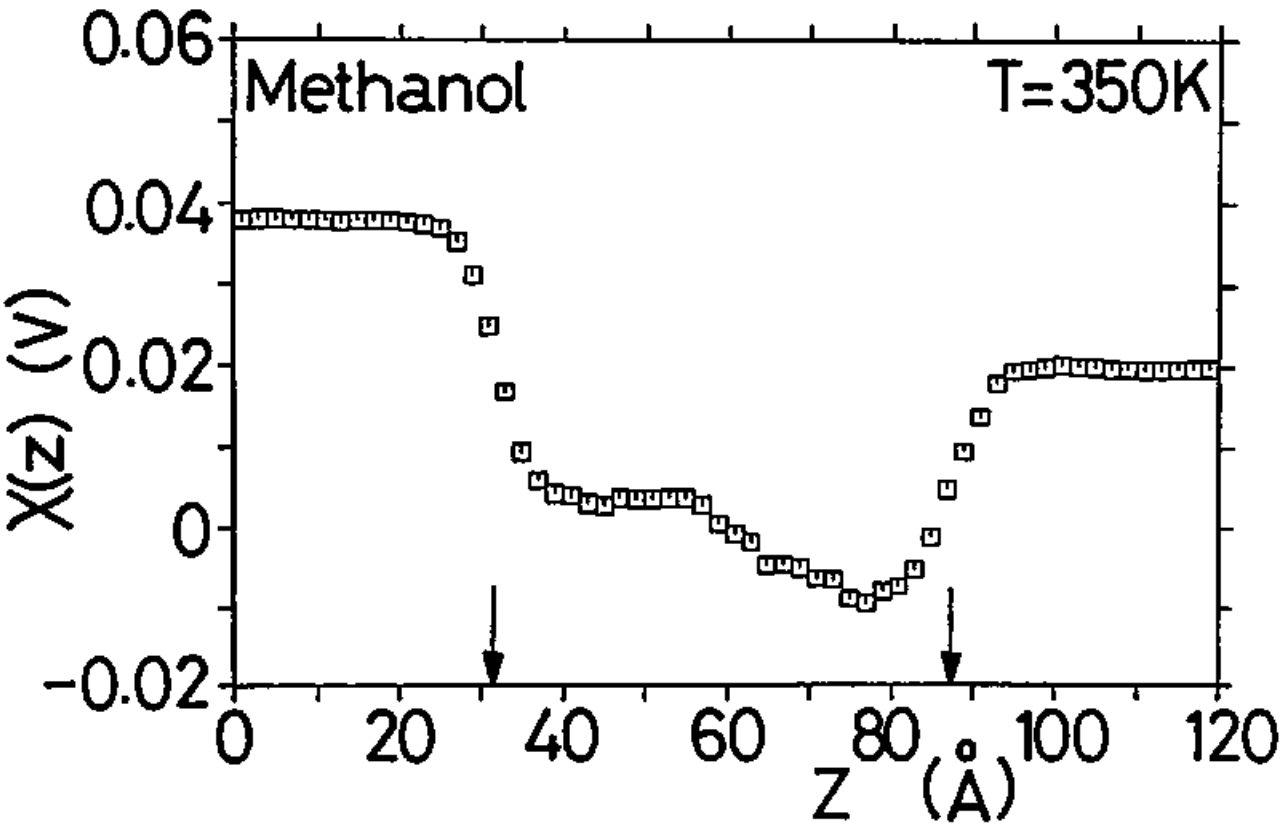

Fig. VI-10. (2) T=350 K.

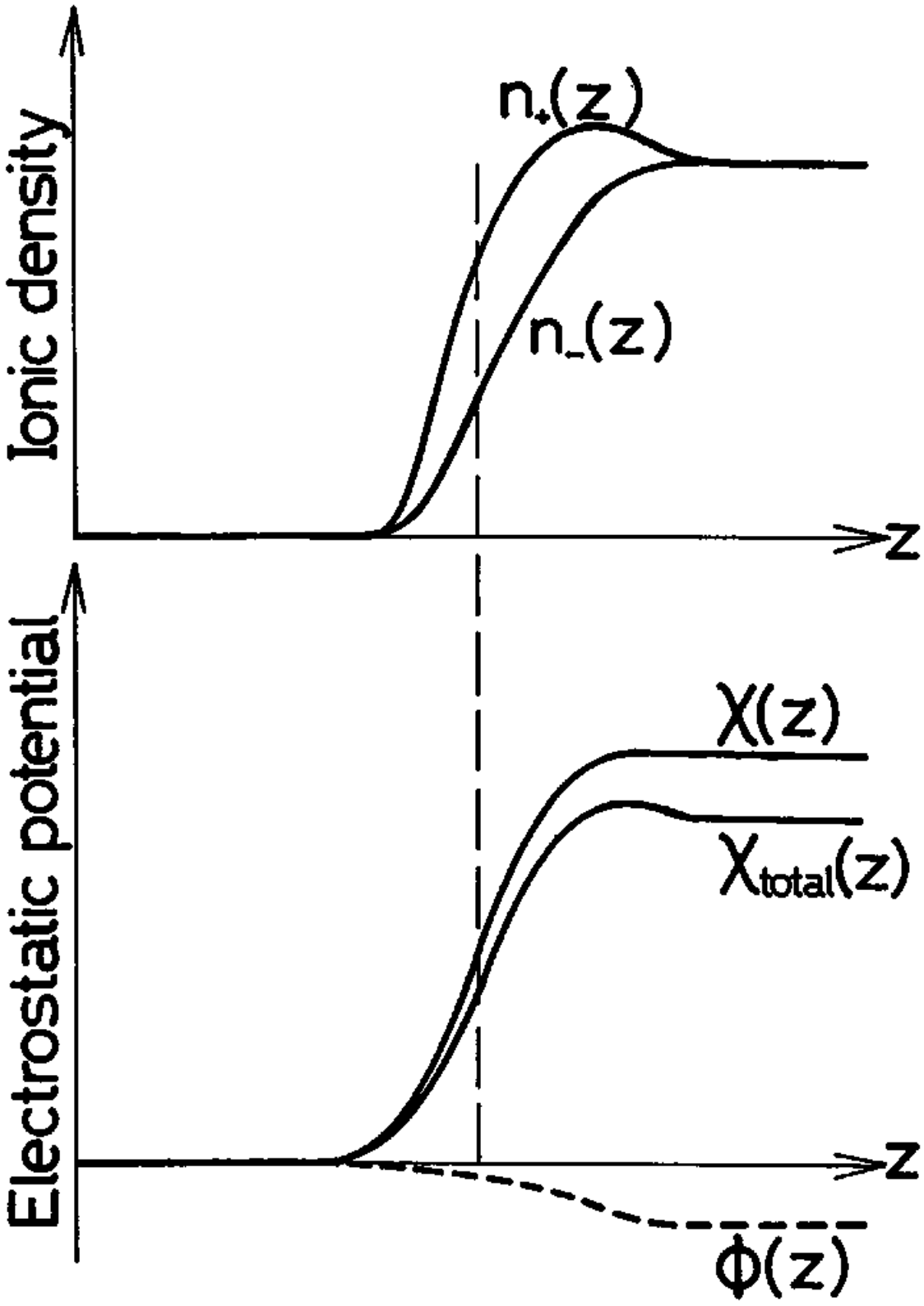
Ionic density
n+(z)
n-(z)
z
Electrostatic potential
χ(z)
χtotal(z)
z
Φ(z)

Fig. VI-11.

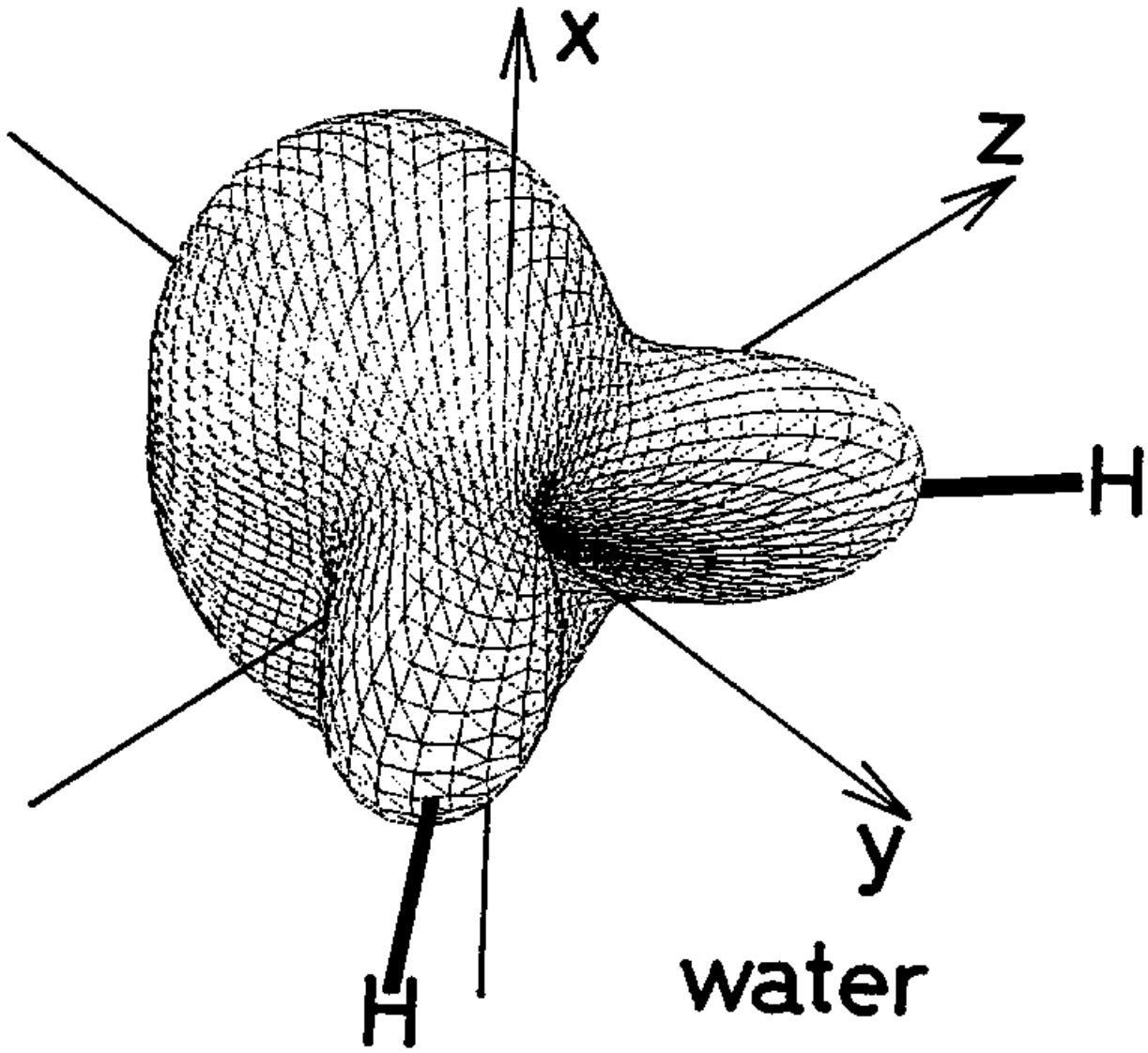

Fig. VI-12.

VI

The river glideth at his own sweet will:
Dear God! the very houses seem asleep;
And all that mighty heart is lying still!

William Wordsworth, COMPOSED UPON WESTMINSTER BRIDGE

Ⅶ. Summary and Problems for Future Study

It was confirmed by MD simulations that the thermodynamic properties of liquid-vapor interface of strongly hydrogen-bonding fluids, water and methanol, are much different from those of simple fluid, LJ system. Although the surface excess energy u_s and the surface excess free energy γ (surface tension) seem to be strongly model-dependent, the surface excess entropy s_s, which is important when one considers the molecular-level structure near the interface, agrees quite well with experimental results. In particular the lowering of s_s of water or methanol is the evidence of structural change near the surface, which can be related to the hydrophobic structural making.

The orientational ordering was mainly investigated in this work. Two different types of characteristic orientation were found for water; in the vapor side of the surface a water molecule has its one hydrogen atom projecting toward the vapor phase, and in the liquid side a molecule tends to lie down on the surface with its both hydrogen atoms slightly directed toward the liquid phase. These orientational orderings can be explained as the energetical stabilization at the sacrifice of one hydrogen bond, like water near hydrophobic walls. The orientational tendency, however, is rather weak and disappears as the temperature rises to 400 K. To the contrary methanol has one typical orientation; hydrophobic methyl group, which can not take part in hydrogen bonding, is put out toward the vapor phase. This effect of hydrophobic group is so drastic that the ordering does not break up to 350 K. Methanol, therefore, can be considered as one of the simplest models of

surfactants.

The surface entropy deficit ΔS^1 due to these orientational orderings was estimated for both systems. While ΔS^1 of methanol is large enough to explain the main cause of the anomalies of surface excess thermodynamic properties, that of water is by an order of magnitude smaller and cannot explain the anomalies by itself, which suggests the importance of higher structural ordering in the case of water.

As a result of such orientation, the surface potential χ, which is important but has been controversial in electrochemistry, can be estimated. The ellipticity coefficient was estimated from the density profile with the Clausius-Mossotti formula, and the anisotropic effect of water due to the orientational ordering was found to be very small; the assumption that density profile has hyperbolic tangent form, however, is inadequate for water and may cause the experimentally observed anomalously thin transition layer of water surface. No such features are observed for methanol surface.

To study interfacial (liquid-vapor, liquid-liquid, or liquid-solid) properties of strongly hydrogen-bonding systems, including various aqueous solutions, in more detail is very necessary not only for pure physical chemistry but also in various fields such as electrochemistry, surface chemistry, biophysical chemistry, and industrial chemistry. It is obvious that hydrophobic groups play an important role in these systems, and the microscopic elucidation of these inhomogeneous systems from this point of view is now widely much required. In particular information about various correlation functions such as many body correlation or time dependent correlation would be very useful in considering such systems. Estimation of

them has been much time consuming task so far, but it will soon become possible thanks to the recent rapid development of computer facilities.

Appendices

海は己れの海鳴りをきき。
天は己れの天を見つめ。

草野心平，BERING-FANTASY

The sea is listening to the rumbling of herself.
The sky is gazing at the space of himself.

Sinpei Kusano

Appendix A. Models of molecules

In this appendix, I briefly describe the models of water and methanol molecules which we used in our simulations.

(1) Model water

It is one of the important problems in quantum chemistry to construct reliable and convenient models of intermolecular potential energy function of water for computer simulation of condensed phase. Up to now several models, such as Rowlinson, [130], ST2[127] and TIPS[133,172] empirical potentials, and MCY[125] nonempirical potential, are usually adopted for various calculations; all of those treat pair potential energy of water dimer. Recently Kataoka examined[141] the Carravetta-Clementi (CC) potential,[142] which is similar to MCY potential in functional form, and found that this CC potential can reproduce semi-quantitatively many of thermodynamic properties of liquid water. He reported the equation of state and the liquid-vapor coexisting line in analytical functions of pressure and temperature, which are convenient for our aim to investigate the properties of liquid-vapor interface. We adopt, therefore, the CC potential although it requires a little more computational time than other empirical potentials because of its functional form as described below.

The shape of the molecule is shown in Fig.A-1, from which we can estimate the electric multipoles of CC water. In particular it is important to point out that the dipole moment is

$$\mu = |\Sigma q_i r_i| = 7.082\times10^{-30}\ \mathrm{Cm},$$

and the quadrupole tensor component Q_{zz} along the dipole, when we choose the center of mass as origin, is

$$Q_{zz} = \tfrac{1}{2}\Sigma q_i(3z_i^2 - r_i^2) = -0.410\times10^{-40}\ \mathrm{Cm}^2.$$

One of experimental values is $\mu=6.19\times10^{-30}$ Cm and $Q_{zz}=-0.434\times10^{-40}$ Cm^2 for isolated molecules.[12]

The functional form of the CC potential is not suitable so much for computer simulation because it includes time-consuming exponential functions; the total potential energy of the system is represented as

$$E = \Sigma\Sigma[\ q_i q_j/r_{ij} + A_{ij}\exp(-B_{ij})\ ], \qquad (A\text{-}1)$$

where partial charges q_i and parameters A_{ij} and B_{ij} are as follows (e is the elementary charge, 1.602×10^{-19} C):

$q_H = 0.658e$, $q_O = -2q_H$,

$A_{OO} = 454.231\times10^3$ kcal/mol, $B_{OO} = 4.756\,\text{Å}^{-1}$.

$A_{HH} = 3.578\times10^3$ kcal/mol, $B_{HH} = 3.845\,\text{Å}^{-1}$.

$A_{OH} = 2.114\times10^3$ kcal/mol, $B_{OH} = 3.176\,\text{Å}^{-1}$.

$A_{OH}' = -0.458\times10^3$ kcal/mol, $B_{OH}' = 2.141\,\text{Å}^{-1}$.

In our simulation the exponential functions are calculated with tabulation and second order interpolation technique, which is described in Appendix B, for economy of CPU time.

(2) Model methanol

As far as we have noticed, Jorgensen's TIPS model[149] is the only intermolecular model potential for computer simulation of methanol that is widely used, so we adopt this model.

This is a sort of empirical potential, in which a methanol molecule is treated as a rigid one and the interaction is represented as a sum of Coulomb terms and Lennard-Jones (12-6) terms. There are three interaction sites on each molecules, i.e., the hydrogen atom, the oxygen atom, and the methyl group. The shape of the molecule is shown in Fig.A-2, from which we can estimate the electric multipoles of TIPS methanol; e.g., the dipole moment μ is 7.36×10^{-30} Cm and the quadrupole tensor component Q_{zz} along the dipole, when we choose the center of mass as origin, is -5.95×10^{-40} Cm^2. One of experimental value is $\mu=5.67\times10^{-30}$ Cm for isolated molecules.[12]

The functional form of the total potential energy of the system is

$$E = \Sigma\Sigma(q_i q_j/r_{ij} + A_i A_j/r_{ij}^{12} - C_i C_j/r_{ij}^{6}), \qquad (A\text{-}2)$$

where partial charges q_i and parameters A_i and C_i are as follows:

q_O=-0.685e, A_O^2= 515×10^{-3} kcal Å^{12}/mol, C_O^2= 525 kcal Å^6/mol,

q_H= 0.40 e, A_H^2= 0×10^{-3} kcal Å^{12}/mol, C_H^2= 0 kcal Å^6/mol,

q_M= 0.285e, A_M^2=7950×10^{-3} kcal Å^{12}/mol, C_M^2=2400 kcal Å^6/mol.

Appendix B. Interpolation technique of mathematical functions

In order to speed up the simulation program, we develop a second-order interpolation technique of FORTRAN intrinsic functions, such as SQRT, EXP, and ERFC. In this appendix, I describe the essence of the technique and some of its results.

The second-order interpolation, by which we mean the parabolic approximation, is one of the simplest ways to guess the value $y=f(x)$ from its neighbor fixed points. Let us consider three fixed points on a curve $y=f(x)$, (x_{2n}, y_{2n}), (x_{2n+1}, y_{2n+1}), and (x_{2n+2}, y_{2n+2}). The parabolic function which connects these points (Fig.B-1) is represented as

$$y = ax^2 + bx + c,$$

$$\begin{aligned} a &= (y_{2n} - 2y_{2n+1} + y_{2n+2}) / D, \qquad \text{(B-1)} \\ b &= [-y_{2n}(x_{2n+1}+x_{2n+2}) + 2y_{2n+1}(x_{2n}+x_{2n+2}) - y_{2n+2}(x_{2n}+x_{2n+1})]/D, \\ c &= (y_{2n}x_{2n+1}x_{2n+2} - 2y_{2n+1}x_{2n}x_{2n+1} + y_{2n+2}x_{2n}x_{2n+1}) / D, \\ D &= x_{2n}^2 - 2x_{2n+1}^2 + x_{2n+2}^2. \end{aligned}$$

When the fixed points are placed at equal intervals, i.e.,

$$x_{2n+2} - x_{2n+1} = x_{2n+1} - x_{2n} = \Delta,$$

the Eq.(B-1) becomes a simpler form,

$$y = d(x)[\{d(x)-1\}G_n - F_n + F_{n+1}] + F_n,$$

$$d(x) = x/2\Delta - n, \qquad (B\text{-}2)$$

$$F_n = y_{2n},$$

$$G_n = 2(y_{2n} - 2y_{2n+1} + y_{2n+2}).$$

What one has to do in advance of calculation is, therefore, to prepare the two numerical tables F_n and G_n. When one wants to get the value f(x), one calculates n as

$$n = [x/2\Delta], \qquad (B\text{-}3)$$

where [ ] is the Gauss's symbol, and one obtains the approximate value through Eq.(B-2).

I show next one example coded in FORTRAN language, which calculates the value of fn(x) in the case of $0 \leqq x \leqq XMAX$ and dividing number NMAX:

```
      IMPLICIT INTEGER*4 (I-N)
      IMPLICIT REAL*8 (D)
      REAL*8 TB1(0:NMAX),TB2(0:NMAX-1)
C*****<< MAKE TABLES >>*****
      DELTA=XMAX/(2.0*NMAX)
      DELINV=0.5/DELTA
      DO 1000 I=0,NMAX,1
        TB1(I)=fn(2*I*DELTA)
1000  CONTINUE
      DO 1100 I=0,NMAX-1,1
        TB2(I)=2.0*(TB1(I)+TB1(I+1))-4.0*fn((2*I+1)*DELTA)
1100  CONTINUE
C*****<< CALCULATION >>*****
      D=X*DELINV
      N=D
      D=D-N
      Y=D*((D-1.0)*TB2(N)-TB1(N)+TB1(N+1))+TB1(N)
```

An example of the results of this interpolation applied to exponential function ($\Delta=1\times10^{-3}$) is showed in Table B-1; it is obvious that this interpolation has enough precision. The additional memory needed in this calculation is rather small, about 400 kbyte in our program, and the speed on vector processor is more than twice as fast as exact calculation.

Appendix C. Equation of state and isothermal compressibility

In this appendix we derive analytic formula of the isothermal compressibility κ from the equation of state empirically represented as a power series.

(1) Water

Kataoka[141] gave two different equations of state (EOS) for CC water; one is G-EOS, which represents the overall feature, and the other is L-EOS, which represents well the liquid state region. Both equations deal with the excess Helmholtz free energy F^e as a power series of density ρ and temperature T,

$$\beta F^e/N = \sum_{pq} A_{pq}(\rho/\rho_0)^p(\beta/\beta_0)^q, \qquad \text{(C-1)}$$

where $\beta=1/k_BT$ (k_B is the Boltzmann constant), N the number of molecule, and 0 represents the standard state,

$$1/\rho_0 = 20\ cm^3/mol, \quad 1/\beta_0 = 500\ K \times k_B. \qquad \text{(C-2)}$$

A_{pq}'s are dimensionless coefficients, listed in Table C-1. Partial differentiation of F^e with volume V gives the excess pressure P^e:

$$\beta P^eV/N = -V\{\frac{\partial}{\partial V}(\beta F^e/N)\}_T$$

$$= \rho\{\frac{\partial}{\partial\rho}(\beta F^e/N)\}_T$$

$$= (\rho/\rho_0)\sum_{pq} pA_{pq}(\rho/\rho_0)^{p-1}(\beta/\beta_0)^q. \qquad (C\text{-}3)$$

For the ideal gas the pressure P^0 is given as

$$\beta P^0 V/N = 1. \qquad (C\text{-}4)$$

The total pressure P is therefore expressed as

$$P = P^0 + P^e$$

$$= (\rho/\beta)[1 + (\rho/\rho_0)\sum_{pq} pA_{pq}(\rho/\rho_0)^{p-1}(\beta/\beta_0)^q]. \qquad (C\text{-}5)$$

The isothermal compressibility κ is thus obtained as

$$\kappa = -(1/V)(\partial V/\partial P)_T$$

$$= (1/\rho)(\partial\rho/\partial P)_\beta$$

$$=(\beta/\rho)[1 + (\rho/\rho_0)\sum_{pq} p^2A_{pq}(\rho/\rho_0)^{p-1}(\beta/\beta_0)^q]^{-1}. \qquad (C\text{-}6)$$

(2) LJ system

Ree[15] reported an analytic expression of the equation of state of LJ system (energy depth ε and core diameter σ) based upon computer simulated

data as density expansion form of pressure:

$$\beta P/\rho = \beta P_{rep}/\rho - (1/T^*)^{1/2}\sum_i iC_i x^i + (1/T^*)\sum_i D_i x^i. \qquad (C\text{-}7)$$

where P_{rep} is the pressure of the repulsive part of the system[174],

$$\beta P_{rep}/\rho = 1 + B_1 x + B_2 x^2 + B_3 x^3 + B_4 x^4 + B_{10} x^{10}. \qquad (C\text{-}8)$$

Here $\beta = 1/k_B T$ and $x = \rho^*/T^{*1/4}$. where $\rho^* = \rho\sigma^3$ is reduced density and $T^* = k_B T/\varepsilon$ is reduced temperature. The coefficients B_i, C_i, and D_i are listed in Table C-2.

The isothermal compressibility κ is obtained by partial differentiation of x with P as

$$\kappa = -(1/V)(\partial V/\partial P)_T$$

$$= (1/\rho)(\partial \rho/\partial P)_\beta$$

$$= (1/x)(\partial x/\partial P)_\beta$$

$$= (\beta\sigma^3/T^{*1/4}x)$$
$$\times\{\sum_i (i+1)B_i x^i - (1/T^*)^{1/2}\sum_i i(i+1)C_i x^i + (1/T^*)\sum_i (i+1)D_i x^i\}^{-1}. \qquad (C\text{-}9)$$

Appendix D. Ellipsometry at orientationally ordered interface

Ellipsometry is a technique which measures the polarization of the light reflected at the interface.[17,18,175] Under certain assumptions one can obtain the information of the interface, such as its thickness and the dielectric constant of the transition layer. The coefficient of ellipticity $\bar{\rho}$, the value of the imaginary part of the ratio of the p and s reflection amplitudes at the Brewster angle, can be represented to the first order with the dielectric constant profile of the transition layer $\varepsilon(z)$ as follows[49,175]:

$$\bar{\rho} = \frac{\pi}{\lambda} \frac{\sqrt{\varepsilon_v + \varepsilon_l}}{\varepsilon_v - \varepsilon_l} \eta_0 \qquad \text{(D-1)}$$

and

$$\eta_0 = \int_{-\infty}^{\infty} dz \frac{[\varepsilon(z) - \varepsilon_v][\varepsilon(z) - \varepsilon_l]}{\varepsilon(z)}, \qquad \text{(D-2)}$$

where λ is the wave length of the incident light, ε_l and ε_v are the dielectric constant (refractive index) of bulk liquid and vapor phase, respectively. Recently Lekner[176] generalized this formula to the case where spatial anisotropy of $\varepsilon(z)$ exists and derived the similar formula to Eq.(D-1), with η_0 replaced by

$$\eta = \int_{-\infty}^{\infty} dz \left\{ \varepsilon_{\parallel}(z) + \frac{\varepsilon_v \varepsilon_l}{\varepsilon_{\perp}(z)} - \varepsilon_v - \varepsilon_l \right\}, \qquad \text{(D-3)}$$

where $\varepsilon_{\perp}(z)$ and $\varepsilon_{\parallel}(z)$ are the dielectric constant normal and parallel to the interface, respectively.

The problem is how one evaluates $\varepsilon(z)$ from the density profile $\rho(z)$. We adopt here one of the simplest (approximate) relations, the Clausius-Mossotti formula[19]:

$$\varepsilon(z)/\varepsilon_0 = \left[1+\frac{8\pi}{3}\frac{\rho(z)}{M}\alpha\right]\Big/\left[1-\frac{4\pi}{3}\frac{\rho(z)}{M}\alpha\right], \qquad \text{(D-4)}$$

where α is the molecular polarizability and ε_0 the dielectric constant of the vacuum. In order to take account of the anisotropy of the transition layer, we represent the dielectric constant as a tensor form:

$$\varepsilon_{kj}(z)/\varepsilon_0 = \left(\delta_{ik}-\frac{4\pi}{3}\frac{\rho(z)}{M}\bar{\alpha}_{ik}\right)^{-1}\left(\delta_{ij}+\frac{8\pi}{3}\frac{\rho(z)}{M}\bar{\alpha}_{ij}\right), \qquad \text{(D-5)}$$

where δ_{ij} is the unit tensor (the Kronecker's delta). The molecular polarizability tensor $\bar{\alpha}_{ij}$, when orientationally averaged with the simulationally evaluated (θ,ϕ) distribution $P(\theta,\phi;z)$, becomes diagonal due to the rotational symmetry of the system around the normal of the surface:

$$\bar{\alpha}_{ij} = \begin{cases} \bar{\alpha}_{\parallel}, & \text{for } i=j=x \text{ or } y. \\ \bar{\alpha}_{\perp}, & \text{for } i=j=z, \\ 0, & \text{otherwise.} \end{cases} \qquad \text{(D-6)}$$

where $\bar{\alpha}_{\parallel}$ and $\bar{\alpha}_{\perp}$ are the orientationally averaged molecular polarizability

parallel and normal to the surface, respectively, which are calculated as follows:

$$\overline{\alpha}_{\parallel} = \frac{1}{2}\int\int d\theta\, d\phi\ P(\theta,\phi;z) \times[\alpha_{xx}(\cos^2\theta\cos^2\phi+\sin^2\phi)+\alpha_{yy}(\cos^2\theta\sin^2\phi+\cos^2\phi)+\alpha_{zz}\sin^2\theta], \tag{D-7}$$

$$\overline{\alpha}_{\perp} = \frac{1}{2}\int\int d\theta\, d\phi\ P(\theta,\phi;z) \times[\alpha_{xx}\sin^2\theta\cos^2\phi+\alpha_{yy}\sin^2\theta\sin^2\phi+\alpha_{zz}\cos^2\theta],$$

where the Jacobian $\sin\theta$ is included in $P(\theta,\phi;z)$. Substituting Eq.(D-6) for Eq.(D-5), one can obtain the following expression:

$$\varepsilon_{\parallel}/\varepsilon_0 = \left(1+\frac{8\pi}{3}\frac{\rho}{M}\overline{\alpha}_{\parallel}\right)\Big/\left(1-\frac{4\pi}{3}\frac{\rho}{M}\overline{\alpha}_{\parallel}\right),$$
$$\varepsilon_{\perp}/\varepsilon_0 = \left(1+\frac{8\pi}{3}\frac{\rho}{M}\overline{\alpha}_{\perp}\right)\Big/\left(1-\frac{4\pi}{3}\frac{\rho}{M}\overline{\alpha}_{\perp}\right). \tag{D-8}$$

This is a generalization of the Clausius-Mossotti formula, Eq.(D-4).

Appendix E. Estimation of surface potential

In this appendix I discuss two different ways to calculate surface potential χ. One is a charge distribution approach,[131,132,134] in which one uses the spatial charge distribution to determine electrostatic field and then integrates the field to obtain the electrostatic potential difference. The other is a dipole moment approach,[129,135] in which one calculates averaged orientation of electric dipole of molecules and spatially integrates it. These two approaches give different results, as shown below, and one may be thrown into a great confusion unless one pays enough attention to the definition of the electrostatic potential; actually it is reported[134] that various models with continuous distributions of charge can change even the sign of χ under the condition of constant dipole moment.

First of all, We show that these two approaches are based on the same expression of electrostatic potential difference. Let us here consider a system in which the density is varying along Z-axis. The formula for the z-component of electric field E(z) (in SI unit) is

$$E(z) = [\, Q_-(z) - Q_+(z) \,] / 2\varepsilon_0 A, \qquad \text{(E-1)}$$

where $Q_+(z)$ [or $Q_-(z)$] is the total charge above (below) the X-Y plane at height z, A the surface area, and ε_0 the dielectric constant of the vacuum. When one uses charge neutrality condition of the whole system, i.e.,

$$\int_{-\infty}^{\infty} dz\, \rho(z) = 0, \qquad \text{(E-2)}$$

one can rewrite the numerator of Eq.(E-1) as

$$Q_-(z)-Q_+(z) = A\left[\int_{-\infty}^{z} dz_1\,\rho(z_1) - \int_{z}^{\infty} dz_1\,\rho(z_1)\right]$$

$$= 2A\int_{-\infty}^{z} dz_1\,\rho(z_1), \qquad \text{(E-3)}$$

where $\rho(z)$ is the charge density. The electric potential $\chi(z)$ can be obtained as the integral of this E(z). Hereafter we set $\chi(-\infty)=0$ for simplicity. The potential difference χ is defined as

$$\chi = \lim_{z\to\infty} \chi(z)$$

$$= -\lim_{z\to\infty} \int_{-\infty}^{z} dz[Q_-(z)-Q_+(z)]/2\varepsilon_0 A$$

$$= -\lim_{z\to\infty} \int_{-\infty}^{z} dz_1 \int_{-\infty}^{z_1} dz_2\,\rho(z_2)/\varepsilon_0$$

$$= -\lim_{z\to\infty} \int_{-\infty}^{z} dz_2\,\rho(z_2) \int_{z_2}^{z} dz_1/\varepsilon_0$$

$$= -\lim_{z\to\infty} \int_{-\infty}^{z} dz_2\,\rho(z_2)(z-z_2)/\varepsilon_0$$

$$= \int_{-\infty}^{\infty} dz_2 \; z_2 \rho(z_2)/\varepsilon_0. \qquad \text{(E-4)}$$

Here we exchange the order of integration for the fourth line and use again the charge neutrality for the last line. The numerator of the last line is the total dipole moment of the system. This expression is the common basis for the two approaches.

The problem is how to calculate this total dipole moment. In the charge distribution approach one obtains directly the electric field E(z) based upon Eq.(E-1) and integrates it. In the dipole moment approach one estimates the total dipole moment as sum of the molecular dipole moments. Recently Wilson .et al. analytically formulated the difference between these two approaches.[134] Their technique is based upon the following Taylor expansion[20] of charge density $\rho(z)$,

$$\rho(z) = -\frac{d}{dz}P_z(z) + \frac{d^2}{dz^2}Q_{zz}(z) - \qquad \text{(E-5)}$$

where $P_z(z)$ is the z-component of the dipole density and $Q_{zz}(z)$ is the zz-component of the quadrupole density. After substitution of this expression into Eq.(E-4) and partial integration, one can obtain the "exact" formula[134]:

$$\chi = \int_{-\infty}^{\infty} dz_2 \; P_z(z_2)/\varepsilon_0 - [Q_{zz}(+\infty)-Q_{zz}(-\infty)]/\varepsilon_0. \qquad \text{(E-6)}$$

Therefore the surface potential is not determined only by molecular dipoles, but depends also on molecular quadrupoles !

As a result of that, the interface of non-polar matter, such as nitrogen, can have non-zero potential difference. This is not so remarkable as may look at first sight. To understand it, let us consider an ideal crystal composed of non-polar model molecules[135] (Fig.E-1); each molecule has a quadrupole moment, the z-component of which is negative. The electrostatic potential (a solid line in Fig.E-1) is therefore positive inside each molecule, and the spatial average of the potential becomes non-zero as shown by a dashed line in the figure, which agrees well with the result of Eq.(E-6). The experimental measurement of χ is, however, usually based on the estimation of electrostatic work needed to move a test charge (ions or electrons) from one bulk phase to another. Can we put the test charge inside the molecule? In the case of soft and large molecules, such as biopolymers, the answer may be yes and one can actually estimate the electrostatic potential spatially averaged in some sense. But for small and rather rigid molecules, like water, we are probably able to measure the potential only at each intermolecular space point; if molecules have no dipole moment, the result will be $\chi \approx 0$.

For the latter case, the dipole moment approach will be useful. To explain it in more detail, let us consider the system composed of rigid molecules** and express the position vector of i-th site (having charge q_i) of each molecule in laboratory-fixed frame as

$$R_i = Ar_j + R_0, \qquad \text{(E-7)}$$

where R_0 is the position of arbitrarily chosen center of each molecule, r_j is

the position of the i-th site in body-fixed frame, and A is the rotational matrix to describe the orientation of the molecule. From computer simulation, we know the distribution of R_0, which is the number density profile $n(z_0)$, and the probability distribution of A at height z_0, which is represented here by $f(A;z_0)$ and can be easily obtained from (θ, ϕ) distribution. The charge density at z is represented as

$$\rho_q(z) = \int_{Z_V}^{Z_L} dz_0 \int dA\ n(z_0) f(A;z_0) \sum_i q_i \delta((Ar_i)_Z + z_0 - z), \qquad \text{(E-8)}$$

where $\delta(x)$ is the Dirac's delta function. When Eq.(E-8) is substituted in Eq.(E-4), we obtain the following expression:

$$\int_{Z_V}^{Z_L} dz\, \rho_q(z) z = \int_{-\infty}^{\infty} dz_0\ n(z_0) \int dA\ f(A;z_0) \int_{Z_V}^{Z_L} dz\ z \sum_i q_i \delta((Ar_i)_Z + z_0 - z)$$

$$= \int_{Z_V}^{Z_L} dz_0\ n(z_0) \int dA\ f(A;z_0) [\sum_i q_i \{(Ar_i)_Z + z_0\}]$$

$$= \int_{Z_V}^{Z_L} dz_0\ n(z_0) \int dA\ f(A;z_0) (A \sum_i q_i r_i)_Z, \qquad \text{(E-9)}$$

where we use charge neutrality of each molecule, $\sum_i q_i = 0$, for the last line. When the molecular dipole P is defined as

$$P = \sum_i q_i r_i, \qquad \text{(E-10)}$$

we can simplify the expression (E-9) as

$$\int dz\, \rho_q(z) z = \int dz_0\, n(z_0) \int dA\, f(A;z_0)(AP)_z$$

$$= \int dz_0\, n(z_0) \langle P_z(z_0) \rangle. \qquad \text{(E-11)}$$

Therefore the potential difference can be expressed only with the sum of molecular dipole moments and the correction with the quadrupole moments of bulk phases does not appear.

We explain how the difference between Eqs.(E-6) and (E-11) comes out. The key exists in the transformation of Eq.(E-9), the first line into the second line, which means that we does not separate each molecule into charged sites. In other word, we neglect contribution of such a molecule as its charged site R_I and its center R_0 exist in different sides of integral boundary z_I or z_V; $z_0 < z_I < z_I$, for example. This assumption is equivalent to considering the electrostatic potential inside and outside of the molecule separately.

Table B-1. Some examples of the results of interpolations. The function is $y=\exp(x)$ and $\Delta=1\times10^{-3}$.

x	Exact	Interpolation	Inter. - Exact
0.54000	0.5827482398696	0.5827482398696	0.000000000000001
0.54016	0.5826550076989	0.5826550077033	0.000000000004437
0.54032	0.5825617904441	0.5825617904479	0.000000000003802
0.54048	0.5824685881029	0.5824685881034	0.000000000000484
0.54064	0.5823754006729	0.5823754006698	-0.000000000003132
0.54080	0.5822822281516	0.5822822281470	-0.000000000004659
0.54096	0.5821890705368	0.5821890705351	-0.000000000001714
0.54112	0.5820959278259	0.5820626278298	0.000000000003892

Table C-1. Coefficients in the equations of states, Eq.C-1, for CC water (Kataoka, 1987; Ref.141).

G-EOS			L-EOS		
p	q	A_{pq}	p	q	A_{pq}
0	-1	0.0	-1	-1	-0.2220869
0	0	0.0	-1	0	3.6157944
0	1	0.0	-1	1	-18.3789792
0	2	3.1807679	-1	2	39.9967884
0	3	-5.9419056	-1	3	-40.3930670
0	4	2.7238863	-1	4	19.5173923
0	5	-0.4205445	-1	5	-3.8310705
1	-1	0.0587421	0	-1	1.1250323
1	0	1.5089905	0	0	0.0
1	1	3.6371539	0	1	90.3543026
1	2	-26.8756039	0	2	-191.9693177
1	3	30.5849404	0	3	183.8455134
1	4	-15.8634460	0	4	-82.9389848
1	5	2.8434336	0	5	14.5930633
2	-1	-0.3288830	1	-1	-1.8968523
2	0	2.8286569	1	0	30.9891198
2	1	-16.6845815	1	1	-146.2148375
2	2	41.1106362	1	2	300.0578154
2	3	-44.2019080	1	3	-284.1159875
2	4	23.8319390	1	4	123.1250824
2	5	-4.5024430	1	5	-20.1654321
3	-1	0.3003771	2	-1	1.2556364
3	0	-2.6169049	2	0	-19.1421732
3	1	14.8803743	2	1	94.3057221
3	2	-29.1987207	2	2	-201.9096123
3	3	27.6103535	2	3	187.5482037
3	4	-14.3644167	2	4	-78.6845661
3	5	2.7566203	2	5	12.2244129
4	-1	-0.0913007	3	-1	-0.3077658
4	0	0.8580968	3	0	4.6769417
4	1	-3.7785341	3	1	-20.7424046
4	2	7.6204051	3	2	47.7529685
4	3	-6.5670215	3	3	-44.1595173
4	4	3.2232452	3	4	18.1884994
4	5	-0.8146288	3	5	-2.7281295

Table C-2. Coefficients in the equations of states, Eq.C-7, for LJ system (Ree, 1980, Ref.151).

i	B_i	C_i	D_i
1	3.629	5.3692	-3.4921
2	7.2641	8.5797	18.8980
3	10.4924	8.1745	-35.5049
4	11.459	-4.2685	31.8151
5		1.6841	-11.1953
10	2.17619		

[Figure captions in Appendices]

Fig.A1. CC model of a water molecule (Ref.142). Four interaction sites are just on the two hydrogen atoms, the oxygen atom, and the virtual lone pair represented as M, which exists between the hydrogen atoms. The hydrogens have partial charge δ=0.658 e, where e is the elementary charge, e=1.602×10^{-19} C, and the lone pair has -2δ.

Fig.A2. TIPS model of a methanol molecule (Ref.149). Three interaction sites are just on the hydrogen atom, the oxygen atom, and the methyl group, each of which has partial charge; δ_1=0.285 e and δ_2=0.40 e. The three axes x, y, z (x is perpendicular to the y-z plane) are principal axes of moment inertia tensor in order of its principal values and form the body-fixed coordinate system. The origin of the frame is the center of mass, which exists between the oxygen atom and the methyl group.

Fig.B1. The scheme of parabolic approximation.

Fig.D1. The surface of ideal Crystal composed of non-polar model molecules having quadrupoles, and the electrostatic potential χ(z) along the crystal axis. The solid line is the true potential, and the dashed line represents the space-averaged one. At every intermolecular space point χ is zero, but averaged potential is positive.

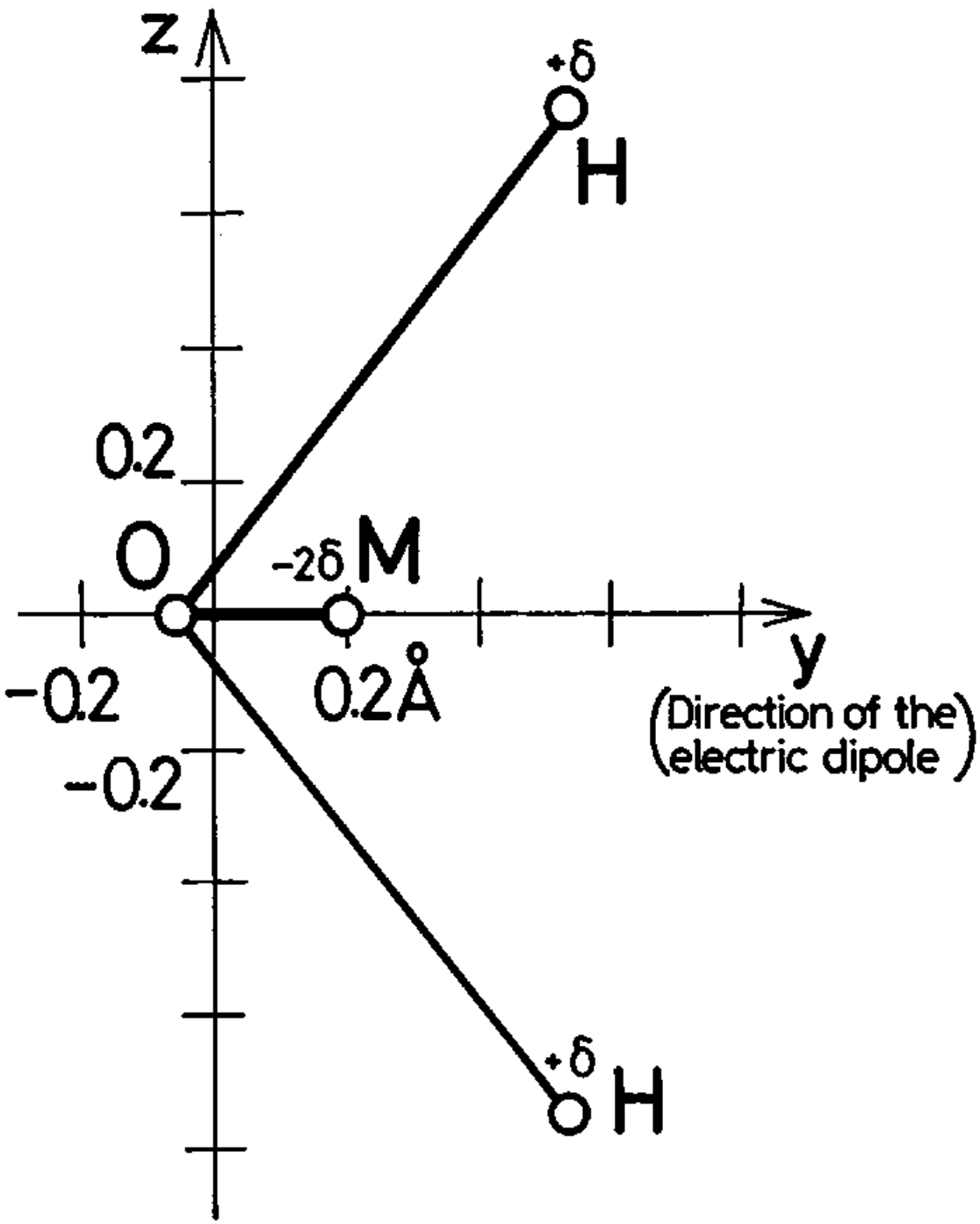

Fig. A1.

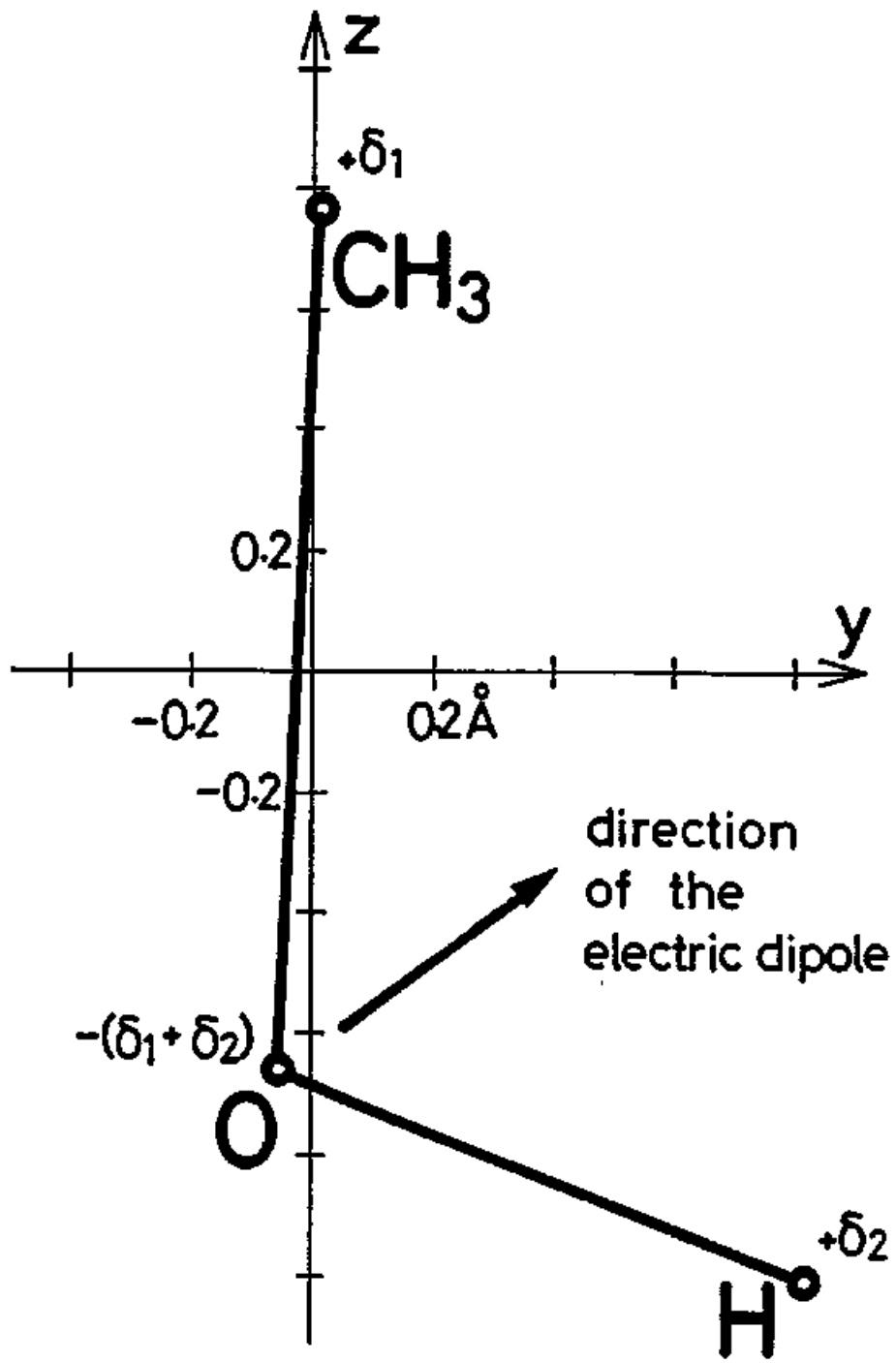
z
+δ1
CH3
0.2
y
-0.2
0.2Å
-0.2
direction
of the
electric dipole
-(δ1+δ2)
O
+δ2
H

Fig. A2.

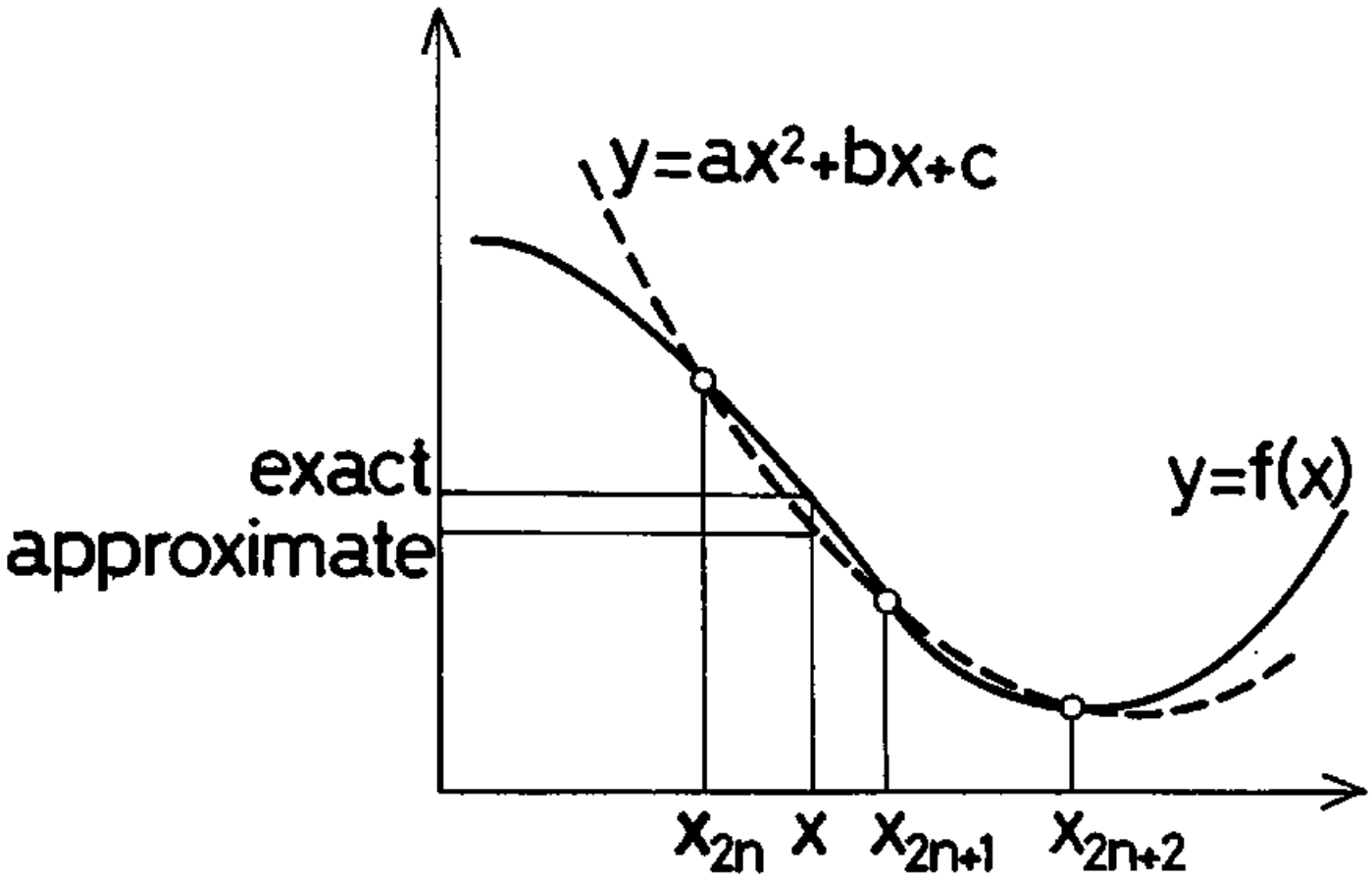

Fig.B1.

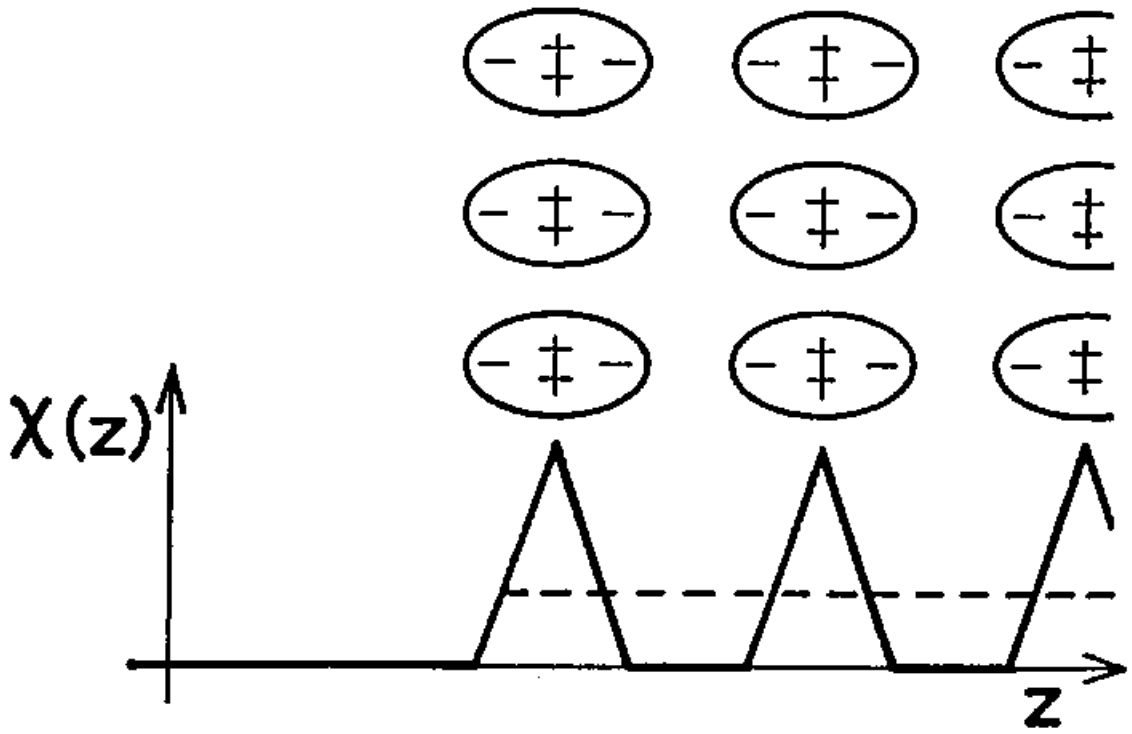

Fig.D1.

References

[Textbooks, monographs, and reviews]

1. Fluid Interfacial Phenomena, ed. by C.A.Croxton (John Wiley & Sons, 1986).

2. J.S.Rowlinson and B.Widom, Molecular Theory of Capillarity (Clarendon, 1982).

3. R.Evans, Adv.Phys., 28,143 (1979).

4. S.Ono and S.Kondo, in Handbuch der Physik X (Springer,1960).

5. J.C.Henniker, Rev.Mod.Phys., 21,322 (1949).

6. D.Nicholson and N.G.Parsonage, Computer Simulation and the Statistical Menanics of Adsorption (Academic Press, 1982).

7. Monte Carlo Methods in Statistical Physics, ed. by K.Binder (Springer, 1979).

8. Applications of the Monte Carlo Method in Statistical Physics, ed. by K.Binder (Springer, 1984).

9. E.A.Guggenheim, Thermodynamics (North-Holland, 1967).

10. Simulation of Liquids and Solids, ed. by G.Ciccotti, D.Frenkel and I.R.McDonald (North-Holland, 1987).

11. Molecular-Dynamics Simulation of Statistical-Mechanical Systems, ed. by G.Ciccotti and W.G.Hoover (1986).

12. C.G.Gray and K.E.Gubbins, Theory of Molecular Fluids, Vol.1, Appendix D (Clarendon, 1984).

13. Handbook of Chemistry and Physics, 69th ed., ed.by R.C.Weast (CRC, 1988).

14. R.C.Reid, J.M.Prausnitz, and B.E.Poling, The Properties of Gases and Liquids, 4th ed., Appendix (McGraw-Hill, 1987).

15. F.Franks and D.S.Reid, in Water, A Comprehensive Treatise, ed. by F.Franks, Vol.2, Chap.5. (Plenum, 1973)

16. F.H.Stillinger, Adv.Chem.Phys., 31,1(1975).

17. P.Drude, Theory of Dielectrics, 2nd ed. (Dover, 1959).

18. R.M.A.Azzam and N.M.Bashara, Ellipsometry and Polarized Light (North-Holland, 1977).

19. H.Fröhlich, Theory of Dielectrics, 2nd ed. (Clarendon, 1958)

20. J.D.Jackson, Classical Electrodynamics (Wiley.1975).

[Original papers]

101. R.Eötvös, Wied.Ann.Physik, 27,448(1886).

102. M.Katayama, Sci.Rep.Tohoku Imp.Univ., 4,373(1916).

103. J.D.van der Waals, Z.Phys.Chem., 13,657(1894).

104. J.W.Cahn and J.E.Hilliard, J.Chem.Phys., 28, 258(1958).

105. S.Fisk and B.Widom, J.Chem.Phys, J.Chem.Phys., 50,3219(1969).

106. J.A.Barker and J.R.Henderson, J.Chem.Phys., 76,6303(1982).

107. F.P.Buff, R.A.Lovett, and F.H.Stillinger, Phys.Rev.Lett., 15,621(1965).

108. C.A.Croxton and R.P.Ferrier, J.Phys., C4,2447(1971).

109. G.A.Chapela, G.Saville, S.M.Thompson, and J.S.Rowlinson, J.Chem.Soc.Faraday Trans.II, 73,1133(1977).

110. J.G.Powles and R.F.Fowler, J.Phys.C, 18,5909(1985).

111. S.M.Thompson and K.E.Gubbins, J.Chem.Phys., 70,4947(1979); S.M.Thompson, K.E.Gubbins, and J.M.Haile, ibid., 75,1325(1981); S.M.Thompson and K.E.Gubbins, ibid., 74,6467(1981).

112. J.Eggebrecht, K.E.Gubbins, and S.M.Thompson, J.Chem.Phys., 86,2286(1987); J.Eggebrecht, S.M.Thompson, and K.E.Gubbins, ibid., 86,2299(1987).

113. P.Tarazona and G.Navascués, Mol.Phys., 47,145(1982); E.Chacon, P.Tarazona, and G.Navascués, J.Chem.Phys., 79,4428(1983); E.Chacon, L.Mederos, G.Navascués, and P.Tarazona, ibid., 82,3802,(1985).

114. J.W.Good, J.Phys.Chem., 61,810(1957).

115. W.Drost-Hansen, Ind.Eng.Chem., 57-4,18(1965); W.Drost-Hansen, J.Geophys.Res., 77,5132(1972), and references therein.

116. G.J.Gittens, J.Colloid and Interface Sci., 30,406(1969).

117. R.Cini, G.Loglio, and A.Ficalbi, J.Colloid and Interface Sci., 41,287(1972).

118. Y.Tominaga, private communication.

119. W.A.Weyl, J.Colloid Sci., 6,389(1951).

120. F.H.Stillinger and A.Ben-Naim, J.Chem.Phys., 47,4431(1967).

121. N.H.Fletcher, Philos.Mag., 18,1287(1968).

122. C.A.Croxton, Physica A, 106,239(1981).

123. W.H.Flygare and R.C.Benson, Mol.Phys., 20,225(1971).

124. B.Borštnik, D.Janežič, and A.Ažman, Acta Phys.Acad.Sci.Hung., 48,297(1976).

125. O.Matsuoka, E.Clementi, and M.Yoshimine, J.Chem.Phys., 64,1351(1976).

126. C.Y.Lee and H.L.Scott, J.Chem.Phys., 73,4591(1980).

127. F.H.Stillinger and A.Rahman, J.Chem.Phys., 60,1545(1974).

128. R.N.Townsend, J.Gryko, and S.A.Rice, J.Chem.Phys., 82,4391(1985).

129. N.I.Christou, J.S.Whitehouse, D.Nicholson, and N.G.Parsonage, Mol.Phys., 55,397(1985).

130. J.S.Rowlinson, Trans.Faraday Soc., 47,120(1951).

131. E.N.Brodskaya and A.I.Rusanov, Mol.Phys., 62,251(1987).

132. M.A.Wilson, A.Pohorille, and L.R.Pratt, J.Phys.Chem., 91,4873(1987).

133. W.L.Jorgensen, J.Chandrasekhar, J.D.Madura, R.W.Impey. and M.L.Klein, J.Chem.Phys., 79,926(1983).

134. M.A.Wilson, A.Pohorille, and L.R.Pratt, J.Chem.Phys., 88,3281(1988); ibid., submitted. (Comment on "Study on the liquid-vapor interface of water...")

135. M.Matsumoto and Y.Kataoka, J.Chem.Phys., submitted. (Reply to Comment)

136. J.G.Kirkwood and F.P.Buff, J.Chem.Phys., 17,338(1949).

137. A.Harashima, Adv.Chem.Phys., 1,203(1958).

138. J.H.Irving and J.G.Kirkwood, J.Chem.Phys., 18,817(1950).

139. J.P.R.B.Walton, D.J.Tildesley, and J.S.Rowlinson, Mol.Phys., 48,1357(1983).

140. M.H.Kalos, J.K.Percus, and M.Rao, J.Stat.Phys., 17,111(1977).

141. Y.Kataoka, J.Chem.Phys., 87,589(1987).

142. V.Carravetta and E.Clementi, J.Chem.Phys., 81,2646(1984).

143. W.Smith and D.Fincham, CCP5 newsletter (Daresbury Lab., England, 1982).

144. L.Verlet, Phys.Rev., 159,98(1967).

145. D.J.Evans, Mol.Phys., 34,317(1977).

146. M.P.Tosi, Solid State Phys., 16,107(1964).

147. S.Nosé and M.L.Klein, Mol.Phys., 50,1055(1983).

148. M.J.P.Nijmeijer, A.F.Bakker, C.Bruin, and J.H.Sikkenk, J.Chem.Phys., 89,3789(1988).

149. W.L.Jorgensen, J.Amer.Chem.Soc., 103,335(1981).

150. J-P.Hansen and L.Verlet, Phys.Rev., 184,151(1969).

151. F.H.Ree, J.Chem.Phys., 73,5401(1980).

152. T.Nakagawa and Y.Oyanagi, in Recent Developments in Statistical Inference and Data Analysis, ed. by K.Matsusita (North-Holland, 1980).

153. A.Braslau, M.Deutsch, P.S.Pershan, A.H.Weiss, J.Als-Nielsen, and J.Bohr, Phys.Rev.Lett., 54,114(1985).

154. M.S.Wertheim, J.Chem.Phys., 65,2377(1976).

155. N.B.Vargaftik, B.N.Volkov, and L.D.Voljak, J.Phys.Chem.Ref.Data, 12,817(1983).

156. R.Strey and T.Schmeling, Ber.Bunsenges.Phys.Chem., 87,324(1983).

157. W.A.P.Luck, Discuss.Faraday Soc., 43,115(1967).

158. P.A.Egelstaff and B.Widom, J.Chem.Phys., 53,2667(1970).

159. I.C.Sanchez, J.Chem.Phys., 79, 405(1983).

160. W.F.Murphy, J.Chem.Phys., 67,5877(1977).

161. V.A.Kizel', J.Exp.Theor.Phys.USSR, 29,658(1955).

162. K.Kinoshita and H.Yokota, J.Phys.Soc.Jpn., 20,1086(1965).

163. J.J.Bridge and A.D.Buckingham, Proc.Roy.Soc., A295,334(1966).

164. D.Beaglehole, Physca 100B,163(1980).

165. A.N.Frumkin, Z.Phys.Chem., 109,34(1924).

166. B.Case and R.Parsons, Trans.Faraday Soc., 631224(1967).

167. A.N.Frumkin, Z.A.Iofa, and M.A.Gerovich, Zhur.Fiz.Khim., 30,1455(1956).

168. D.J.Schiffrin, Trans.Faraday Soc., 66(2464(1970).

169. J.R.Farrell and P.McTigue, J.Electroanal.Chem., 139,37(1982); J.R.Farrell and P.McTigue, ibid., 163,129(1984); A.Borazio, J.R.Farrel, and P.McTigue, ibid., 193,103(1985).

170. C.Y.Lee, J.A.McCammon, and P.J.Rossky, J.Chem.Phys., 80,4448(1984).

171. J.P.Valleau and A.A.Gardner, J.Chem.Phys., 86,4162(1987).

172. B.Jorgensen, J.Chem.Phys., 77,4156(1982).

173. P.Linse, J.Chem.Phys., 86,4177(1987).

174. J.P.Hansen, Phys.Rev., A2,221(1971).

175. D.Beaglehole, Physica 100B,163(1980).

176. J.Lekner, Mol.Phys., 49,1385(1983).